DISSERTATION ZUR ERLANGUNG DES DOKTORGRADES
DER FAKULTÄT FÜR CHEMIE UND PHARMAZIE
DER LUDWIG-MAXIMILIANS-UNIVERSITÄT MÜNCHEN

Evaluation of energetic plasticizers for GAP-based formulations

Synthesis and characterization of nitrofurazanyl ethers

Patrick Lieber
aus Baden-Baden, Deutschland
2025

Erklärung

Diese Dissertation wurde im Sinne von § 7 der Promotionsordnung vom 28. November 2011 von Herrn Prof. Dr. Dr. h.c. Thomas M. Klapötke betreut.

Eidesstattliche Versicherung

Diese Dissertation wurde eigenständig und ohne unerlaubte Hilfe erarbeitet.

Pfinztal, 2. Dezember 2025

_____

Patrick Lieber

Dissertation eingereicht am 3. Dezember 2025

1. Gutachter: Prof. Dr. Dr. h.c. Thomas M. Klapötke

2. Gutachter: apl. Prof. Dr. Konstantin L. Karaghiosoff

Mündliche Prüfung am 17. Februar 2026

Und weiter, weiter geht der Lauf

tut euch, ihr alten Tore, auf!

Leicht ist mein Sinn und frei mein Pfad

gehab dich wohl, du Musenstadt!

Gustav Schwab, 1814.

Danksagung

Mein besonderer Dank gilt **Prof. Dr. Dr. h.c. Thomas M. Klapötke**, der mich als „Externen“ in seinen Arbeitskreis aufgenommen und so diese Dissertation ermöglicht hat. Ich bin ihm zudem dankbar, dass ich ihn jederzeit unkompliziert kontaktieren konnte und er häufig so prompt antwortete, dass seine Rückmeldungen meist noch am selben Tag bei mir eintrafen. Trotz der Distanz zwischen Karlsruhe und München konnte ich mich immer auf die Unterstützung meines Doktorvaters verlassen.

Dr. Uwe Schaller danke ich herzlich für die intensive Begleitung dieser Doktorarbeit am Fraunhofer ICT. Deine zahlreichen Anregungen zu Synthesewegen, Charakterisierungsmethoden und Anwendungen waren für diese Arbeit unverzichtbar. In vielen Gesprächen hast du meine Fragen beantwortet und mir Einblicke verschafft, die weit über rein chemisches Fachwissen hinausgehen. Auch wenn es an das Korrekturlesen von Manuskripten ging, warst du immer zur Stelle.

Dr. Stefan Löbbecke und **Dr. Dusan Boskovic**, danke ich für das Vertrauen, das sie mir mit der Einstellung als Doktorand und später mit der Leitung von Projekten entgegenbrachten.

Für die schnelle und unkomplizierte Aufnahme in die Gruppe Chemische Prozesstechnik sowie die kollegiale und konstruktive Arbeitsatmosphäre danke ich **Gonzalo Araya Vargas, Mirjam Brassat, Jeremy M. Brixner, Angelika Eberhardt, Hartmut Kröber, Dr. Alexander Mendel, Barbara Bertin Mente, Slobodan Panic, Dr. Calogero Piscopo, Dr. Angelos Polyzoidis, Maud Schwarzer, Heinrich Wegner** und **Dr. Michael Mössinger** herzlich.

Ein besonderer Dank gilt:

- **Tobias Türcke** für die Hilfe beim Auffinden und in Betrieb nehmen von allen möglichen Dingen und beim Zerschlagen bürokratischer Knoten. Außerdem ist er ein Top-Experte für Quizrunden in der Mittagspause, Außenwirtschaftsrecht, Gefahrgut und die Organisation von Barbara-Feiern und Betriebsausflügen.
- **Ligia Radulescu** für den Hinweis auf die NTREM und die legendären Abende in Pardubice. Es war mir stets eine Freude mit dir das Fraunhofer ICT auf Konferenzen gebührend zu vertreten und gemeinsam neue Kontakte in der kleinen, aber feinen Welt der Energetischen Materialien zu knüpfen.

Dr. Thomas Keicher, **Gudrun Dornick**, **Tim Nickel** und **Jan-Benedikt Müller** von der Synthesegruppe danke ich herzlich für ihre Freundlichkeit und Hilfsbereitschaft.

Wenka Schweikert und **Stefan Müller** danke ich für die Unterstützung bei der Schwingungsspektroskopie und dass sie mir den uneingeschränkten Zugang zu ihren Spektrometern für diese Arbeit anvertraut haben.

Dr. Peter Schultz danke ich für die große Hilfsbereitschaft bei allen Fragen zur Kristallographie und besonders die Unterstützung bei der Einkristallstrukturanalyse.

Ich danke außerdem **Dr. Jasmin Lechner** und **Dr. Maximilian Benz** sowie allen Doktorandinnen und Doktoranden und Mitarbeitenden des Arbeitskreises in München für die freundliche Aufnahme und kollegiale Zusammenarbeit.

Ein Dank gilt meiner studentischen Hilfskraft **Mike Schäfer**, der mit der Synthese von Edukten einen wichtigen Beitrag zu dieser Arbeit geleistet hat. Ebenso danke ich meinen Praktikantinnen **Nane Timme**, **Lena Luisa Fercic** und **Sarah Sounier** sowie meiner Bachelorandin **Nea Ana Langkamp** für ihre engagierte Mitarbeit und den Beitrag, den sie zum Gelingen dieser Arbeit geleistet haben. Mein Dank gilt auch **Samira Kalapos** und **Chiara Vetter** für ihre wertvolle Unterstützung während der Praxisphasen ihrer Ausbildung zu Chemielaborantinnen.

Ich bedanke mich bei meinen engagierten Chemielehrern **Björn Baumann** und **Nina Schille**, die mich früh für die Chemie begeisterten und mir den richtigen Weg wiesen.

Meinen Corpsbrüdern der **Friso-Cheruskia** in Karlsruhe danke ich für unzählige fröhliche Abende, die Segelurlaube und viele andere gemeinsame Abenteuer und Erlebnisse, die meine Studien- und Promotionszeit wie im Flug vergehen ließen.

Von Herzen danke ich meinen Eltern, **Maria** und **Horst**, für ihre bedingungslose Unterstützung und ihren beständigen Rückhalt.

Zuletzt gilt mein tief empfundener Dank meiner wunderbaren Ehefrau **Aline**, deren unerschütterliche Unterstützung, Geduld und Liebe mich in den vergangenen fünf Jahren durch alle Höhen und Tiefen dieser Arbeit getragen haben.

Contents

1 Introduction

1.1 Energetic materials

The research on energetic materials is interdisciplinary. Those who devote themselves to it inevitably leave the familiar terrain and enter unknown areas of chemistry, physics, material science, chemical engineering, and computer science. Many more scientific disciplines and sub-disciplines could be listed here. Accordingly, the classification of energetic materials also varies depending on the perspective. Energetic materials can be classified according to their chemical substance class or divided into materials of civil or military use. Figure 1 shows the most common classification of pure energetic materials, mixtures or formulations according to their use as explosive, propellant or pyrotechnic composition.[1] In addition, energetic binders and plasticizers are also considered to be energetic materials.[2] Common subcategories include gun propellants, rocket propellants, and primary and secondary explosives.[3–6]

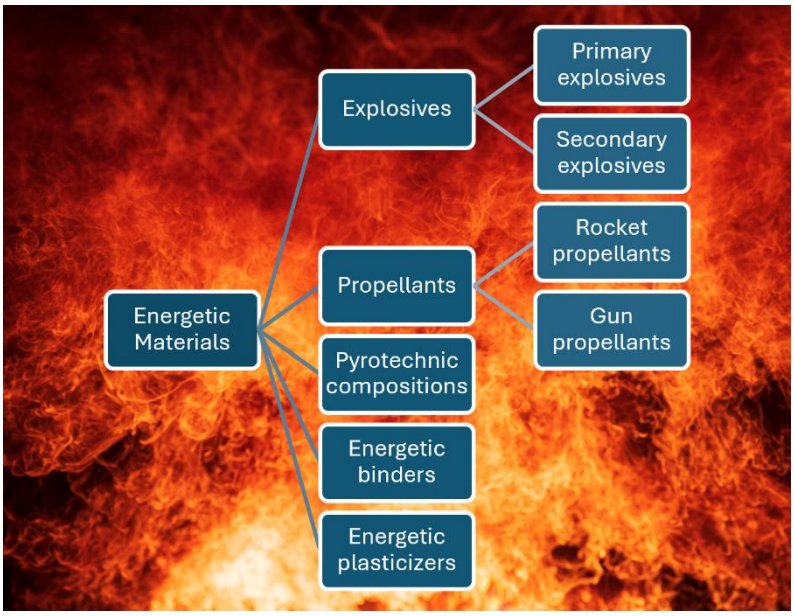

Figure 1 Classification of energetic materials by their application.

Pyrotechnic compositions produce effects such as heat[7], light[8], sound[9], gas[10], or smoke[11], or a combination of these. They are used in distress flares and smoke grenades, as well as less obvious applications such as igniters and as delay elements. The effects of pyrotechnic compositions are always based on a reaction between an oxidizer and a

reducing agent contained in the mixture. Therefore, they do not require additional atmospheric oxygen to perform their function.

Propellants are burned in a controlled manner to accelerate an object. They are divided into two main groups: gun propellants and rocket propellants.[2] Gun propellants ignite while the projectile initially seals the barrel. This results in a sharp pressure increase due to gas generation at a nearly fixed volume. In contrast, a solid rocket motor's chamber pressure self-regulates through the balance of pressure-dependent mass flow through the choked nozzle and pressure-dependent propellant burn rate. Therefore, the combustion pressures of gun propellants are generally much higher than those of rocket propellants. The specific impulse corresponds to the change in momentum per unit mass of the propellant and is the most important performance parameter for this group of energetic materials.[12] Rocket propellants are further divided into liquid and solid propellants according to their aggregate state.[2] Liquid propellants are mainly used in civil spaceflight due to a complex storage and refueling process.[13] Solid propellants, which are used in all kinds of military applications and as boosters for civilian spaceflight, are further classified as homogeneous or heterogeneous.[14] Homogeneous propellants are uniform mixtures of one or more components, while heterogeneous propellants, also known as composite propellants, are a mixture of relatively pure phases like oxidizer granules or aluminum particles in a polymer binder.[2] Figure 2 illustrates the two-dimensional structure of a common composite propellant, which consists of HTPB as the polymer binder and an organic fuel, ammonium perchlorate as the oxidizer, and aluminum as a metal fuel.

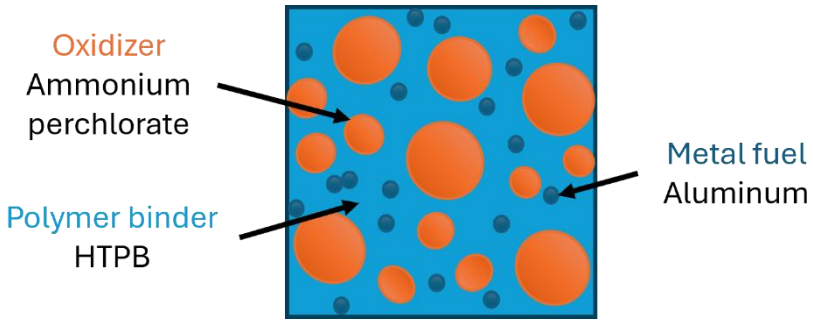

Figure 2 Internal two-dimensional structure of a common composite propellant.

Explosives are used to create a shock wave by detonation. The force of this shock wave can be utilized for various applications such as demolition, resource extraction or

weapon systems. A detonation is a self-sustaining reaction that occurs faster than the speed of sound under formation of a detonation wave with a shock front, while a deflagration is a very rapid burning under buildup of pressure that does not exceed the speed of sound.[2,15] Explosives are divided into primary and secondary explosives. While primary explosives generally have a high sensitivity and undergo a rapid deflagration-to-detonation (DDT) transition after ignition, secondary explosives must be initiated by a shock wave in order to detonate.[1,16] A general performance parameter for secondary explosives is the detonation velocity.[17,18] Blasting oils such as nitroglycerin are primary explosives, but they are also used in homogeneous propellants based on nitrocellulose (NC) because of their high chemical energy, their positive oxygen balance and their plasticizing effect.[19–21] Figure 3 shows the molecular structures of traditional and new secondary explosives, and Figure 4 shows those of typical primary explosives.

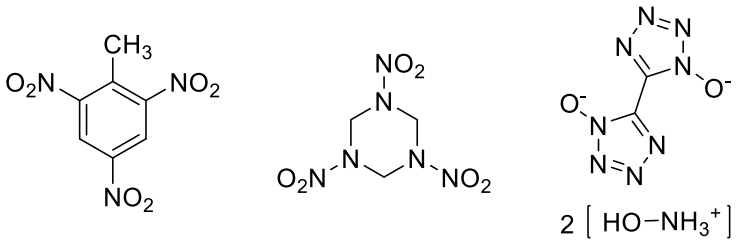

Figure 3 Molecular structures of secondary explosives trinitrotoluene (TNT), hexogen (RDX), and dihydroxylammonium 5,5′-bistetrazolyl-1,1'-diolate (TKX-50) including the year in which they were published for the first time.

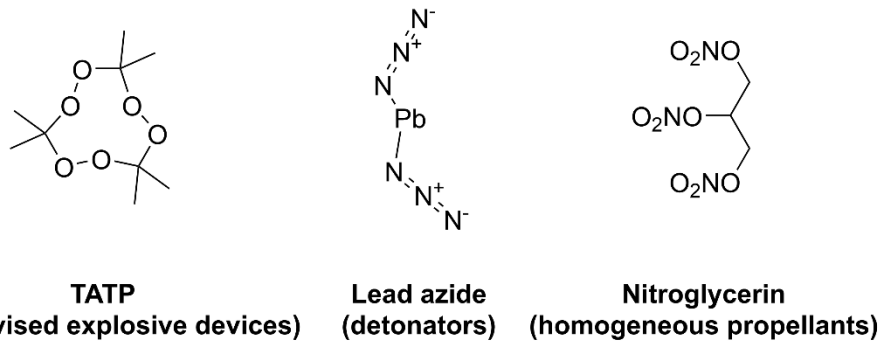

Figure 4 Molecular structures of primary explosives triacetone triperoxide (TATP), lead azide (LA), and nitroglycerin (NG) including their main application.

Energetic binders and **energetic plasticizers** also fall under the category of energetic materials. These groups are central to this thesis and will be discussed in more detail in the following sections.

1.2 Energetic binders

Chemically pure energetic materials are rarely used in applications. Instead, they are used in formulations with other energetic and non-energetic components. Energetic binders are organic polymers that act as an elastic matrix for fillers such as explosives, oxidants or reducing agents.[22] Unlike inert binders, such as the widely used hydroxyl-terminated polybutadiene (HTPB), energetic binders contain energy-rich functional groups, called explosophores, which result in a contribution to the total energy of the formulation.

A long-known energetic binder is nitrocellulose (NC).[1] It is still widely used in double base propellants, but has the disadvantage of being made from cotton, which is a natural product, making it difficult to obtain a consistent quality.[22] Figure 5 illustrates the repeat units of HTPB and NC. However, the main issue with NC is the acid-induced autocatalytic decomposition of the nitrate ester groups, which requires the use of stabilizers.[23]

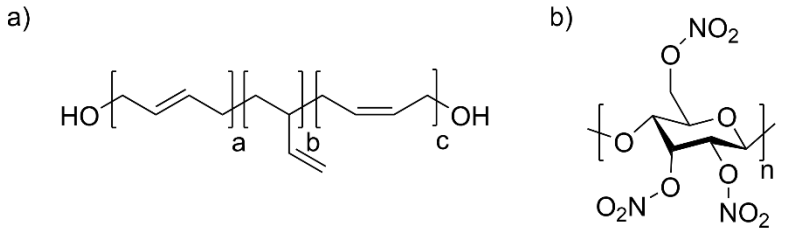

Figure 5 Repeat units of a) hydroxyl-terminated polybutadiene (HTPB) and b) nitrocellulose (NC).

Over the years, new synthetic polymers have been discovered to overcome the challenges associated with NC as a natural product. Formulations containing modern cross-linked binders are typically processed in a cast-cure process in which the fillers, prepolymers, and curing agents are first mixed before the mixture is poured into a mold and then cured. According to their explosophores energetic binders can be divided into those containing nitro or nitrate ester groups and those containing azide groups.

An azide-based energetic polymer that is frequently mentioned in the literature for exceptional properties is glycidyl azide polymer (GAP).[24] Other compounds that have been documented include poly-BAMO, poly-AMMO, and poly(allyl azide) (PAA).[25–27] Figure 6 shows the repeat units of the named azide-containing polymers.

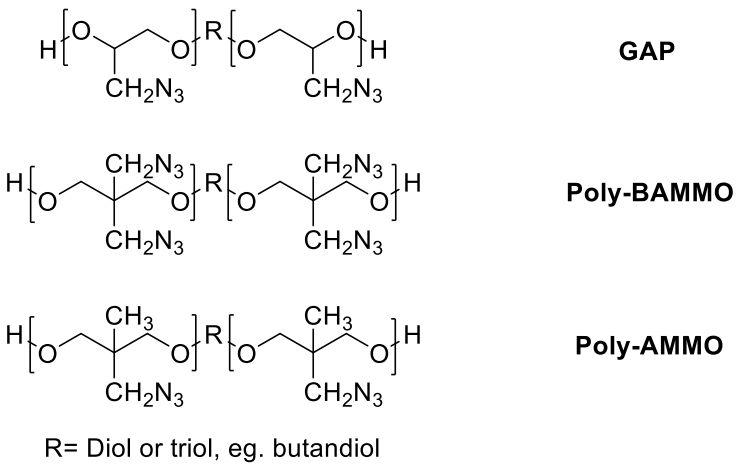

Figure 6 Molecular structure of selected azide-based binders for isocyanate curing.

For hydroxyl-terminated binders, isocyanates are generally used as curing agents, which react under formation of polyurethanes. However, other curing strategies are also used.[28] For example, PAA is cured with diacrylates by formation of triazole-linkers as shown in Figure 7.[29]

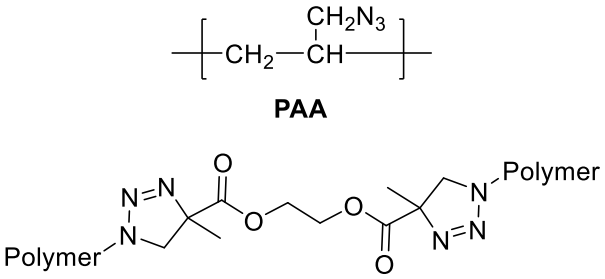

Figure 7 Molecular structure of PAA and a triazole linker formed during the curing of PAA with ethylene glycol dimethacrylate (EGDMA).

Binders that contain nitrate ester or nitro groups often have a better oxygen balance compared to azides, but simultaneously often have weaker mechanical properties. Poly-GLYN was one of the most anticipated compounds, but it has serious stability problems when combined with isocyanate crosslinkers.[30] A more recent approach is the one-pot synthesis of nitro-HTPB.[31,32] Figure 8 depicts the repeat units of the named examples for nitro and nitrate ester-containing polymers.

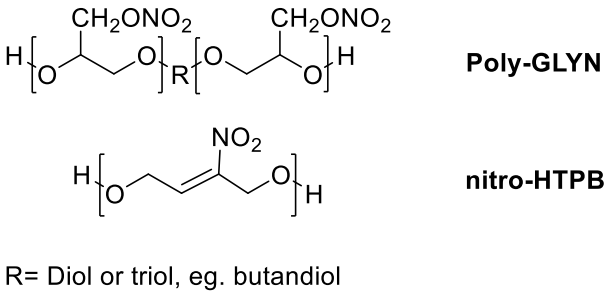

Figure 8 Molecular structure of poly-GLYN and nitro-HTPB.

1.3 Energetic plasticizers

Plasticizers are typically organic liquids with high boiling points that are used to modify the mechanical properties of polymers. They lower the glass transition temperature (T_g), the temperature at which a polymer changes from a brittle state to a flexible, rubber-like state. Furthermore, plasticizers decrease the elastic modulus (E) by raising strain (ε) and lowering stress (σ) in the linear-elastic section of the stress-strain curve (Equation 1). Figure 9 illustrates the impact of plasticization on the stress-strain curve of a polymer. These adjustments help to prevent fractures or surface detachment, even at low temperatures. Also, plasticizers reduce the viscosity of uncured formulations, thereby improving their processability during casting.[22,33]

$$E = \frac{\sigma}{\varepsilon} \tag{1}$$

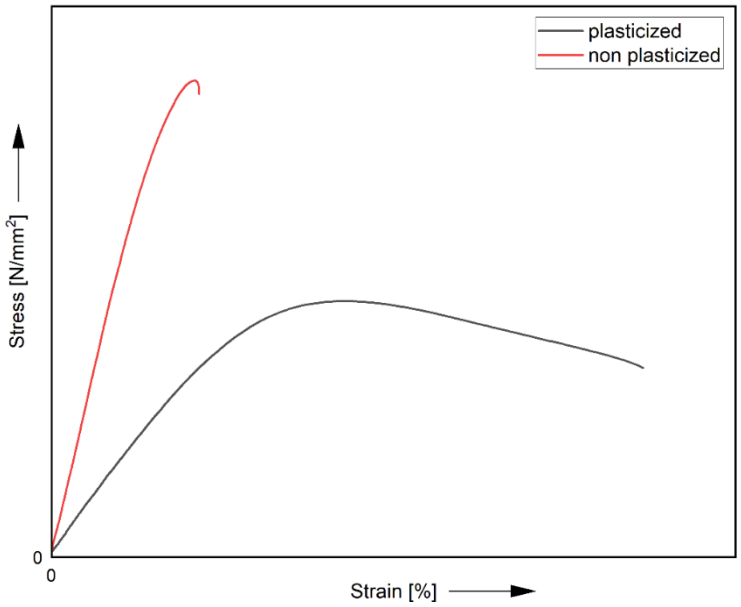

Figure 9 Exemplary stress-strain curves of a plasticized and a non-plasticized polymer.

However, these effects can also be achieved by adding inert plasticizers. In the civil plastics industry, phthalates are used in large quantities. Bis(2-ethylhexyl) phthalate (DEHP) and dioctyl phthalate (DIOP) were historically used in building materials and consumer products. Especially in the case of the widely used plastic polyvinyl chloride (PVC), which only becomes useful through the use of plasticizers.[34] However, due to their biological activity as endocrine disruptors[35], they have been replaced by other compounds such as di(propylheptyl) orthophthalate (DPHP) with a higher molecular weight.[36] In a mixture with anionic phthalate and tri-n-butyl citrate, DIOP is used until today in the renowned Czech plastic explosive SEMTEX. In the well-known US American plastic explosive C4, the plasticizers bis(2-ethylhexyl) adipate (DEHA, sometimes also abbreviated as DOA) and bis(2-ethylhexyl) sebacate are used.[37] DEHA is also commonly used as a plasticizer for HTPB-based composite propellants. Due to its large aliphatic structure, it is well miscible with HTPB. Additionally, studies have shown that DEHA has no negative influence on the thermal ageing process. [38] A selection of the named inert plasticizers is shown in Figure 10.

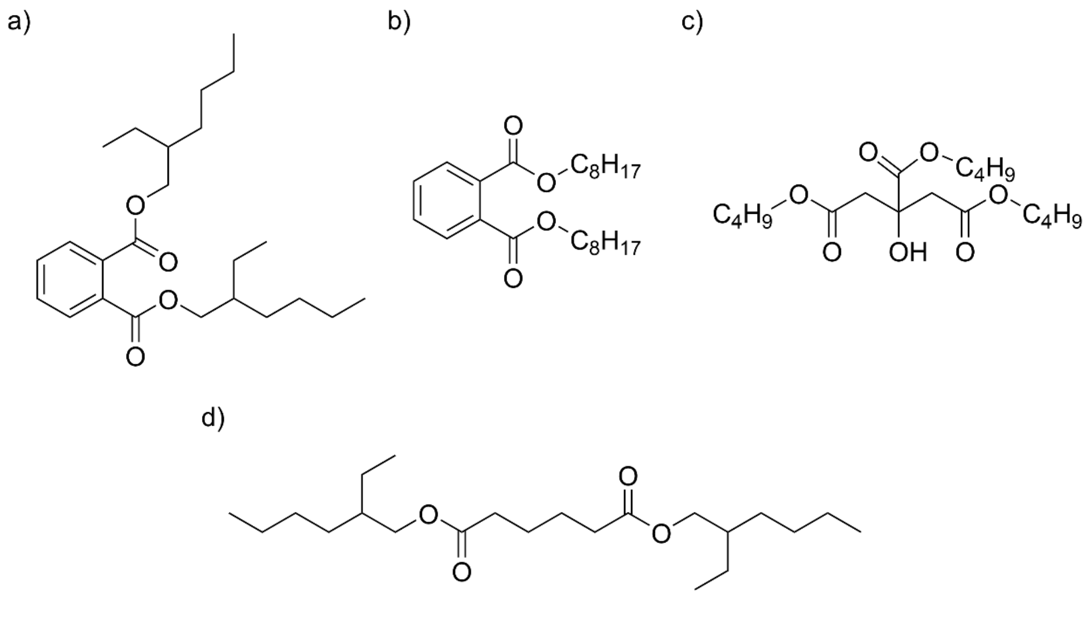

Figure 10 Selection of inert plasticizers used in SEMTEX and C4 type plastic explosives a) bis(2-ethylhexyl) phthalate (DEHP) b) dioctyl phthalate (DIOP) c) tri-n-butyl citrate d) bis(2-ethylhexyl) adipate (DEHA, sometimes also abbreviated as DOA).

One disadvantage of inert plasticizers is their low energy content. In contrast, energetic plasticizers contain explosophoric groups, such as nitro, nitramino, azido, and nitrate

esters. These groups contribute to the oxygen balance and energetic performance of a formulation.[39] It should also be noted that plasticizers have the ability to dissolve other components of a formulation. This behavior can significantly impact the long-term stability of formulations. Therefore, solubility is a decisive factor for compatibility of a plasticizer with the environmentally friendly, low-signature ammonium dinitramide (ADN) oxidizer. For example, Ek et al. demonstrated that the solubility of ADN depends heavily on the length of the polyethylene glycol chains within a plasticizer molecule.[40]

1.3.1 Energetic plasticizers based on nitrate esters

Aliphatic nitrate esters are the oldest group of energetic plasticizers. Figure 11 shows the molecular structure of exemplary compounds. These compounds are characterized by a high oxygen balance, as well as high impact sensitivity, autocatalytic decomposition in the presence of acids, and low thermal stability.[39,41,42] They are mainly used in double base NC propellants.[43]

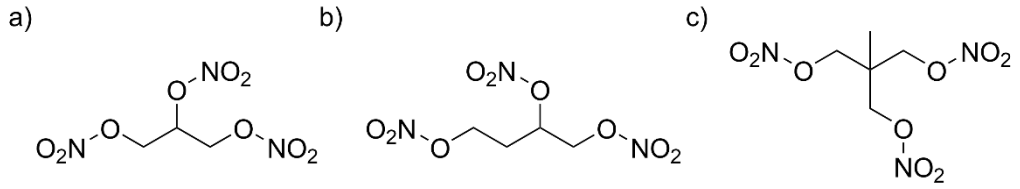

Figure 11 Selected nitrate ester-based energetic plasticizers a) nitroglycerin b) 1,2,4-butanetriol trinitrate (BTTN) c) trimethylolethane trinitrate (TMETN).

1.3.2 Energetic plasticizers based on nitro and nitramines

Another large group of energetic plasticizers is based on nitramines or nitro groups. These compounds are often characterized by a lower impact sensitivity, a lower T_g, and a lower oxygen balance than nitrate esters.[44–46] Figure 12 shows a selection of representative molecular structures.

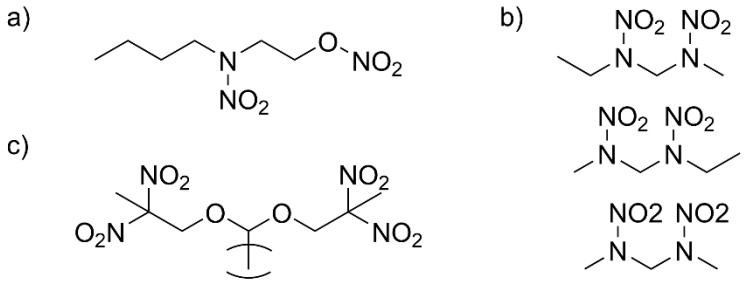

Figure 12 Selected nitramine and nitro-based energetic plasticizers a) 2-(butyl(nitro)amino)ethyl nitrate (Bu-NENA) b) mixture of three dinitrodiazaalkanes (DNDA-57) c) bis-2,2-dinitropropyl acetal/ formal (BDNPA/F).

Energetic plasticizers can positively impact the combustion properties of a propellant. When formulated with RDX and NC, the mixture of 2,4-dinitro-2,4-diazapentane (DNDA-5), 2,4-dinitro-2,4-diazahexane (DNDA-6), and 3,5-dinitro-3,5-diazaheptane (DNDA-7), known as DNDA-57, enables temperature-independent combustion. This allows for more efficient use of gun chamber pressure and reduces barrel erosion.[47–49]

1.3.3 Energetic plasticizers based on azides

A relatively new and promising group are azide-based plasticizers. Due to their azide functional group, these plasticizers have a high enthalpy of formation and an exceptional high nitrogen content.[50] The molecular structures of two azide-based energetic plasticizers are shown in Figure 13. Azide terminated oligomers of GAP (GAP-A) have been successfully utilized as energetic plasticizers.

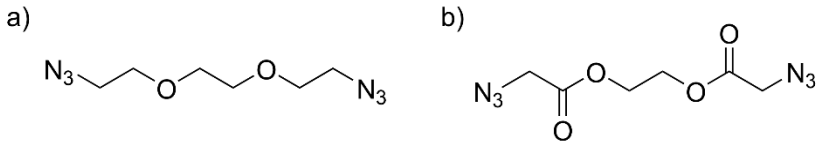

Figure 13 Molecular structures of the azide-based energetic plasticizers a) 1,2-bis(2-azidoethoxy)ethane (BATEG) and b) ethane-1,2-diyl bis(2-azidoacetate) (EGBAA).

Azide containing plasticizers are frequently used in combination with GAP. However, plasticizers containing azide may be unsuitable for HTPB and other binders with unsaturated bonds. Azides react with unsaturated alkenes via an 1,3-dipolar cycloaddition to form triazolines.[51] Triazolines of HTPB are unstable and decompose, releasing nitrogen.[52] With terminal alkynes, on the other hand, a stable crosslinking occurs via the Huisgen reaction.[53]

1.3.4 Energetic plasticizers based on heterocyclic structures

Energetic ionic liquids (EILs) derived from azoles are used as heterocyclic plasticizers. Ionic liquids have the advantage of easy synthesis, low volatility and high-temperature stability. Jafari et al. showed that incorporating EILs, particularly those with smaller or more flexible anions like dicyanamide, into GAP can significantly lower T_g by altering the polymer's density and free volume behavior.[54] Schaller et al. synthesized 4-amino-1-butyl-1,2,4-triazolium dinitramide (C4 DN) via a two-step process from commercially available materials. Figure 14 shows the molecular structure of C4 DN which exhibits desirable properties for use as a plasticizer, such as a low T_g of −74 °C.[55]

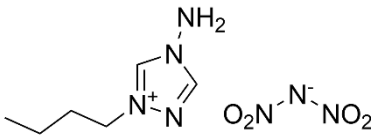

Figure 14 Molecular structure of the energetic ionic liquid 4-amino-1-butyl-1,2,4-triazolium dinitramide (C4 DN).

Although there are studies on heterocyclic plasticizers based on oxadiazole and isoxazole derivatives, these compounds do not exhibit a glass transition.[56,57] While heterocycles are common components of energetic materials, they are rarely used in plasticizers.

1.4 Plasticization

The first theories on the mechanism of plasticization were developed in the 1940s. After the early concepts of lubricity and gel theory were developed simultaneously, the free volume theory was developed in the 1950s as a more precise concept that is still widely used today to explain viscoelastic properties.

1.4.1 Lubricity theory

The lubricity theory is closely associated with the work of Kirkpatrick[58], Clark[59], and Houwink[60]. Its fundamental premise is that a plasticizer reduces the intramolecular friction between the polymer molecules. This goes hand in hand with the assumption that in a flexible polymer material, the polymer molecules must slide over each other.

The function of the plasticizer is to lubricate the movement of molecules, thereby reducing their internal resistance to sliding.

Kirkpatrick describes the molecular functions of a plasticizer as one part that attaches to the polymer and acts as a solvent and the other part that is a pendant portion and acts as a lubricant between the polymer molecules. Therefore, each plasticizer requires certain molecular properties: functional groups that attract counterparts in the polymer and plasticizer, a proper arrangement of these groups in relation to each other to allow the attractive forces to work, a suitable geometry of the entire plasticizer molecule to produce the desired effects.[58] The model was extended by Clark[59] to include the notion of intermolecular voids filled by plasticizers, resulting in a structure of parallel alternating layers of polymers lubricated by layers of plasticizers that break the intermolecular bonds between the polymer chains, as illustrated in Figure 15.

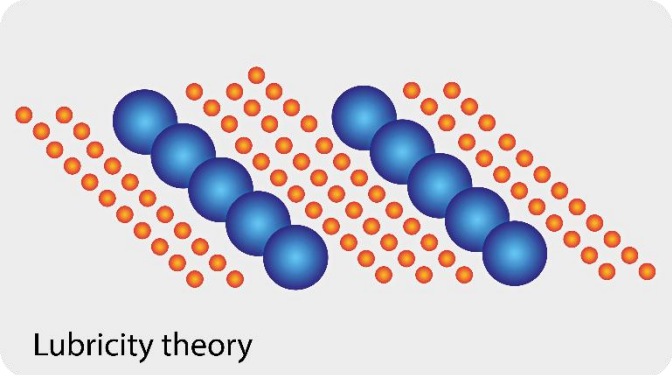

Figure 15 Schematic representation of the sliding layers of polymer (blue balls) and plasticizer (orange balls) as described in the lubricity theory.

1.4.2 Gel theory

In gel theory, polymers are formed by a three-dimensional honeycomb structure that is maintained by loose attachments between polymer molecules along their chains. Solvation-desolvation and aggregation-deagglomeration equilibria exist between the polymer and the plasticizer molecules. The stiffness of polymers is primarily attributed to the resistance of their three-dimensional structure. In the gel theory, the plasticizer reduces the number of points at which polymers attach to polymers as depicted in Figure 16, allowing the polymer material to be deformed without breaking. Despite lubricating the slip planes, the plasticizer reduces the rigidity of the polymer material by reducing the aggregation of the polymer molecules.

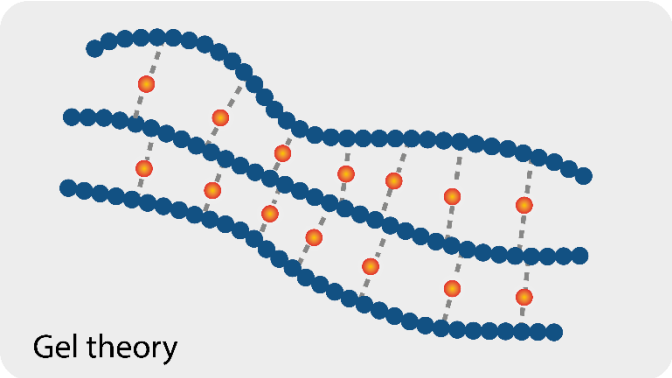

Figure 16 Schematic representation of the plasticizer molecules (orange balls) reducing the number of contact points between the polymer chains (blue balls) and thereby decreasing rigidity of the material as described in the gel theory.

1.4.3 Free volume theory

The free volume theory was postulated for the first time by Fox and Flory.[61] In the context of plasticized polymers, it attempts to explain how the glass transition temperature decreases with increasing plasticizer content. The viscosity at glass transition temperature was found to be approximately 10^{12} Pa s for all polymers, independent of their chemical structure.[61] In this way, the viscosity, the free volume between the molecules and the glass transition temperature can be set in relation to each other. At the glass transition point, all materials have the same "fractional free volume". In addition to the viscoelastic properties, a number of other properties of a polymer such as heat capacity, thermal expansion coefficient and dielectric coefficient also change at the glass transition.[62] Figure 17 illustrates how the addition of a plasticizer increases the free volume of a polymer structure by forming voluminous sections of low order.

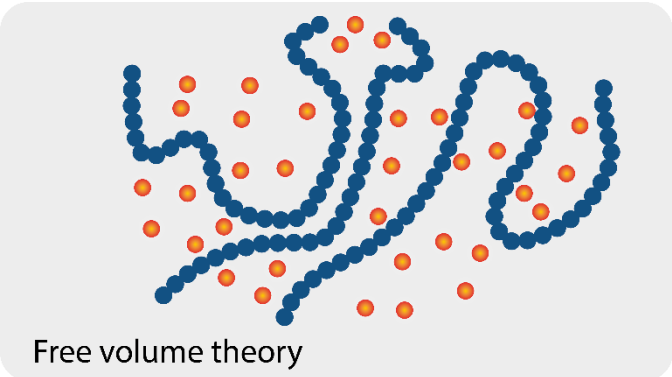

Figure 17 Schematic representation of a plasticizer (orange balls) inserting between polymer chains (blue balls), thereby increasing the polymer material's free volume.

1.5 Oxadiazoles

1.5.1 General chemistry

Oxadiazoles are five-membered heteroaromatic rings that are considered as high-energy compounds. While they formally satisfy Hückel's rule (possessing 6 π-electrons), their aromaticity is weakened due to significant electron density localization around the electronegative nitrogen and oxygen atoms. Figure 18 shows the four oxadiazole isomers.

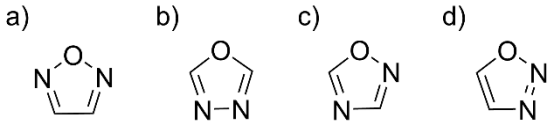

Figure 18 Molecular structure of the four oxadiazole isomers a) 1,2,5-oxadiazole (furazan) b) 1,3,4-oxadiazole c) 1,2,4-oxadiazole d) 1,2,3-oxadiazole.

Furazans were extensively studied in Russia, particularly during the Soviet era. [63] Much of this research was published in the West only later — sometimes not until after the dissolution of the Soviet Union.[64] The furazan ring is particularly attractive for energetic applications because it has the highest formation enthalpy of all oxadiazole rings.[65] It is surpassed only by its N-oxide derivative, furoxan.[66] On the other hand, 1,2,3-oxadiazole compounds are not suitable as starting materials for synthesizing energetic materials because they tend to form the unstable diazoketone tautomer.[67] Compared to other five-membered heterocycles like triazoles, oxadiazoles have a better oxygen balance and lower enthalpy of formation. One exception is furoxan, an extremely energy-rich compound whose derivatives are often very mechanically sensitive.[63]

1.5.2 3,4-Dinitrofurazan

3,4-Dinitrofurazan (DNF) is a highly energetic liquid and a rare organic oxidizer. It has an oxygen balance of 10.00%, which is superior to the 3.52% oxygen balance of nitroglycerin. It was first synthesized in 1978 at the Zelinsky Institute of Organic Chemistry in Moscow. However, this work was not published until 1993.[64] The original synthesis was carried out from 3,4-diaminofurazan (DAF), which can be synthesized in two steps from glyoxime and hydroxylamine, as shown in Scheme 1.[68,69] Today, DAF can be purchased commercially in kilogram quantities.

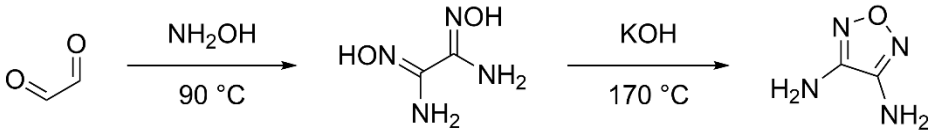

Scheme 1 Synthesis of 3,4-diaminofurazan from glyoxime as reported by A. K. Zelenin et al.

The synthesis of DNF involves the oxidation of both amines to nitro groups. Due to the deactivating effect of the electron-deficient ring, DAF is a weak nucleophile, necessitating harsh reaction conditions. A high yield of 94% is reported by the original synthesis, which uses an oxidizing mixture of 93% hydrogen peroxide, 98% sulfuric acid, and sodium tungstate.[70] The original synthesis by Novikova et al. is shown in Scheme **2**.

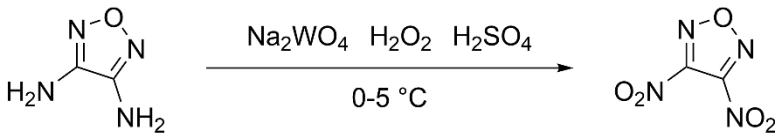

Scheme 2 Synthesis of 3,4-dinitrofurazan (DNF) from 3,4-diaminofurazan as reported by T. S. Novikova et al.[70]

Ren et al. reported the synthesis of DNF with a 58% yield using 50% hydrogen peroxide in an ionic liquid.[71] A. B. Sheremetev et al. demonstrated the nucleophilic substitution of one or both nitro groups when synthesizing a variety of nitrofurazanyl ethers from DNF using N- and O-nucleophiles.[72,73] The synthetic work in this doctoral thesis is thus based in particular on the pioneering work of M. D. Coburn, A. K. Zelenin, T. S. Novikova and A. B. Sheremetev.

1.6 References

[1] R. Meyer, J. Köhler, A. Homburg, *Explosives*, Wiley-VCH, s.l., **2016**.
[2 T. M. Klapötke, *Chemistry of high-energy materials*, De Gruyter, Berlin, Boston, **2022**.
[3] E.-C. Koch, *High Explosives, Propellants, Pyrotechnics*, Walter de Gruyter GmbH, Berlin/Boston, **2021**.
[4] M. Gozin, L. L. Fershtat, *Nitrogen-Rich Energetic Materials*, Wiley-VCH GmbH, Weinheim, **2022**.
[5] J. Akhavan, *The chemistry of explosives*, Royal Society of Chemistry, London, **2022**.
[6] J. P. Agrawal, *High energy materials. Propellants, explosives and pyrotechnics*, Wiley-VCH, Weinheim, **2010**.
[7] A. Ulas, G. A. Risha, K. K. Kuo, *Propellants, Explos., Pyrotech.* **2006**, *31*, 311.
[8] G. Steinhauser, T. M. Klapötke, *Angew. Chem., Int. Ed. Engl.* **2008**, *47*, 3330.
[9] Y. Verbovytskyy, D. Juknelevicius, *Propellants, Explos., Pyrotech.* **2023**, *48*.
[10] K. Engelen, M. H. Lefebvre, A. Hubin, *Propellants, Explos., Pyrotech.* **2002**, *27*, 290.

[11] E.-C. Koch, S. Cudziło, *Angew. Chem., Int. Ed. Engl.* **2016**, *55*, 15439.
[12] G. P. Sutton, O. Biblarz, *Rocket Propulsion Elements*, John Wiley & Sons, **2011**.
[13] A. de Iaco Veris, *Fundamental Concepts of Liquid-Propellant Rocket Engines*, Springer International Publishing; Imprint Springer, Cham, **2021**.
[14] A. Davenas, *J. Propul. Power* **2003**, *19*, 1108.
[15] E. B. Smirnov, A. N. Averin, B. G. Loboiko, O. V. Kostitsyn, Y. A. Belenovskii, K. M. Prosvirnin, A. N. Kiselev, *Combust Explos Shock Waves* **2012**, *48*, 309.
[16] X.-G. Dai, Y.-S. Wen, F.-L. Huang, H. Huang, Y.-M. Huang, *Propellants, Explos., Pyrotech.* **2014**, *39*, 563.
[17] M. H. Keshavarz, H. R. Pouretedal, *Propellants, Explos., Pyrotech.* **2005**, *30*, 105.
[18] R. Matyáš, S. Zeman, W. Trzciński, S. Cudziło, *Propellants, Explos., Pyrotech.* **2008**, *33*, 296.
[19] D. A. Reese, L. J. Groven, S. F. Son, *Propellants, Explos., Pyrotech.* **2014**, *39*, 205.
[20] F. Volk, M. A. Bohn, G. Wunsch, *Propellants, Explos., Pyrotech.* **1987**, *12*, 81.
[21] X. Zou, W. Zhang, Z. Zhang, Y. Gu, X. Fu, Z. Ge, Y. Luo, *Propellants, Explos., Pyrotech.* **2021**, *46*, 1662.
[22] H. G. Ang, S. Pisharath, *Energetic polymers. Binders and plasticizers for enhancing performance*, Wiley-VCH-Verl., Weinheim, **2012**.
[23] T. B. Brill, P. E. Gongwer, *Propellants, Explos., Pyrotech.* **1997**, *22*, 38.
[24] S. K. Boopathi, N. Hadjichristidis, Y. Gnanou, X. Feng, *Nat. Commun.* **2019**, *10*, 293.
[25] B. Gaur, B. Lochab, V. Choudhary, I. K. Varma, *J. Therm. Anal. Calorim.* **2003**, *71*, 467.
[26] S. Pisharath, H. G. Ang, *Polym. Degrad. Stab.* **2007**, *92*, 1365.
[27] C. Mura, S. Fruci, P. Lamia, M. Cappello, S. Filippi, G. Polacco, *J. Energ. Mater.* **2016**, *34*, 216.
[28] B. S. Min, Y. C. Park, J. C. Yoo, *Propellants, Explos., Pyrotech.* **2012**, *37*, 59.
[29] I. K. Varma, *Macromol. Symp.* **2004**, *210*, 121.
[30] Leeming W. B. H., Marshall E. J., Bull H., et al., *Proceedings Of The 27th international annual conference of ICT* **1996**.
[31] M. E. Colclough, N. C. Paul in *ACS symposium series, Vol. 623* (Ed.: L. F. Albright), American Chemical Society, Washington, DC, **1996**, pp. 97–103.
[32] C. Shekhar Pant, M. S. S. N. M. Santosh, S. Banerjee, P. K. Khanna, *Propellants, Explos., Pyrotech.* **2013**, *38*, 748.
[33] G. Wypych, *Handbook of plasticizers*, ChemTec Publishing, Toronto, **2023**.
[34] J. Kubát, L.-Å. Nilsson, M. Rigdahl, *Mater. Sci. Eng.* **1982**, *53*, 199.
[35] M. Manikkam, R. Tracey, C. Guerrero-Bosagna, M. K. Skinner, *PloS one* **2013**, *8*, e55387.
[36] R. Nagorka, J. Koschorreck, *Environ. Pollut.* **2020**, *262*, 114237.
[37] M. A. Ivy, L. T. Gallagher, A. D. Ellington, E. V. Anslyn, *Chem. Sci.* **2012**, *3*, 1773.
[38] J. A. F. F. Rocco, J. E. S. Lima, A. G. Frutuoso, K. Iha, M. Ionashiro, J. R. Matos, M. E. V. Suárez-Iha, *J. Therm. Anal. Calorim.* **2004**, *77*, 803.
[39] S. Singh, S. Raveendran, D. R. Kshirsagar, Somraj, A. Kumar, C. J. Bhongale, M. Gupta, *Propellants, Explos., Pyrotech.* **2022**, *47*.
[40] S. Ek, J. Johansson, M. Brantlind, H. Ellis, M. Skarstind in *Proceedings of the 22nd Seminar on New Trends in Research of Energetic Materials (NTREM)*, **2019**, pp. 81–87.
[41] F. Jin, Y. Wu, H. Wu, J. Yang, H. Li, X. Liu, X. Hou, *Propellants, Explos., Pyrotech.* **2024**, *49*.
[42] Y. Sun, S. Ni, X.-M. Pan, *J. Mol. Model.* **2019**, *25*, 346.
[43] H. Boukeciat, A. F. Tarchoun, D. Trache, A. Abdelaziz, R. Ahmed Hamada, A. Bouhantala, C. Bousstila, S. Hanafi, M. Dourari, T. M. Klapötke, *Materials* **2022**, *15*.
[44] X. Qi, H. Li, Y. Zhao, N. Yan, *J. Hazard. Mater.* **2019**, *362*, 303.
[45] Z. Yuan, S.-L. Yang, F. Zhao, L. Liu, M. Zhang, Y. Wang, W. Zheng, J. Pei, S. Hu, *Langmuir* **2024**, *40*, 27228.

[46] A. Edgar, J. Yang, M. Chavez, M. Yang, D. Yang, *J. Energ. Mater.* **2020**, *38*, 483.
[47] R. Vijayalakshmi, N. H. Naik, G. M. Gore, A. K. Sikder, *J. Energ. Mater.* **2015**, *33*, 1.
[48] D. Mueller, W. Langlotz in *Procced of the 36th international annual conference of the ICT*, **2005**.
[49] D. Mueller, W. Langlotz in *21st International Symposium on Ballistics,* Adelaide, Australia, **2004**.
[50] D. B. Vinogradov, P. V. Bulatov, E. Yu. Petrov, V. A. Tartakovsky, *Mendeleev Commun.* **2022**, *32*, 720.
[51] K. B. Mishra, *Org. Biomol. Chem.* **2025**, *23*, 5483.
[52] M. F. Lemos, L. C. Mendes, M. A. Bohn, *J. Appl. Polym. Sci.* **2021**, *138*.
[53] S. Reshmi, K. P. Vijayalakshmi, D. Thomas, R. Rajeev, C. P. Reghunadhan Nair, *Combust. Flame* **2016**, *167*, 380.
[54] N. Jafari, B. Arab, N. Zekri, R. Fareghi-Alamdari, *Propellants, Explos., Pyrotech.* **2020**, *45*, 615.
[55] U. Schaller, J. Lang, V. Gettwert, J. Hürttlen, V. Weiser, T. Keicher, *Propellants, Explos., Pyrotech.* **2022**, *47*.
[56] G. E. Cabrera, T. A. Reid, E. C. Johnson, J. A. Orlicki, N. Z. Burns, J. J. Sabatini, *ChemPlusChem* **2022**, *87*, e202200096.
[57] Q. Xue, F. Bi, J. Zhang, J. Zhang, B. Wang, M. Wu, *FirePhysChem* **2023**, *3*, 16.
[58] A. Kirkpatrick, *J. Appl. Phys.* **1940**, *11*, 255.
[59] F. W. Clark, *Chem. Ind.* **1941**, *60*, 225.
[60] R. Houwink, *Proc. XI Cong. Pure Appl. Chem.* **1947**, 575.
[61] T. G. Fox, P. J. Flory, *J. Appl. Phys.* **1950**, *21*, 581.
[62] Y. Zhang, X. Geng in *Processing and development of polysaccharide-based biopolymers for packaging* (Ed.: Y. Zhang), Elsevier, Amsterdam, **2020**, pp. 1–19.
[63] A. B. Sheremetev, N. N. Makhova, W. Friedrichsen, *Adv. Heterocycl. Chem.* **2001**, *78*, 65.
[64] K. Y. Suponitsky, A. F. Smol'yakov, I. V. Ananyev, A. V. Khakhalev, A. A. Gidaspov, A. B. Sheremetev, *ChemistrySelect* **2020**, *5*, 14543.
[65] L. L. Fershtat, I. V. Ovchinnikov, M. A. Epishina, A. A. Romanova, D. B. Lempert, N. V. Muravyev, N. N. Makhova, *ChemPlusChem* **2017**, *82*, 1309.
[66] M. Gozin (Ed.) *Nitrogen-Rich Energetic Materials*, John Wiley & Sons Incorporated, Newark, **2023**.
[67] M. T. Nguyen, A. F. Hegarty, J. Elguero, *Angew. Chem., Int. Ed. Engl.* **1985**, *24*, 713.
[68] A. K. Zelenin, M. L. Trudell, *J. Heterocycl. Chem.* **1997**, *34*, 1057.
[69] M. D. Coburn, *J. Heterocycl. Chem.* **1968**, *5*, 83.
[70] T. S. Novikova, T. M. Mel'nikova, O. V. Kharitonova, V. O. Kulagina, N. S. Aleksandrova, A. B. Sheremetev, T. S. Pivina, L. I. Khmel'nitskii, S. S. Novikov, *Mendeleev Commun.* **1994**, *4*, 138.
[71] H.-P. Ren, Z.-W. Liu, J. Lu, Z.-T. Liu, *Ind. Eng. Chem. Res.* **2011**, *50*, 6615.
[72] A. B. Sheremetev, O. V. Kharitonova, E. V. Mantseva, V. O. Kulagina, E. V. Shatunova, N. S. Aleksandrova, T. M. Mel'nikova, E. A. Ivanova, D. E. Dmitriev, V. Eman et al., *Russ. J. Org. Chem.* **1999**, *35*, 1525.
[73] A. B. Sheremetev, V. O. Kulagina, I. A. Kryazhevskikh, T. M. Melnikova, N. S. Aleksandrova, *Russ. Chem. Bull.* **2002**, *51*, 1533.

2 Concept and objectives

Although plasticizers constitute only a small fraction of modern polymer-based formulations compared to fillers and binders, they play a crucial role in tailoring mechanical properties and combustion characteristics. Due to their low required quantities, plasticizers also facilitate a rapid transition from synthesis to application-oriented research.

In particular, energetic binders such as glycidyl azide polymer (GAP), which is being extensively studied at Fraunhofer ICT, require plasticizers that are specifically designed to meet their performance demands. However, the energetic plasticizers currently available suffer from limitations such as insufficient energy content, inadequate plasticizing effect, or high volatility.

Therefore, the primary objective of this dissertation is the development of novel energetic plasticizers and the evaluation of their physical and energetic properties. These new compounds are also assessed for their compatibility with GAP-based systems. In order to achieve thermal and energetic performance superior to existing materials, a novel molecular design approach was adopted based on the incorporation of the nitrofurazanyl heterocycle.

The research strategy comprises the following key steps:

1. Development and implementation of a continuous synthesis process for DNF to ensure sufficient availability of this critical starting material.
2. Screening of side chains to investigate their influence on the thermal and energetic properties of nitrofurazanyl ethers.
3. Compatibility studies with GAP-based formulations, including analysis of interactions with formulation components and evaluation of mechanical and thermal behavior.
4. Manufacturing and performance testing of a complete energetic formulation and comparison with reference formulations containing energetic plasticizers in use.

The overarching goal of this work is to develop a new energetic plasticizer for GAP-based formulations that significantly lowers the T_g, enhances mechanical flexibility at room temperature, and increases the overall energy content, while maintaining thermal and long-term stability comparable to or better than existing systems.

3 Synthesis and characterization of novel nitrofurazanyl ethers as potential energetic plasticizers

Patrick Lieber*, Uwe Schaller, Thomas M. Klapötke

as published in: *RSC Advances* **2025**, 15, 12577–12584

DOI: 10.1039/D5RA01282A

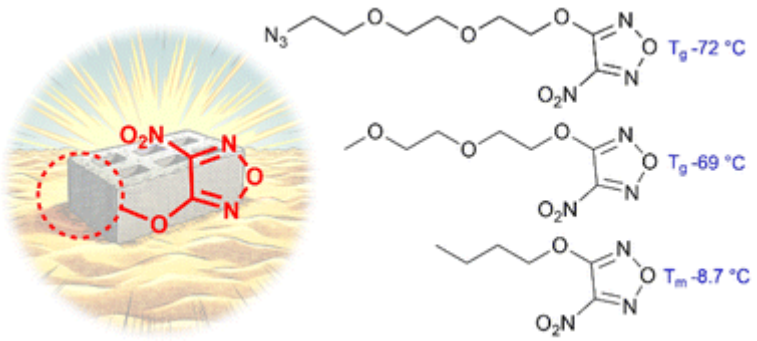

3.1 Abstract

Energetic plasticizers are used to improve the mechanical properties of advanced energetic formulations while increasing the overall energy content. Although nitro-1,2,5-oxadiazoles (nitrofurazans) possess excellent energetic properties such as a favorable oxygen balance and high heat of formation, their use as plasticizers has received little attention in the scientific literature. Four nitrofurazanyl ethers were synthesized by substitution of dinitrofurazan with linear alkoxides. The synthesized compounds were extensively analyzed by Fourier-transform infrared (FT-IR) spectroscopy, Raman spectroscopy, differential scanning calorimetry (DSC), thermogravimetric analysis (TGA), electrospray ionization (ESI) mass spectroscopy, mechanical sensitivity test, ^{1}H nuclear magnetic resonance (NMR) spectroscopy and ^{13}C NMR spectroscopy. They have lower mechanical sensitivity (> 40 J) compared to modern energetic plasticizers in use, including 2,2-dinitropropyl formal/acetal (BDNPA/F), n-butylnitratoethylnitramine (BuNENA), and dinitrodiazaalkanes (DNDA-57). In addition, the most promising compound 3-(2-(2-(2-azidoethoxy)ethoxy)ethoxy)-4-nitro-1,2,5-oxadiazole (NFPEG3N3)

exhibits competitive thermal properties, with a lower glass transition temperature of -72 °C compared to BDNPA/F (-67 °C) and a higher thermal decomposition temperature of 179 °C compared to BuNENA (173 °C). The enthalpy of formation and heat of explosion of NFPEG3N3 were calculated to be -41.7 kJ mol^{-1} and 3421 J g^{-1}, respectively. The impact of NFPEG3N3 on the glass transition temperature, viscosity and decomposition of the energetic binder glycidyl azide polymer (GAP)-diol was investigated and showed a remarkable decrease in viscosity (45.4%) and glass transition temperature (-3.3 °C) when compared to benchmark plasticizers in 10wt% mixtures. These results demonstrate the potential of NFPEG3N3 as an insensitive and highly energetic plasticizer.

3.2 Introduction

Energetic plasticizers are critical to the development of advanced solid propellants and polymer-bonded explosives.[1–4] Typically, these plasticizers are high-boiling organic liquids that improve the mechanical properties and lower the glass transition temperature of binders. They also help reduce the viscosity during processing and can modify the burn rate of energetic formulations. Unlike inert plasticizers, energetic plasticizers contain energetic groups such as nitro, nitrate ester, nitramino, and azido, which increase the overall energy of the formulation. Depending on the application, the ideal properties for energetic plasticizers can vary and sometimes be contradictory. In general, they should have high heat of formation, high oxygen balance, low glass transition temperature, low migration tendency, low viscosity, high thermal stability and low mechanical sensitivity.[5] Investigation of the glass transition temperature depression, viscosity reduction and decomposition temperature shift of a liquid plasticizer-binder mixture compared to pure binder samples provides initial insight into the suitability of a new compound.[6] Known energetic plasticizers such as 2,2-dinitropropyl formal/acetal[7,8] (BDNPA/F), n-butylnitratoethylnitramine[9] (BuNENA) and dinitrodiazaalkanes[10] (DNDA-57) primarily consist of a saturated, linear carbon backbone, augmented by heteroatoms, most of which form energetic side groups (Figure 1). Studies on heterocycle-based energetic plasticizers remain limited in the

literature although heterocyclic building blocks are energy-rich and have been extensively studied for secondary and primary explosives.[11–13]

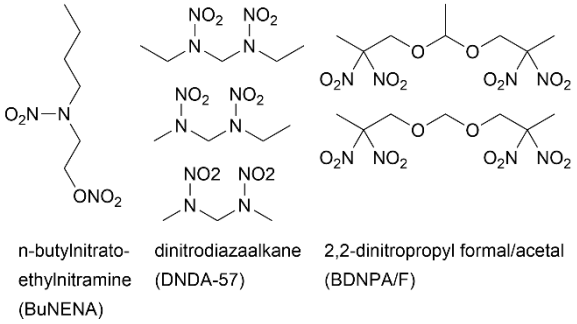

Figure 1 Examples for energetic plasticizers in use.

In particular, oxadiazoles may be advantageous for plasticizers due to their higher oxygen content compared to triazoles or tetrazoles. Among the oxadiazole isomers, the 1,2,5-oxadiazole (furazan) ring has the highest heat of formation at 216 kJ mol^{-1}.[15–17] Notably, 3,4-dinitrofurazan (DNF) is a liquid at room temperature, with a melting point of -15 °C.[18–20] Although its synthesis is challenging, we have recently improved its safety by using a flow process.[21] Derivatization of DNF via nucleophilic substitution is a straightforward reaction, as demonstrated by Sheremetev et al.[22,23] In this work we present novel energetic plasticizers that exploit the outstanding energetic properties of the nitrofurazan structure.

3.3 Results and discussion

3.3.1 Synthesis

The starting material chosen for the synthesis was 3,4-diaminofurazan (DAF). Products were obtained by two-step syntheses (Scheme 1). First, DNF was obtained by complete amine oxidation of DAF with a mixture of hydrogen peroxide, sulfuric acid and sodium tungstate at 60 °C according to the flow chemistry procedure we reported.[21] DNF is a sensitive primary explosive. However, in the context of the synthesis shown here, it can be safely handled and stored diluted in anhydrous dichloromethane solution. Side chains were introduced by nucleophilic substitution with sodium and lithium alkoxides, eliminating a nitro group as the corresponding nitrite. NFOEt was prepared based on literature methods.[22] The purity of the longer-chain compounds NFPEG2Me and

NFPEG3N3 was verified using HPLC (S6). Non-commercially available alkoxides were synthesized by deprotonation of the alcohols with n-butyllithium in tetrahydrofuran. The deprotonation of the alcohols and the substitution reaction were performed at -94 °C. The prepared alkoxides were then used in the substitution reaction without further purification.

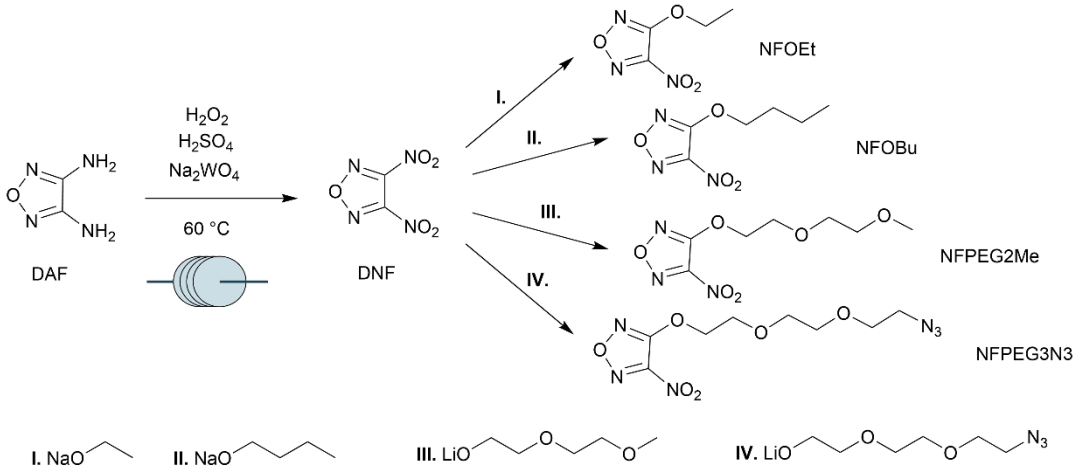

Scheme 1 Synthesis of nitrofurazanyl ethers starting from DAF.

3.3.2 Physicochemical properties

An overview of the properties of the synthesized nitrofurazanyl ethers is given in Table 1, in comparison to conventional energetic plasticizers. The heat of explosion and gas volume generated were determined using the ICT Thermodynamic Code.[24]

Table 1 Comparison of conventional energetic plasticizers in use to synthesized nitrofurazanyl ethers.

Compound	T_g[a] [°C]	T_m[b] [°C]	T_{TGA}[c] [°C]	T_{dec}[d] [°C]	IS[e] [J]	ϱ[f] [g cm^{-3}]	Q_x[g] [J g^{-1}]	OB_{CO2}[h] [%]	N[i] [%]	V_x[j] [cm^3 g^{-1}]
BDNPA/F[k]	-67		182	207	3	1.39	3469	-57.6	17.6	957
DNDA-57[k]	-52		159	221	3	1.35	3848	-72.3	30.9	1078
BuNENA[k]	-82		152	173	6	1.22	3573	-104.3	17.4	1045
NFOEt		8.7	65	233	> 40	1.33	3976	-65.4	26.4	928
NFOBu		-6.2	88	191	> 40	1.21	3379	-106.9	22.5	940
NFPEG2Me	-69		135	156	> 40	1.30	3004	-92.6	18.2	956
NFPEG3N3	-72		167	179	> 40	1.34	3421	-88.8	29.2	948

[a] Glass transition temperature measured by DSC. [b] Melting point measured by DSC. [c] Temperature at maximum mass loss rate measured by TGA. [d] Thermal decomposition temperature (onset) measured by DSC in pressure-tight crucibles. [e] Impact sensitivity measured by BAM drop hammer. [f] Density. [g] Heat of explosion calculated by ICT-Thermodynamic Code (water liquid). [h] Oxygen balance calculated on CO_2. [i] Nitrogen content. [j] Gas volume calculated by ICT-Thermodynamic code without H_2O at 25 °C. [k] physical properties of conventional energetic plasticizers partially from Schaller et al.[14]

The compounds show a heat of explosion ranging from 3004 J g^{-1} to 3976 J g^{-1} and a generated gas volume ranging from 928 cm^3 g^{-1} to 956 cm^3 g^{-1}, which are similar to energetic plasticizers in use. However, significant differences are observed for the glass transition temperature. The glass transition temperature of the ethylene glycol type side chain-containing ethers NFPEG2Me and NFPEG3N3 are -69 °C and -72 °C, respectively (Figure 2a).

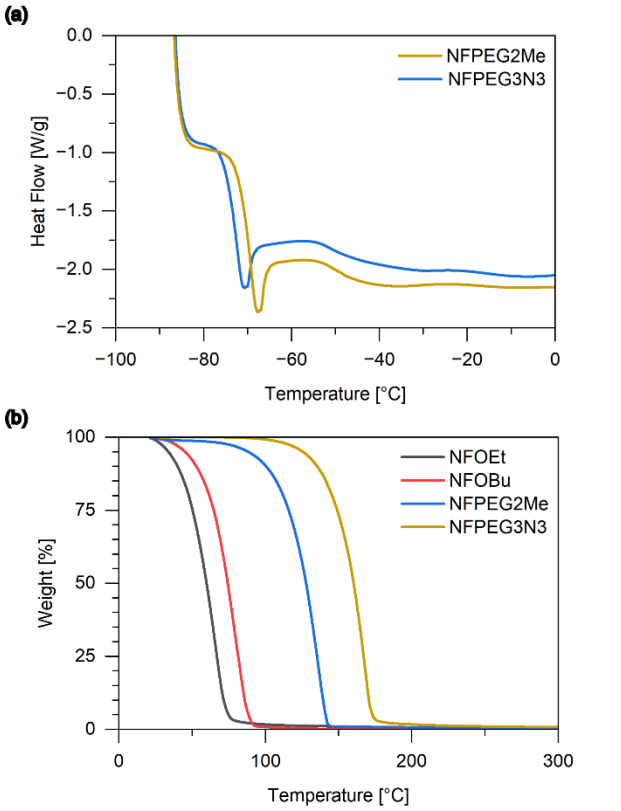

Figure 2 (a) Glass transition temperature curves obtained by DSC (b) Thermal mass loss curves obtained by TGA.

These are slightly higher than the glass transition temperature of BuNENA (-82 °C), but lower than that of BDNPA/F (-67 °C). In contrast, NFOEt and NFOBu do not exhibit a glass transition, but rather melting points at 8.66 °C and -6.19 °C, respectively. The thermal stability of the compounds was analyzed by DSC in pressure-tight stainless steel crucibles and TGA under nitrogen flow. The alkyl ethers showed significantly higher thermal stability than the ethylene glycol ethers in DSC but evaporated at lower temperatures as shown in the TGA (Figure 2b). The exothermic onsets for NFPEG2Me and NFPEG3N3 in DSC were found to be 156 °C and 179 °C, respectively. The complex

DSC curves suggest a multi-stage decomposition processes (S4). Until now we have no information about the exact mechanism of the decomposition of these substances. Compared to the reference plasticizers, NFPEG2Me shows a lower thermal stability while NFPEG3N3 outperforms BuNENA. These properties suggest that, depending on the side chain, the new materials could potentially be used as plasticizers in energetic formulations such as solid rocket propellants. They could also potentially be used as high-explosive plasticizers or in modern gun propellant formulations. The ethylene glycol type ethers have an oxygen balance slightly higher than BuNENA and NFPEG3N3 has a high nitrogen content of 29.2%, comparable to DNDA-57. In general, a compound with a higher oxygen balance tends to be more explosive, powerful, or sensitive.[25] The densities of the synthesized compounds are between 1.30 g cm^{-3} and 1.34 g cm^{-3}, except for NFOBu which has a much lower density of 1.21 g cm^{-3}. NFPEG3N3 has a density similar to that of GAP diol (1.34 g cm^{-3}) which ensures a good miscibility. The impact sensitivity was determined by using standard BAM techniques.[26] All nitrofurazanyl ethers have been found to be non-impact sensitive within UN regulations (> 40 J). As a result, they exhibit superior sensitivity compared to conventional energetic plasticizers. NFPEG3N3 has a low viscosity of 32 mPa·s at 20 °C, ensuring adequate processability over a wide temperature range.

3.3.3 Infrared spectroscopy

The infrared spectra of the nitrofurazanyl ethers and DNF were analyzed, and specific group frequencies were identified (Figure 3).[27] While the 1,2,5-oxadiazole ring vibration is found at 1570 cm^{-1} for DNF, it shifts to 1560 cm^{-1} for the ethers. The asymmetric stretching of the nitro group also shifts from 1538 cm^{-1} to 1548-1544 cm^{-1}. In contrast the symmetric stretching of NO_2 shows no shift and is found at 1350 cm^{-1} for all compounds. Specific frequencies for an allylic ether occur at 1203 cm^{-1} and 828 cm^{-1} indicating the replacement of a nitro group by the alkoxy substituents. The characteristic N=N stretching of the azide group is found for NFPEG3N3 at 2106 cm^{-1}. The analysis shows that the IR spectroscopy allows rapid identification and reaction control in this case.

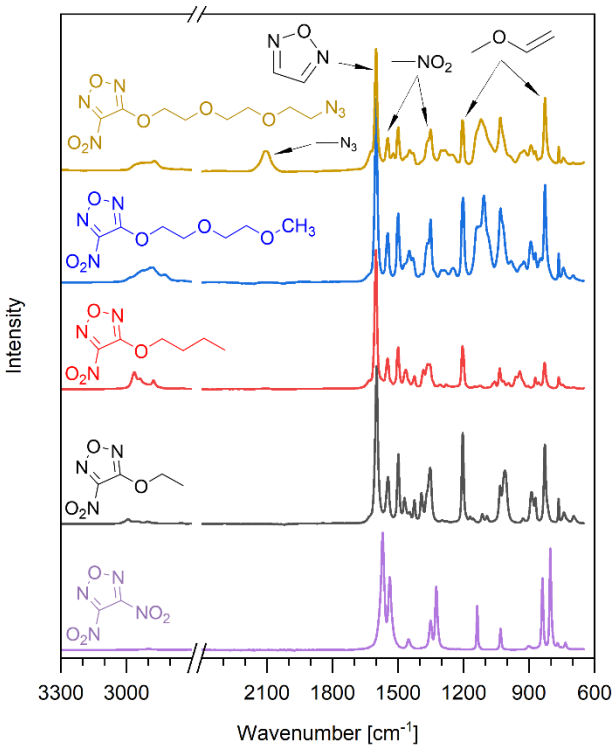

Figure 3 Infrared spectra of synthesized nitrofurazanyl ethers and 3,4-dinitrofurazan.

3.3.4 Calculation of the formation enthalpy

The standard enthalpy of formation of the synthesized nitrofurazanyl ethers in liquid-state was calculated from the gas-phase enthalpy of formation and the vaporization enthalpy using density functional theory calculations within the Gaussian 16 software package.[28] The vaporization enthalpies were estimated using the semi-empirical methods of Politzer[29], Rice[30] and improved Rice[31] (Table 2). In our experience, for molecules without any enthalpy data in literature, an average of all three methods gives the best results as it provides the broadest empirical base. The methods are based on geometry optimizations and calculations of the ground state energy with the DFT functional/basis set combinations B3PW91/6-31G** and B3LYP/6-31G*. The improved method of Rice utilizes B3LYP/6-311++G(2df,2p) for calculation of the electronic energy of the ground state. The functional/basis set combinations B3PW91/aug-cc-pVTZ and B3LYP/aug-cc-pVTZ were also used to find and validate the energetic ground state. Since the accuracy of the DFT methods is not sufficient for the calculations of the gas phase enthalpy of formation with the atomization method, geometry optimizations and ground state energy calculations were performed with the so-called composite methods CBS-QB332,33, G434,35 and G4MP235 (Table 3, Figure 4). Finally, the standard enthalpy

of formation of the liquid phase was determined by combining results of the precise G4 calculations and average value of the three semi-empirical values for the vaporization enthalpy (Table 4). The standard enthalpy of formation of the liquid state for NFOEt, NFOBu, NFPEG2Me, and NFPEG3N3 were found to be -13.8 kJ mol^{-1}, -72.7 kJ mol^{-1}, -339.5 kJ mol^{-1}, and -41.7 kJ mol^{-1}, respectively.

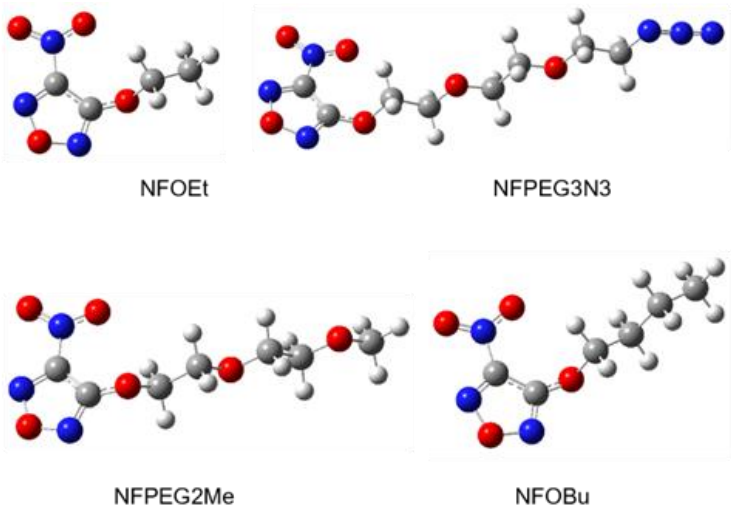

Figure 4 Molecular structures of the synthesized nitrofurazanyl ethers geometry optimized using the G4 composite method.

Table 2 Vaporization enthalpies calculated by the methods of Rice and Politzer.

$\Delta H^{\emptyset}_{vap.}$ [kJ/mol]	Politzer	Rice	Rice II	Average
NFOEt	53.5	58.5	62.6	58.2
NFOBu	60.8	68.7	74.9	68.1
NFPEG2Me	69.7	80.5	88.4	79.6
NFPEG3N3	78.6	92.5	103.1	91.4

Table 3 Gas-phase heat of formation calculated by composite methods.

$\Delta_f H^{\emptyset}_m$ [kJ/mol]	CBS-QB3	G4	G4MP2
NFOEt	29.2	44.4	56.7
NFOBu	-17.7	-4.5	7.7
NFPEG2Me	-285.2	-260.0	-244.0
NFPEG3N3	26.8	49.7	70.0

Table 4 Standard heat of formation in the liquid phase.

	$\Delta_f H^{\emptyset}_m(l)$ [kJ/mol]	$\Delta_f H^{\emptyset}_m(l)$ [kcal/mol]
NFOEt	-13.8	-3.31
NFOBu	-72.7	-17.36
NFPEG2Me	-339.5	-81.14
NFPEG3N3	-41.7	-9.98

3.3.5 Impact of NFPEG3N3 in mixtures with GAP diol

In addition to the mechanical properties of the cured formulation, plasticizers are also critical to the processability of the uncured formulation. Therefore, we studied the viscosity change of mixtures of GAP diol and NFPEG3N3 with ratios from pure GAP diol to 40wt% at 10 °C to 100 °C (Figure 5a). Newtonian behavior was observed for all measured compounds and mixtures. With increasing plasticizer concentration, the viscosity decreases at all measured temperatures, but each increase in plasticizer concentration has a smaller effect than the previous one. In direct comparison with other plasticizers at 10wt% NFPEG3N3 shows a superior viscosity reduction of GAP diol from 4560 mPa·s to 2490 mPa·s at 20 °C. This result is slightly better than BuNENA, which reduced the viscosity of GAP diol to 2560 mPa·s in our measurement (Figure 5b).

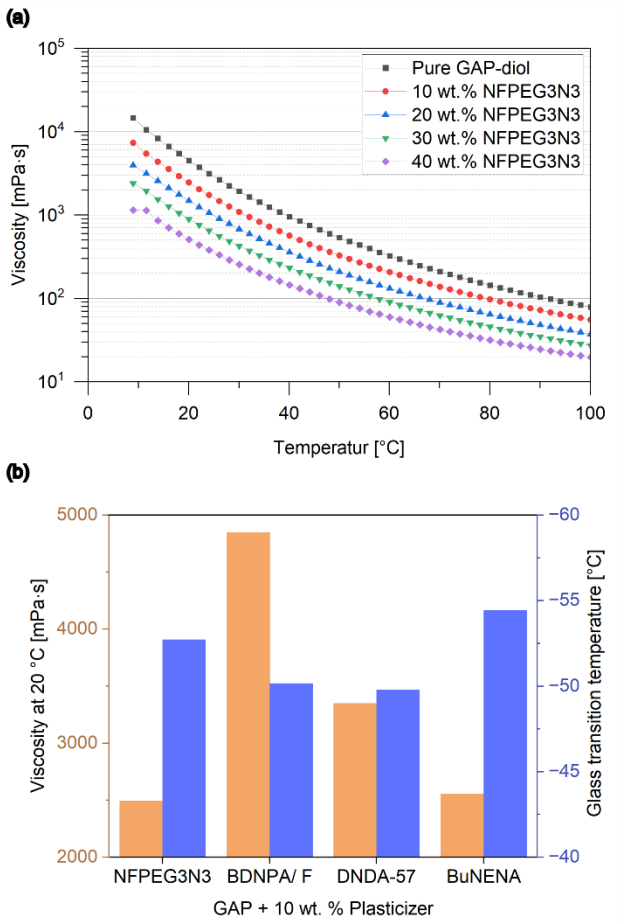

Figure 5 (a) Logarithmic representation of temperature and NFPEG3N3 concentration impact on the viscosity of GAP diol. (b) Viscosity and glass transition temperature of GAP diol with 10wt% of NFPEG3N3 and selected plasticizers in use.

NFPEG3N3 also shows a competitive lowering of the glass transition temperature from -49.4 °C to -52.7 °C. At concentrations up to 40wt% a linear decrease of the glass transition temperature compared to pure GAP diol was observed (Figure 6a). First results on the compatibility of GAP and NFPEG3N3 could be received by TGA measurements of mixtures and pure substances (Figure 6b). Two separate decomposition peaks were found for all investigated mixtures. The first decomposition event can be attributed to NFPEG3N3 which shows a mass loss in TGA at 167 °C as a pure substance and in a 10wt% mixture in GAP diol. The second decomposition event could be attributed to the GAP diol and took place constantly at 231 °C without any influence of the presence or content of NFPEG3N3.

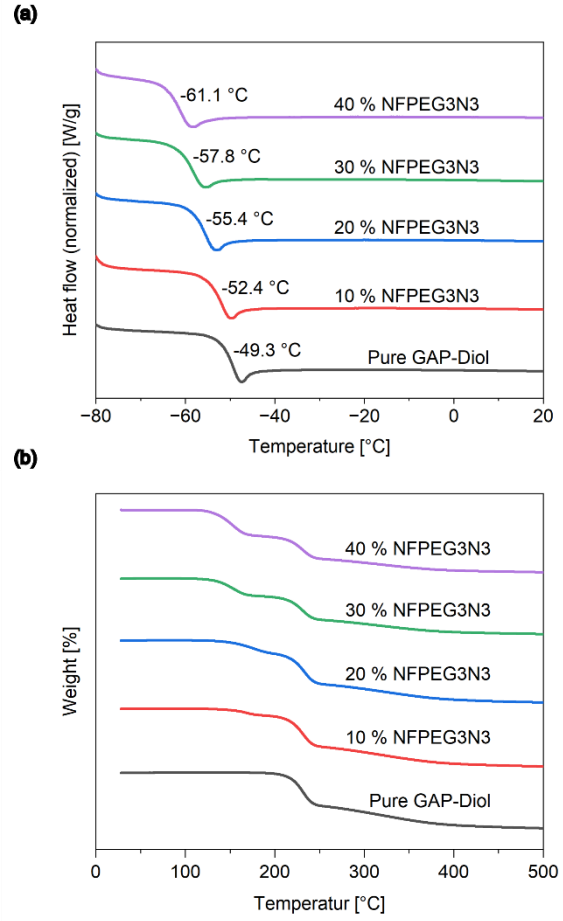

Figure 6 (a) Glass transition temperatures of pure GAP diol and mixtures with NFPEG3N3 obtained by DSC. (b) TGA curves of pure GAP diol and mixtures with NFPEG3N3.

3.4 Conclusion

In this study, three new nitrofurazanyl ethers were synthesized in high yields. Theoretical calculations show that nitrofurazanyl ethers with ethylene glycol-type side chains have promising energetic properties, including high heat of explosion and large generated gas volume. All synthesized ethers were found to be non-impact sensitive within UN regulations.[26] Among the synthesized compounds, NFPEG3N3 emerged as the most promising candidate for use as an energetic plasticizer. Remarkably, NFPEG3N3 outshines BuNENA with its superior oxygen balance, nitrogen content and decomposition temperature, while maintaining a low glass transition temperature of -72 °C and viscosity of 32 mPa·s at 20 °C. In addition, NFPEG3N3 demonstrated a significant ability to reduce viscosity and glass transition temperature when formulated with GAP diol. NFPEG3N3 does not adversely affect the decomposition temperature of GAP diol, even at concentrations up to 40wt%. These results demonstrate for the first time the potential of nitrofurazanyl ethylene glycol ethers as advanced energetic plasticizers.

3.5 Experimental

3.5.1 Materials and instruments

BuNENA and BDNPA/F were purchased from Chemring. DNDA-57 was obtained from N. D. Zelinsky Institute of Organic Chemistry (Moscow, Russia). DAF was purchased from Chemicalpoint (Deisenhofen, Germany). 2-(2-(2-Azidoethoxy)ethoxy)ethan-1-ol (PEG3N3) was purchased from Abcr (Karlsruhe, Germany). GAP diol charge 03S19 (MW 1814 g mol^{-1}, EQ 1228 g mol^{-1}, functionality 1.5) was supplied from Eurenco. Other chemicals were purchased from Sigma Aldrich, Merck, or Carl Roth. Unless otherwise stated, all chemicals were used without further purification. A cooling bath from liquid nitrogen and acetone was used for low temperature reactions. ^{1}H-NMR and ^{13}C-NMR spectra were recorded on a 400 MHz Bruker AV-400 spectrometer. The melting point and glass transition temperature were recorded on a TA instruments Q1000 differential scanning calorimeter (DSC) at a heat rate of 10 °C min^{-1} using pierced aluminum crucibles. Glass transition temperatures were measured from heating up after cooling to -90 °C. Reported glass transition temperatures are inflection point temperatures.

Reported melting points are peak temperatures. Measurements were carried out under nitrogen flux (25 ml min^{-1}). The thermal decomposition temperature was measured on the same apparatus at a heat rate of 5 °C min^{-1} in pressure-tight steel crucibles (F20) purchased from the Swiss Institute for the Promotion of Safety. Thermogravimetric analysis (TGA) was performed on a TA Q500 apparatus with a heating rate of 5 °C min^{-1} in a platinum 100 µL pan under nitrogen flux (25 ml min^{-1}). Reported values are the central points, according to DIN ENISO 11358. Infrared (IR) spectra were recorded on a Thermo Scientific iS 50 FTIR spectrometer in attenuated total reflection (ATR) mode. Raman spectra were recorded on a Bruker FT MultiRAM spectrometer at 1064 nm (Nd:YAG laser). Densities were determined by scale and volumetric flask. Elemental analyses were performed on a Thermo Flash EA with helium as carrier gas. Carbon, hydrogen and nitrogen were determined at a combustion temperature of 900 °C using a tin sleeve and oxygen at 1090 °C using a silver sleeve. High-resolution mass spectra were recorded on a Thermo Fisher QExactive Plus spectrometer using electrospray ionization (ESI). Mechanical sensitivity was measured on a BAM drop hammer. A high-pressure liquid chromatography system Agilent 1200 equipped with a ZorbaxBonus RP 4.6x2500 mm column and a diode array detector was used to verify the purity of NFPEG2Me and NFPEG3N3. Gradient determinations were performed by injecting 5 µL acetonitrile diluted samples of the products. The mobile phase was acetonitrile/water with 0.1% trifluoroacetic acid (gradient from 20:80 to pure acetonitrile in 15 minutes) the flow rate was 1.0 ml/min.

3.5.2 Quantum and thermochemical calculations

Quantum chemical calculations were performed with the software Gaussian 16.[28] The molecular structures were calculated as singlets in their electronic ground states and verified as true minima by frequency calculations (no imaginary frequencies). The electrostatic potential of the optimized structures was investigated using the software Multiwfn.[36,37] Thermochemical data were calculated using ICT-thermodynamic code.[24]

3.5.3 General procedure for the preparation of nitrofurazanyl ethers

General procedure 1: Preparation of the alkoxide solution

To a solution of the alcohol in THF, 2.5 M n-butyllithium in hexane was added at -94 °C and under protective atmosphere. The reaction mixture was slowly warmed up to

ambient temperature. The alkoxide solution was subsequently used for the substitution without further purification.

General procedure 2: Substitution

To a solution of DNF in DCM, the alkoxide solution was added at -94 °C under protective atmosphere. The reaction mixture was slowly warmed up to ambient temperature. Then it was washed with water (2 x 300 ml) and the organic phase was dried over Na2SO4. The solvent was removed, and the residue was purified by basic alumina column chromatography using 25vol% ethyl acetate-petroleum ether to deliver a pure product.

Synthesis of 3,4-dinitro-1,2,5-oxadiazole (DNF)

DNF was prepared according to the literature.[21] It was received as a colorless solution in dichloromethane (21.74 g L^{-1}, 50%). IR (ATR, cm^{-1}): 1570, 1538, 1451, 1351, 1325, 1137, 1031, 902, 839, 803, 769, 734, 615, 475. 13C NMR (400 MHz, CDCl3) δ [ppm]=152.72 (t, J=20.2 Hz).

Synthesis of 3-ethoxy-4-nitro-1,2,5-oxadiazole (NFOEt)

NFOEt (440 mg, 73%) was prepared according to the literature and received as a colorless oil.[22] Mp 7.1 °C. TGA 65 °C. T_{dec} 233 °C. Found: C, 30.15; H, 3.25; N, 26.4; O, 40.2%; M^- (mass spectrum), 159.0275. $C_4H_5N_3O_4$ requires C, 30.2; H, 3.2; N, 26.4; O, 40.2%; M^-, 159.0280. IR (ATR, cm^{-1}): 2992, 1597, 1545, 1498, 1471, 1446, 1425, 1393, 1353, 1298, 1204, 1170, 1156, 1114, 1093, 1033, 1011, 928, 889, 871, 828, 765, 741, 696, 593. Raman (1064 nm, cm^{-1}): 2991, 2945, 2898, 2877, 2768, 2721, 1728, 1605, 1550, 1501, 1454, 1426, 1369, 1355, 1279, 1207, 1116, 1094, 1016, 928, 872, 831, 767, 742, 696, 598, 448. ^{1}H NMR (400 MHz, $CDCl_3$) δ [ppm]=4.55 (q, J=7.1 Hz, 2H), 1.55 (t, J=7.1 Hz, 3H) ppm. ^{13}C NMR (101 MHz, $CDCl_3$) δ [ppm]=158.19, 151.62 (t, J=17.5 Hz), 70.80, 14.29. Impact sensitivity > 40 J. Friction sensitivity > 360 N. ϱ 1.33 ± 0.02 g cm^{-3}.

Synthesis of 3-butoxy-4-nitro-1,2,5-oxadiazole (NFOBu)

The reaction has been performed by following general procedure 2. 20wt% sodium butoxide in butanol (10.65 g, 22.11 mmol) and DNF (3.37 g, 21.06 mmol) in dichloromethane (180 ml) were used. The product was obtained as colorless oil (3.11 g, 79%). Mp -7.2 °C. TGA 86 °C. T_{dec} 191 °C. Found: C, 38.5; H, 4.9; N, 22.3; O, 34.1%; M^- (mass spectrum), 187.0591. $C_6H_9N_3O_4$ requires C, 38.5; H, 4.85; N, 22.45; O, 34.2%; M^-, 187.0593. IR (ATR, cm^{-1}): 2964, 2938, 2877, 1598, 1546, 1498, 1464, 1424, 1383, 1353, 1203,

1057, 1034, 1017, 994, 960, 942, 872, 857, 827, 765, 746, 592, 496. Raman (1064 nm, cm^{-1}): 2940, 2918, 2877, 2743, 1603, 1550, 1500, 1453, 1426, 1356, 1303, 1263, 1232, 1204, 1147, 1127, 1059, 1036, 994, 961, 944, 906, 871, 832, 766, 696, 596, 438. ^{1}H NMR (400 MHz, $CDCl_3$) δ [ppm]=4.48 (t, *J*=6.5 Hz, 2H), 1.94 – 1.81 (m, 2H), 1.59-1.43 (m, 2H), 0.99 (t, *J*=7.4 Hz, 3H). ^{13}C NMR (101 MHz, $CDCl_3$) δ [ppm]=158.39, 151.63, 74.59, 30.61, 18.90, 13.68. Impact sensitivity > 40 J. Friction sensitivity > 360 N. ϱ 1.21 ± 0.02 g cm^{-3}.

Synthesis of 3-(2-(2-methoxyethoxy)ethoxy)-4-nitro-1,2,5-oxadiazole (NFPEG2Me)

The reaction has been performed by following the general procedures 1 and 2. Diethylene glycol monomethyl ether (1.44 ml, 1.47 g,12.24 mmol), THF (5 ml), 2.5 M n-butyllithium in hexane (5 ml, 12.48 mmol) and DNF (1.96 g, 12.24 mmol) in DCM (90 ml) were used. The product was obtained as pale yellow liquid (2.31 g, 81%). T_g -69.2 °C. TGA 135 °C. T_{dec} 156 °C. Found: C, 34.95; H, 4.8; N, 17.9; O, 41.2%; $[M+H]^+$ (mass spectrum), 234.0710. $C_7H_{11}N_3O_6$ requires C, 36.1; H, 4.8; N, 18.0; O, 41.2%; $[M+H]^+$, 234.0726. IR (ATR, cm^{-1}): 2883, 1599, 1547, 1499, 1448, 1432, 1351, 1300, 1248, 1202, 1107, 1031, 983, 924, 892, 872, 828, 765, 743, 698, 591, 497. Raman (1064 nm, cm^{-1}): 2947, 2895, 2830, 2742, 1604, 1550, 1501, 1472, 1446, 1431, 1368, 1287, 1243, 1205, 1132, 1032, 926, 872, 831, 766, 743, 699, 594, 441. ^{1}H NMR (400 MHz, CDCl3) δ [ppm]=4.63 (ddd, J=5.8, 3.3, 1.2 Hz, 2H), 3.93 (ddd, J=5.8, 3.4, 1.3 Hz, 2H), 3.74-3.67 (m, 2H), 3.57-3.51 (m, 2H), 3.36 (d, J=1.2 Hz, 3H). ^{13}C NMR (101 MHz, CDCl3) δ [ppm]=158.40, 151.58, 73.75, 72.00, 71.03, 68.63, 59.16 ppm. Impact sensitivity > 40 J. Friction sensitivity > 360 N. ϱ 1.30 ± 0.02 g cm^{-3}.

Synthesis of 3-(2-(2-(2-azidoethoxy)ethoxy)ethoxy)-4-nitro-1,2,5-oxadiazole (NFPEG3N3)

The reaction has been performed by following the general procedures 1 and 2.

2-(2-(2-azidoethoxy)ethoxy)ethan-1-ol (2.65 g, 15.15 mmol), THF (10 ml), 2.5 M n-butyllithium in hexane (6 ml, 15.2 mmol) and DNF (2.42 g, 15.15 mmol) in DCM (140 ml) were used. The product was obtained as yellow liquid (3.50 g, 80%). T_g -72.4 °C. TGA 167 °C. T_{dec} 179 °C. Found: C, 32.9; H, 4.2; N, 28.0; O, 33.45%; $[M+H]^+$ (mass spectrum), 289.0882. $C_8H_{12}N_6O_6$ requires C, 33.3; H, 4.2; N, 29.2; O, 33.3%; $[M+H]^+$, 289.0897. IR (ATR, cm^{-1}): 2872, 2100 ($-N_3$), 1599, 1547, 1499, 1446, 1351, 1284, 1205, 1119, 1032, 923, 891, 871, 852, 827, 765, 743, 697, 645, 591, 557, 505. Raman (1064 nm, cm^{-1}): 2944, 2875, 2096, 1604, 1549, 1501, 1472, 1446, 1430, 1368, 1286, 1247, 1126, 1033, 992, 923, 872, 831, 165, 742, 699,

645, 593, 440. ^{1}H NMR (400 MHz, $CDCl_3$) δ [ppm]=4.61-4.54 (m, 2H), 3.93-3.86 (m, 2H), 3.71-3.64 (m, 2H), 3.68-3.58 (m, 4H), 3.31 (dq, J=4.7, 2.4 Hz, 2H). ^{13}C NMR (101 MHz, $CDCl_3$) δ [ppm]=158.29, 73.62, 71.03, 70.72, 70.17, 68.58, 50.69. Impact sensitivity > 40 J. Friction sensitivity > 360 N. ϱ 1.34 ± 0.02 g cm^{-3}.

3.6 Data availability

The data supporting this article, including infrared spectra, NMR spectra, mass spectra, DSC curves and HPLC chromatograms have been included as part of the ESI.

3.7 Acknowledgment

The authors are thankful to Dr. D. Boskovic, Dr. V. Gettwert, Dr. T. Keicher and Dr. A. Omlor for guidance and support throughout the study. We thank H. Schuppler for TGA and DSC analysis, Y. Kasimir for elemental analysis, S. Huber (LMU Munich) for mechanical sensitivity tests, U. Förter-Barth for rheological measurements, W. Schweikert for Raman and IR measurements, L. Hirsch (KIT Karlsruhe) for mass spectroscopy, T. Ohmer-Scherrer (KIT Karlsruhe) for NMR spectroscopy and M. Schwarzer for HPLC method development. The authors also would like to acknowledge the German Ministry of Defense for funding this work, and support provided by the WTD91.

3.8 References

1 D. Kumari, K. D. B. Yamajala, H. Singh, R. R. Sanghavi, S. N. Asthana, K. Raju and S. Banerjee, Application of Azido Esters as Energetic Plasticizers for LOVA Propellant Formulations, Propellants Explos. Pyrotech., 2013, 38, 805–809.

2 L. A. Wingard, E. C. Johnson, P. E. Guzmán, J. J. Sabatini, G. W. Drake, E. F. C. Byrd and R. C. Sausa, Synthesis of Biisoxazoletetrakis(methyl nitrate): A Potential Nitrate Plasticizer and Highly Explosive Material, Eur. J. Org. Chem., 2017, 2017, 1765–1768.

3 R. S. Damse and A. Singh, Evaluation of Energetic Plasticisers for Solid Gun Propellant, Def. Sci. J., 2008, 58, 86–93.

4 S. Hafner, V. A. Hartdegen, M. S. Hofmayer and T. M. Klapötke, Potential Energetic Plasticizers on the Basis of 2,2-Dinitropropane-1,3-diol and 2,2-Bis(azidomethyl)propane-1,3-diol, Propellants Explos. Pyrotech., 2016, 41, 806–813.

5 H. G. Ang and S. Pisharath, Energetic polymers. Binders and plasticizers for enhancing performance, Wiley-VCH-Verl., Weinheim, 1st edn., 2012.

6 S. K. Shee, S. T. Reddy, J. Athar, A. K. Sikder, M. B. Talawar, S. Banerjee and M. A. Shafeeuulla Khan, Probing the compatibility of energetic binder poly-glycidyl nitrate with energetic plasticizers: thermal, rheological and DFT studies, RSC Adv., 2015, 5, 101297–101308.

7 V. Grakauskas, Polynitroalykyl ethers, J. Org. Chem., 1973, 38, 2999–3004.

8 K. Selim, S. zkar and L. Yilmaz, Thermal characterization of glycidyl azide polymer (GAP) and GAP-based binders for composite propellants, J. Appl. Polym. Sci., 2000, 77, 538–546.
9 K. P. C. Rao, A. K. Sikder, M. A. Kulkarni, M. M. Bhalerao and B. R. Gandhe, Studies on n-Butyl Nitroxyethylnitramine (n-BuNENA): Synthesis, Characterization and Propellant Evaluations, Propellants Explos. Pyrotech., 2004, 29, 93–98.
10 R. Vijayalakshmi, N. H. Naik, G. M. Gore and A. K. Sikder, Linear Nitramine (DNDA-57): Synthesis, Scale-Up, Characterization, and Quantitative Estimation by GC/MS, J. Energ. Mater., 2015, 33, 1–16.
11 Z. Xu, G. Cheng, H. Yang, X. Ju, P. Yin, J. Zhang and J. M. Shreeve, A Facile and Versatile Synthesis of Energetic Furazan-Functionalized 5-Nitroimino-1,2,4-Triazoles, Angew. Chem., Int. Ed. Engl., 2017, 56, 5877–5881.
12 M. A. Roux, M. Zeller, E. F. C. Byrd and D. G. Piercey, Synthesis and characterization of the energetic 5,7-diamino-2-nitro-1,2,4-triazolo[1,5-a]-1,3,5-triazine, Propellants Explos. Pyrotech., 2023, 48. DOI: 10.1002/prep.202300125.
13 J. Li, Y. Liu, W. Ma, T. Fei, C. He and S. Pang, Tri-explosophoric groups driven fused energetic heterocycles featuring superior energetic and safety performances outperforms HMX, Nat. Commun., 2022, 13, 5697.
14 U. Schaller, J. Lang, V. Gettwert, J. Hürttlen, V. Weiser and T. Keicher, 4-Amino-1-Butyl-1,2,4-Triazolium Dinitramide – Synthesis, Characterization and Combustion of a Low-Temperature Dinitramide-Based Energetic Ionic Liquid (EIL), Propellants Explos. Pyrotech., 2022, 47. DOI: 10.1002/prep.202200054.
15 L. L. Fershtat and N. N. Makhova, 1,2,5-Oxadiazole-Based High-Energy-Density Materials: Synthesis and Performance, ChemPlusChem, 2020, 85, 13–42.
16 W.-L. Cao, Q.-N. Tariq, Z.-M. Li, J.-Q. Yang and J.-G. Zhang, Recent advances on the nitrogen-rich 1,2,4-oxadiazole-azoles-based energetic materials, Def. Technol., 2022, 18, 344–367.
17 T. S. Hermann, T. M. Klapötke, B. Krumm and J. Stierstorfer, Synthesis, Characterization, and Properties of Di- and Trinitromethyl-1,2,4-Oxadiazoles and Salts, Asian J. Org. Chem., 2018, 7, 739–750.
18 A. B. Sheremetev, Efficient synthesis of nitrofurazans using HOF • MeCN, Russian Chemical Bulletin, 2022, 71, 1818–1820.
19 T. S. Novikova, T. M. Mel'nikova, O. V. Kharitonova, V. O. Kulagina, N. S. Aleksandrova, A. B. Sheremetev, T. S. Pivina, L. I. Khmel'nitskii and S. S. Novikov, An Effective Method for the Oxidation of Aminofurazans to Nitrofurazans, Mendeleev Commun., 1994, 4, 138–140.
20 K. Y. Suponitsky, A. F. Smol'yakov, I. V. Ananyev, A. V. Khakhalev, A. A. Gidaspov and A. B. Sheremetev, 3,4-Dinitrofurazan: Structural Nonequivalence of ortho -Nitro Groups as a Key Feature of the Crystal Structure and Density, ChemistrySelect, 2020, 5, 14543–14548.
21 P. Lieber, U. Schaller and T. M. Klapötke, in Proceedings of the 26th Seminar on New Trends in Research of Energetic Materials (NTREM), Pardubice, Czech Republic, 2024.
22 A. B. Sheremetev, O. V. Kharitonova, E. V. Mantseva, V. O. Kulagina, E. V. Shatunova, N. S. Aleksandrova and L. I. Khmel'nitskii, Nucleophilic substitution in the furazan series. Reactions with O-nucleophiles, Russ. J. Org. Chem., 1999, 35, 1525–1537.
23 A. B. Sheremetev, V. O. Kulagina, I. A. Kryazhevskikh, T. M. Melnikova and N. S. Aleksandrova, Nucleophilic substitution in the furazan series. Reactions of nitrofurazans with ammonia, Russian Chemical Bulletin, 2002, 51, 1533–1539.
24 S. Kelzenberg, P.-B. Kempa, S. Wurster, M. Herrmann and T. Fischer, New version of the ICT-thermodynamic code, 45th International Annual Conference of ICT - Energetic Materials Particles, Processing, Applications, Karlsruhe, 2014.

25 R. Haiges and K. O. Christe, Energetic high-nitrogen compounds: 5-(trinitromethyl)-2H-tetrazole and -tetrazolates, preparation, characterization, and conversion into 5-(dinitromethyl)tetrazoles, Inorg. Chem., 2013, 52, 7249–7260.
26 Manual of Tests and Criteria - Eighth Revised Edition, United Nations, New York, 5th edn., 2023.
27 G. Socrates, Infrared and Raman characteristic group frequencies. Tables and charts, Wiley, Chichester, 3rd edn., 2010.
28 M. J. Frisch, G. W. Trucks, H. B. Schlegel, G. E. Scuseria, M. A. Robb, J. R. Cheeseman, G. Scalmani, V. Barone, G. A. Petersson, H. Nakatsuji, X. Li, M. Caricato, A. V. Marenich, J. Bloino, B. G. Janesko, R. Gomperts, B. Mennucci, H. P. Hratchian, J. V. Ortiz, A. F. Izmaylov, J. L. Sonnenberg, D. Williams-Young, F. Ding, F. Lipparini, F. Egidi, J. Goings, B. Peng, A. Petrone, T. Henderson, D. Ranasinghe, V. G. Zakrzewski, J. Gao, N. Rega, G. Zheng, W. Liang, M. Hada, M. Ehara, K. Toyota, R. Fukuda, J. Hasegawa, M. Ishida, T. Nakajima, Y. Honda, O. Kitao, H. Nakai, T. Vreven, K. Throssell, Montgomery, Jr., J. A., J. E. Peralta, F. Ogliaro, M. J. Bearpark, J. J. Heyd, E. N. Brothers, K. N. Kudin, V. N. Staroverov, T. A. Keith, R. Kobayashi, J. Normand, K. Raghavachari, A. P. Rendell, J. C. Burant, S. S. Iyengar, J. Tomasi, M. Cossi, J. M. Millam, M. Klene, C. Adamo, R. Cammi, J. W. Ochterski, R. L. Martin, K. Morokuma, O. Farkas, J. B. Foresman and D. J. Fox, Gaussian˜16 Revision C.01, 2016.
29 P. Politzer, Y. Ma, P. Lane and M. C. Concha, Computational prediction of standard gas, liquid, and solid-phase heats of formation and heats of vaporization and sublimation, Int. J. Quantum Chem., 2005, 105, 341–347.
30 B. M. Rice, S. V. Pai and J. Hare, Predicting heats of formation of energetic materials using quantum mechanical calculations, Combustion and Flame, 1999, 118, 445–458.
31 E. F. C. Byrd and B. M. Rice, Improved prediction of heats of formation of energetic materials using quantum mechanical calculations, J. Phys. Chem. A, 2006, 110, 1005–1013.
32 J. M. Simmie and K. P. Somers, Benchmarking Compound Methods (CBS-QB3, CBS-APNO, G3, G4, W1BD) against the Active Thermochemical Tables: A Litmus Test for Cost-Effective Molecular Formation Enthalpies, J. Phys. Chem. A, 2015, 119, 7235–7246.
33 G. A. Petersson and M. A. Al-Laham, A complete basis set model chemistry. II. Open-shell systems and the total energies of the first-row atoms, J. Chem. Phys., 1991, 94, 6081–6090.
34 S. Rayne and K. Forest, A G4MP2 and G4 Theoretical Study into the Thermochemical Properties of Explosophore Substituted Tetrahedranes and Cubanes, Propellants Explos. Pyrotech., 2011, 36, 410–415.
35 L. A. Curtiss, P. C. Redfern and K. Raghavachari, Gaussian-4 theory using reduced order perturbation theory, J. Chem. Phys., 2007, 127, 124105.
36 T. Lu and F. Chen, Multiwfn: a multifunctional wavefunction analyzer, J. Comput. Chem., 2012, 33, 580–592.
37 T. Lu, A comprehensive electron wavefunction analysis toolbox for chemists, Multiwfn, J. Chem. Phys., 2024, 161. DOI: 10.1063/5.0216272.

3.9 Supplementary information

^{1}H and ^{13}C NMR spectra (S1)

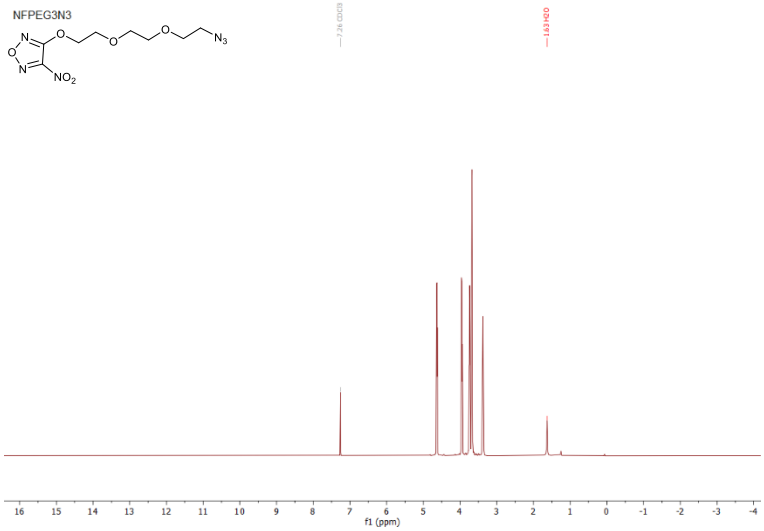

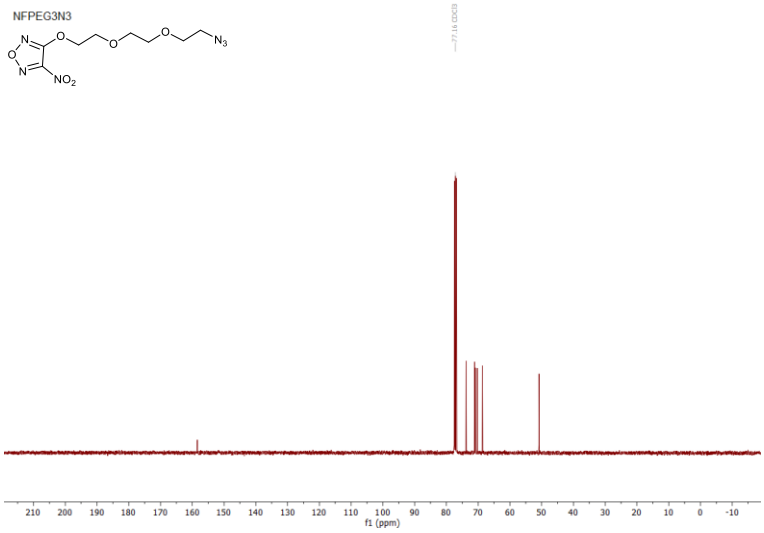

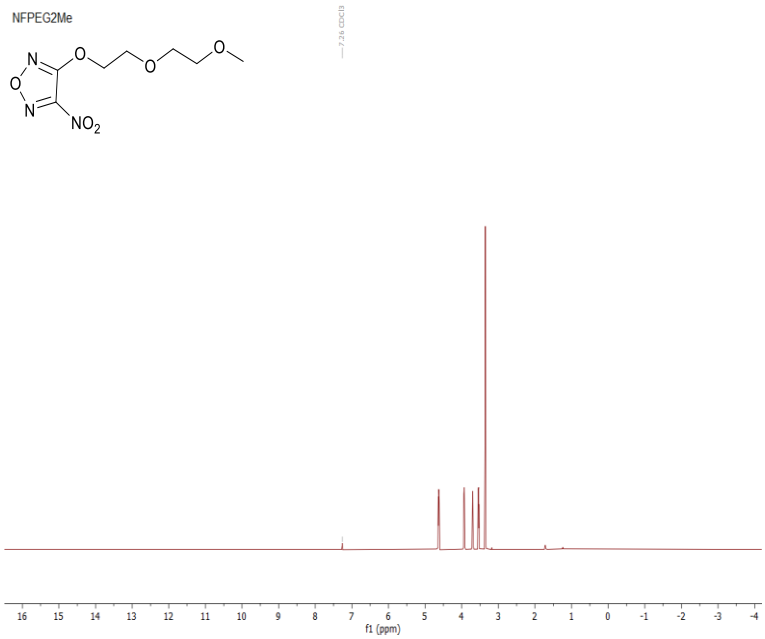

NFPEG2Me

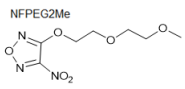

NFOBu

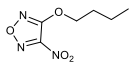

NFOBu

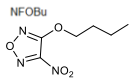

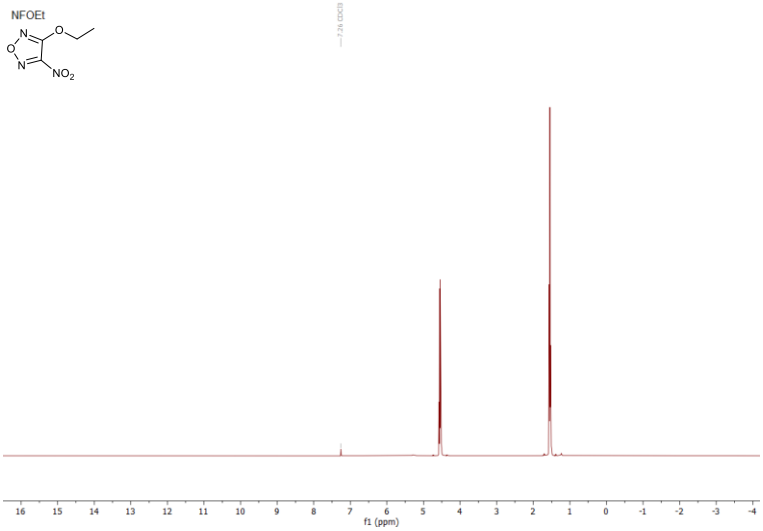
NFOEt
O
N
O
N
NO2
7.26 CDCl3
16 15 14 13 12 11 10 9 8 7 6 5 4 3 2 1 0 -1 -2 -3 -4
f1 (ppm)

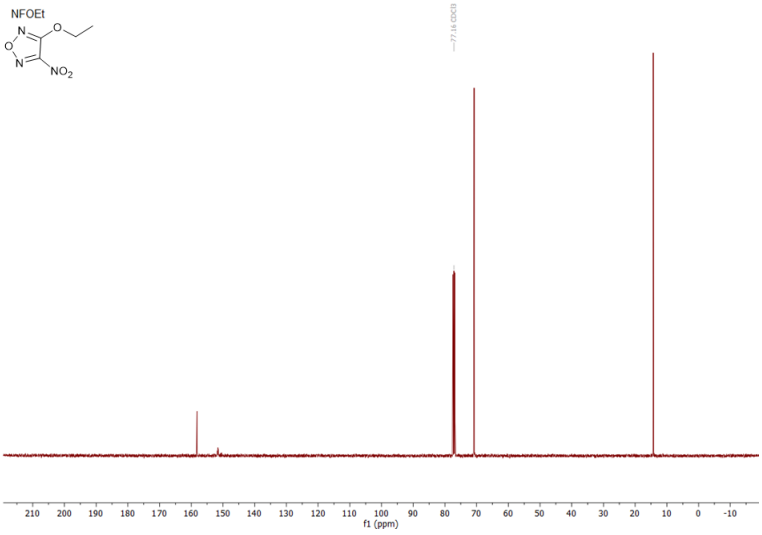
NFOEt
O
N
O
N
NO2
77.16 CDCl3
210 200 190 180 170 160 150 140 130 120 110 100 90 80 70 60 50 40 30 20 10 0 -10
f1 (ppm)

Infrared spectra (S2)

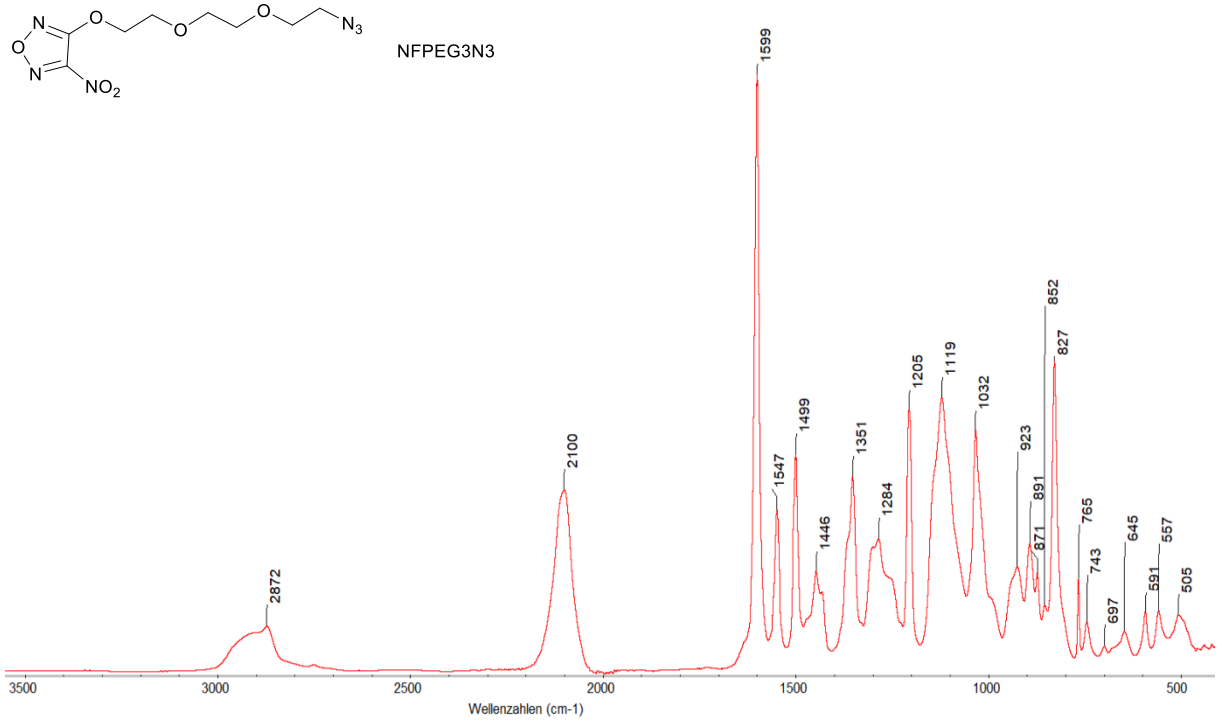

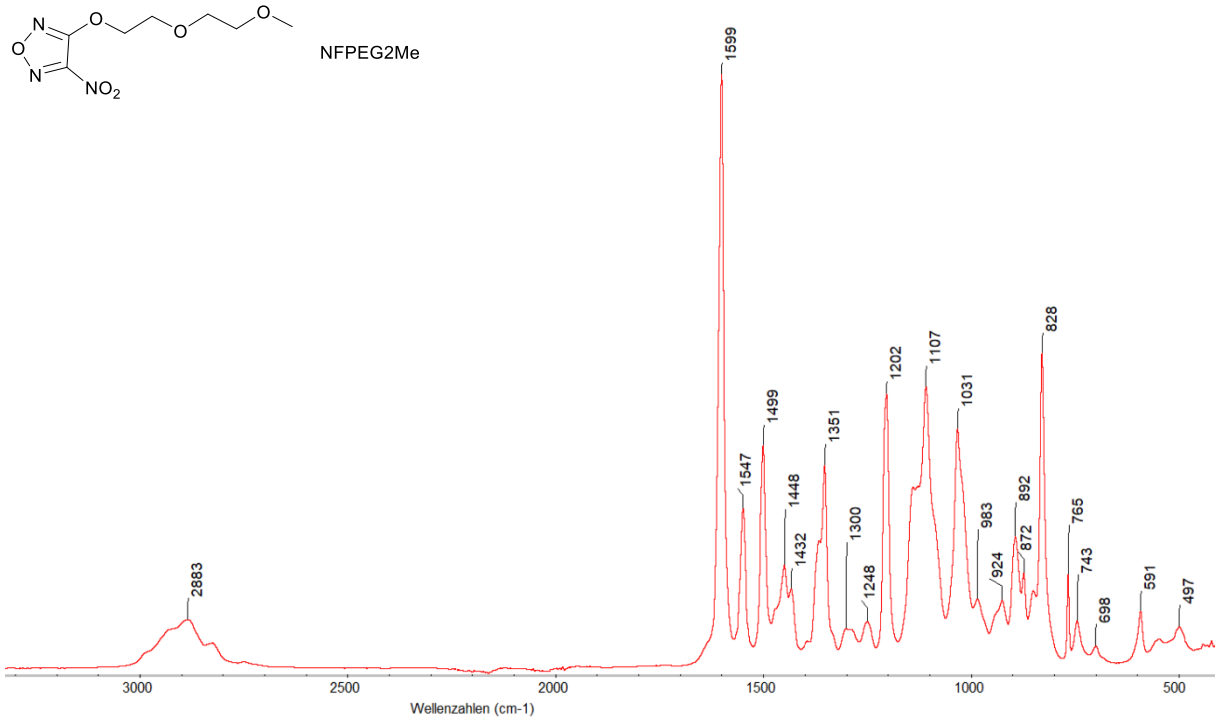

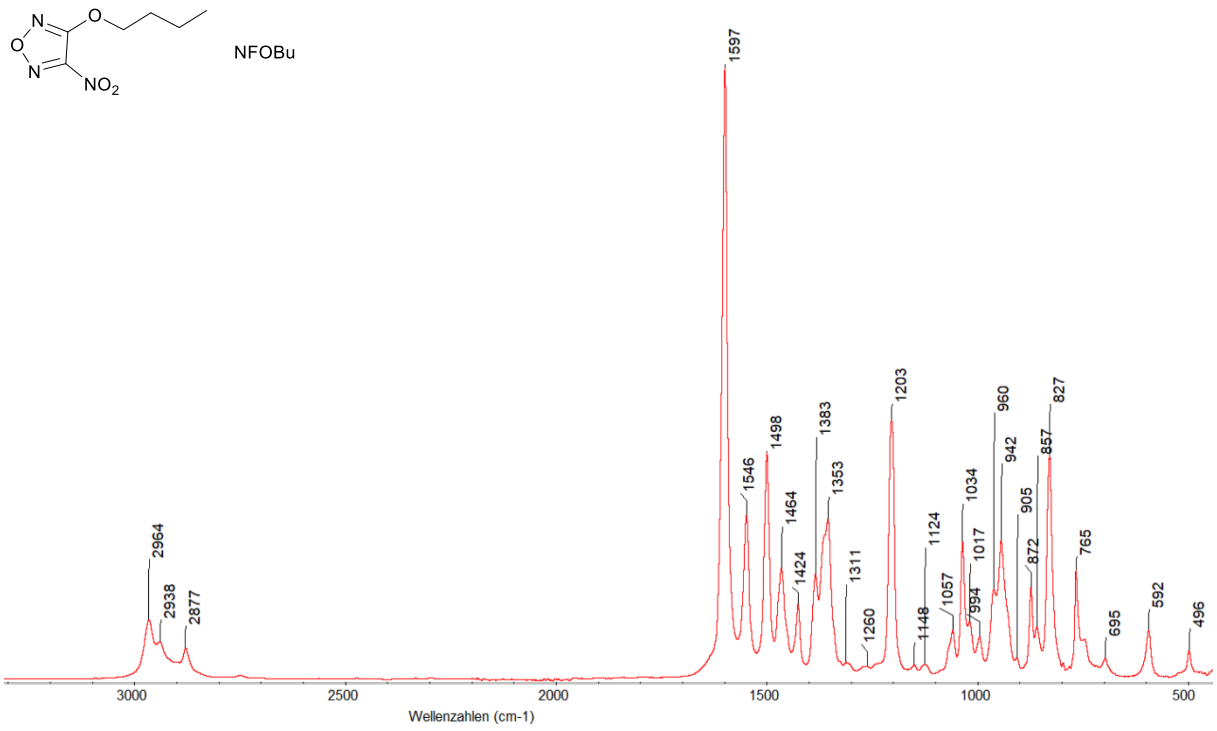
NFOBu
1597
1546
1498
1464
1424
1383
1353
1311
1260
1203
1148
1124
1057
1034
1017
994
960
942
905
872
857
827
765
695
592
496
2964
2938
2877
3000
2500
2000
1500
1000
500
Wellenzahlen (cm-1)

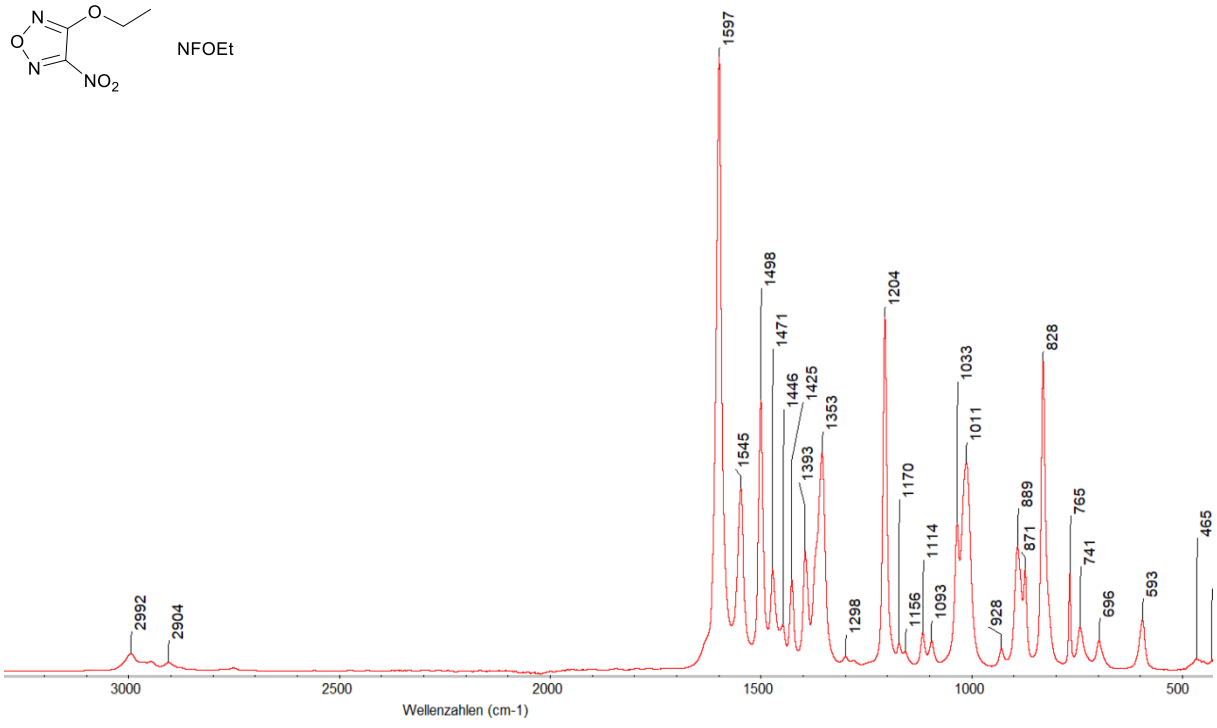
NFOEt
1597
1545
1498
1471
1446
1425
1393
1353
1298
1204
1170
1156
1114
1093
1033
1011
928
889
871
828
765
741
696
593
465
2992
2904
3000
2500
2000
1500
1000
500
Wellenzahlen (cm-1)

Mass spectra (S3)

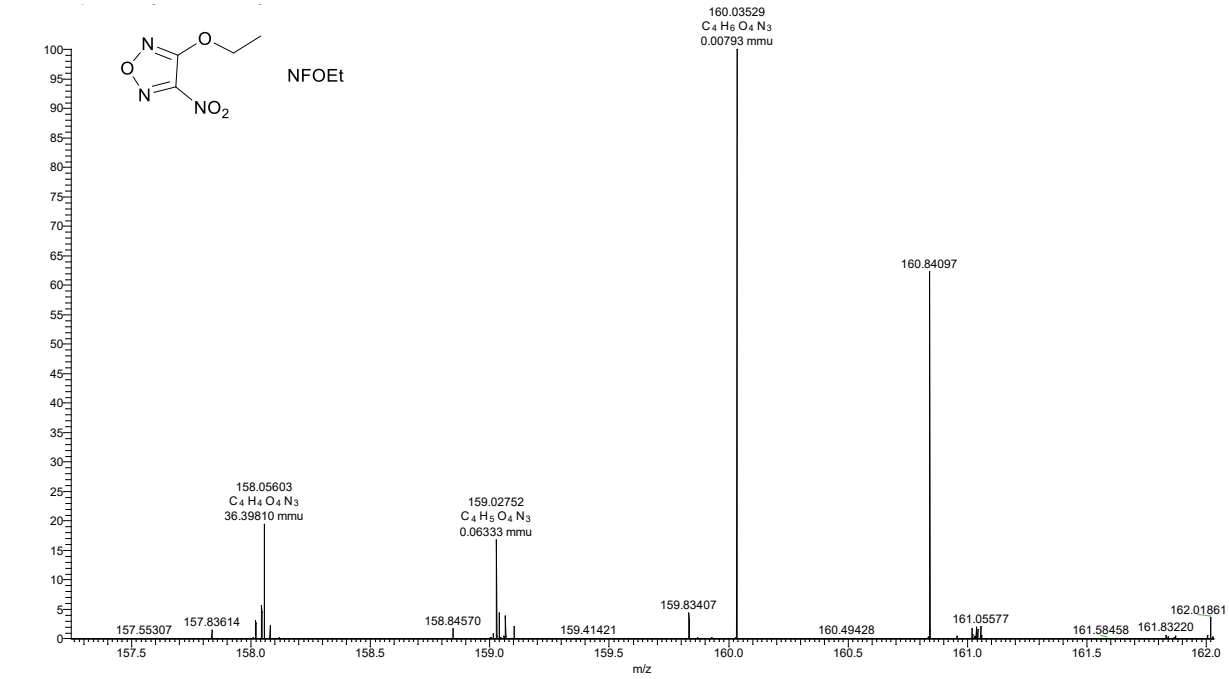

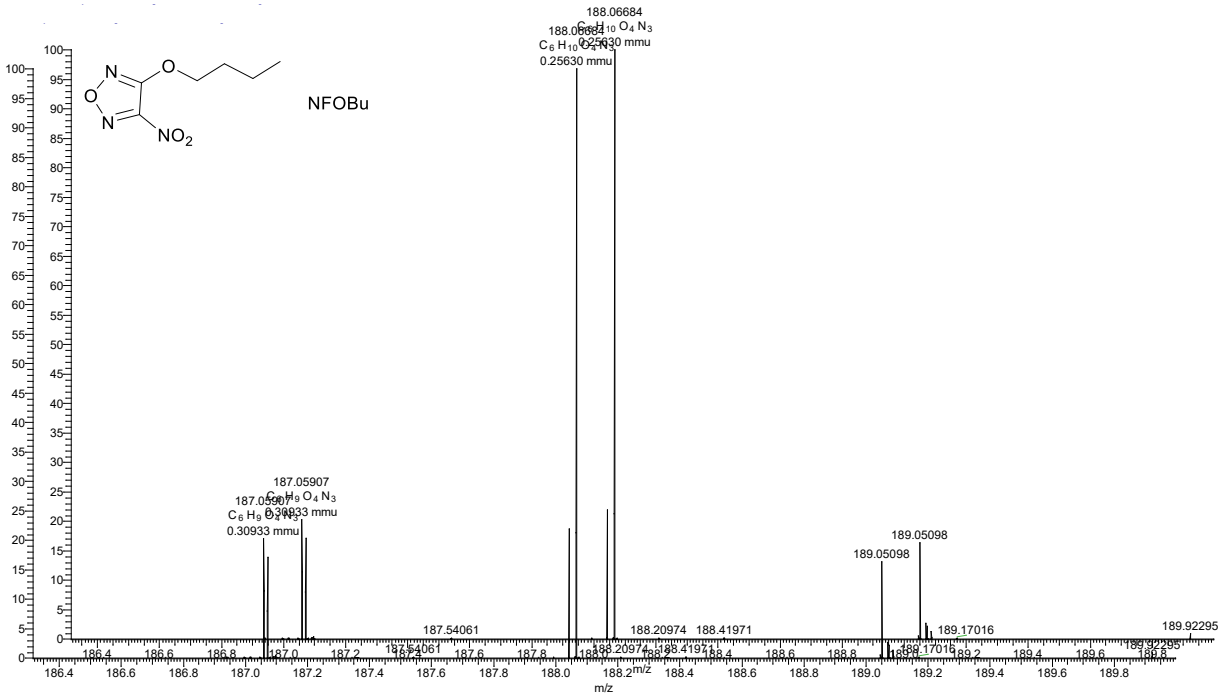

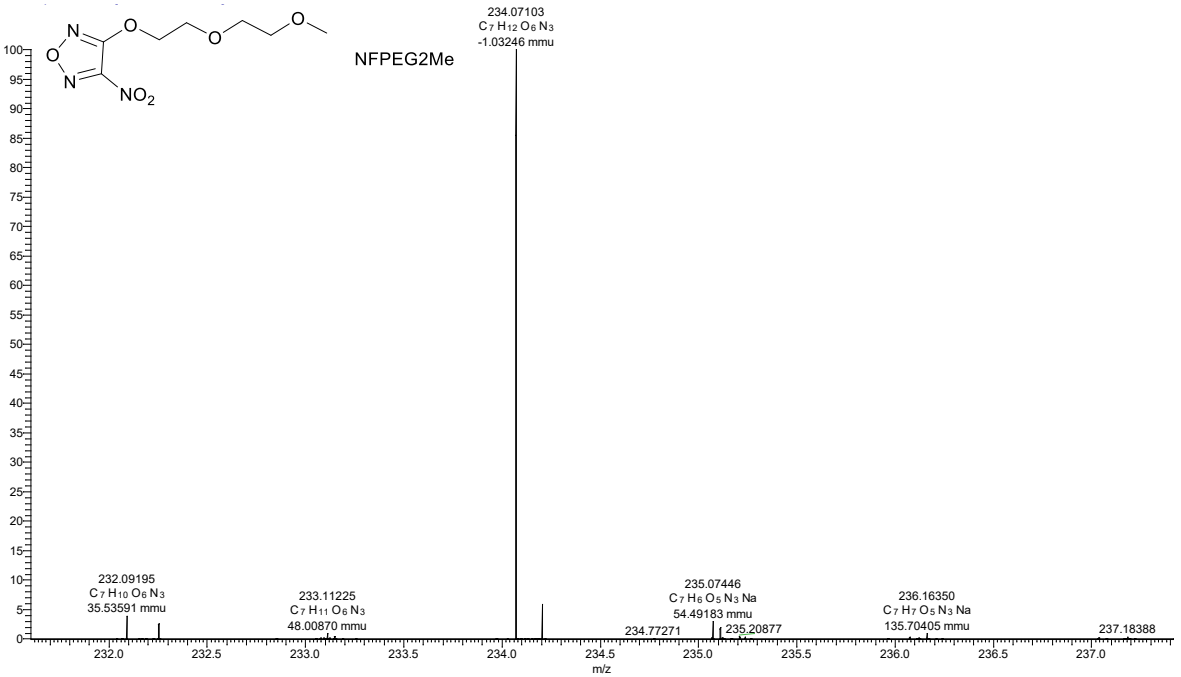
NFPEG2Me
234.07103
C7 H12 O6 N3
-1.03246 mmu
232.09195
C7 H10 O6 N3
35.53591 mmu
233.11225
C7 H11 O6 N3
48.00870 mmu
234.77271
235.07446
C7 H8 O5 N3 Na
54.49183 mmu
235.20877
236.16350
C7 H7 O5 N3 Na
135.70405 mmu
237.18388
m/z

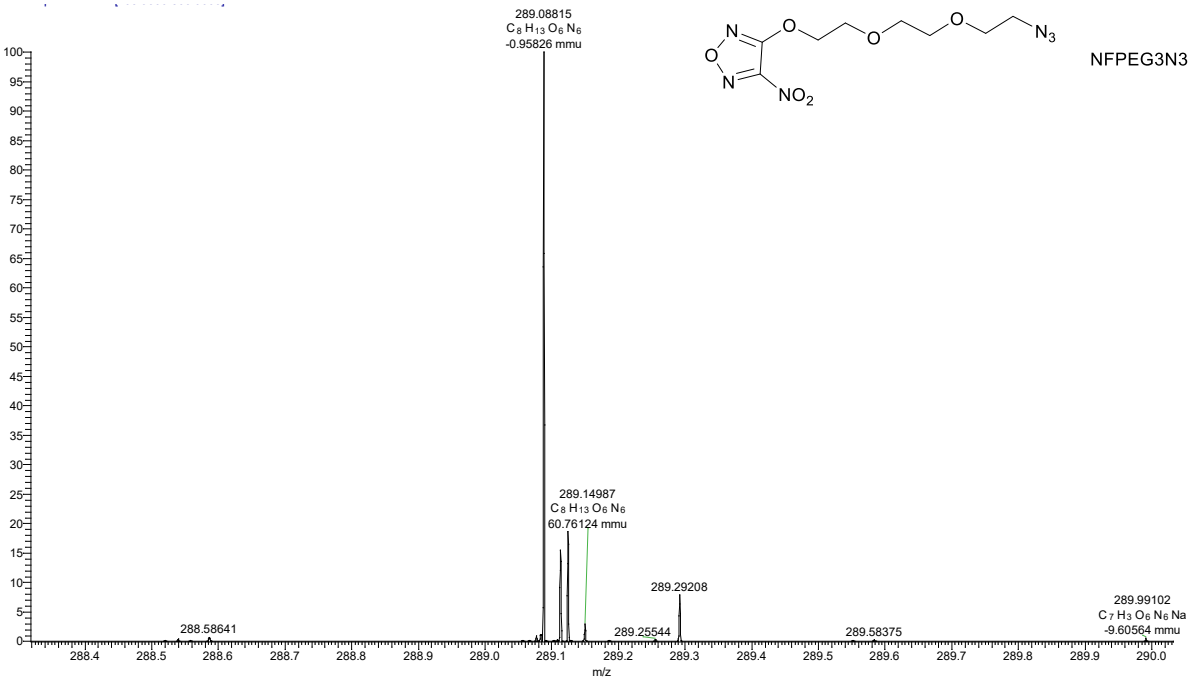
NFPEG3N3
289.08815
C8 H13 O6 N6
-0.95826 mmu
289.14987
C8 H13 O6 N6
60.76124 mmu
288.58641
289.25544
289.29208
289.58375
289.99102
C7 H3 O6 N6 Na
-9.60564 mmu
m/z

Pressure-tight crucible DSC (S4)

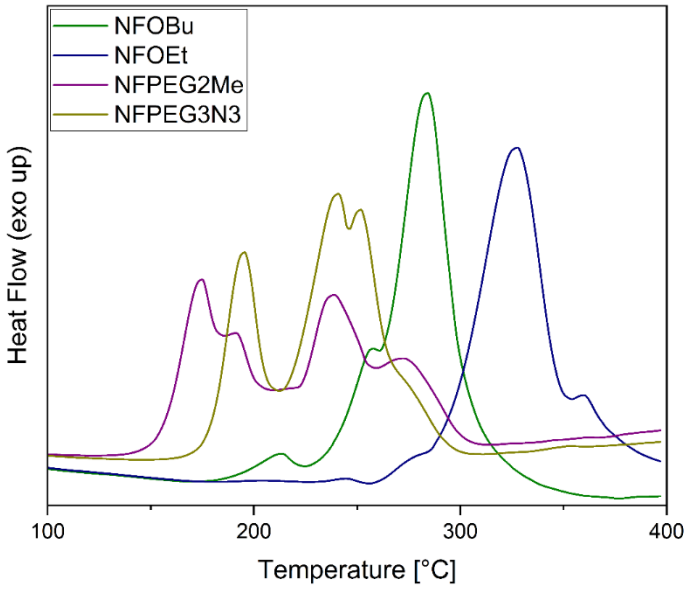

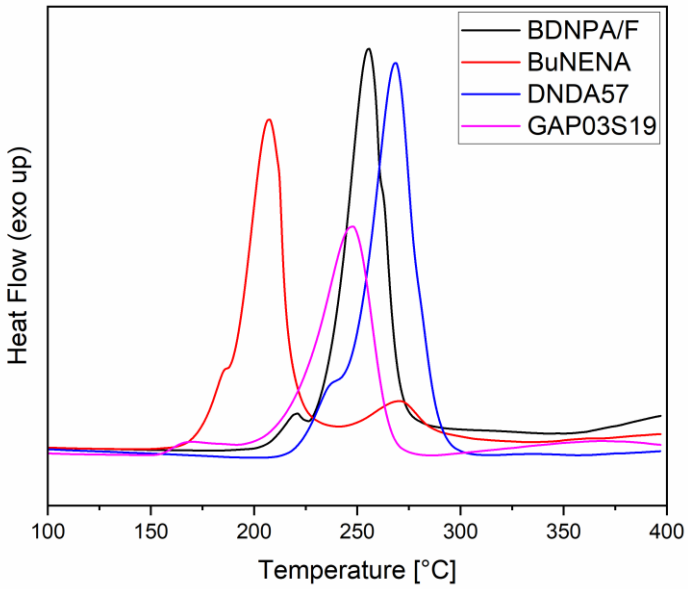

Perforated aluminum crucible DSC (S5)

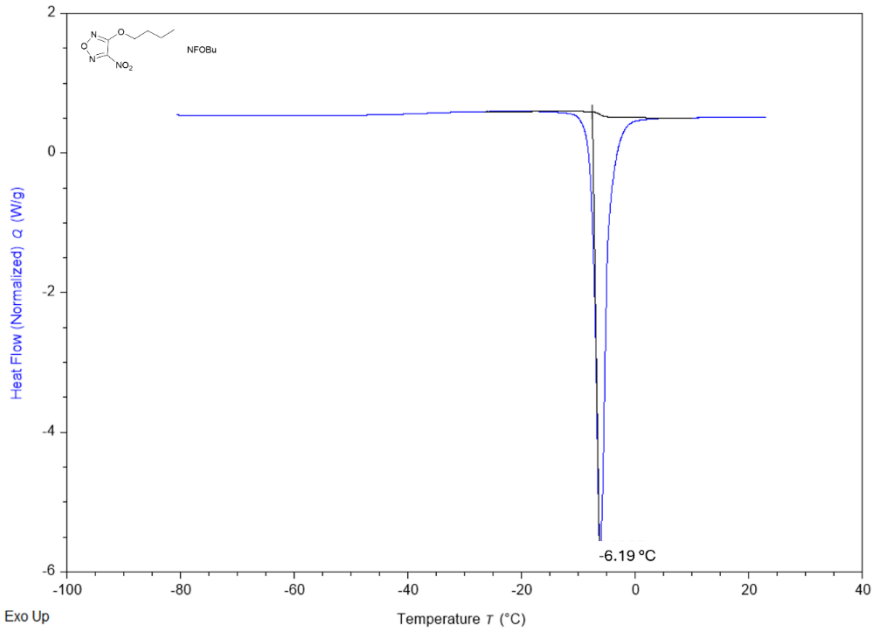

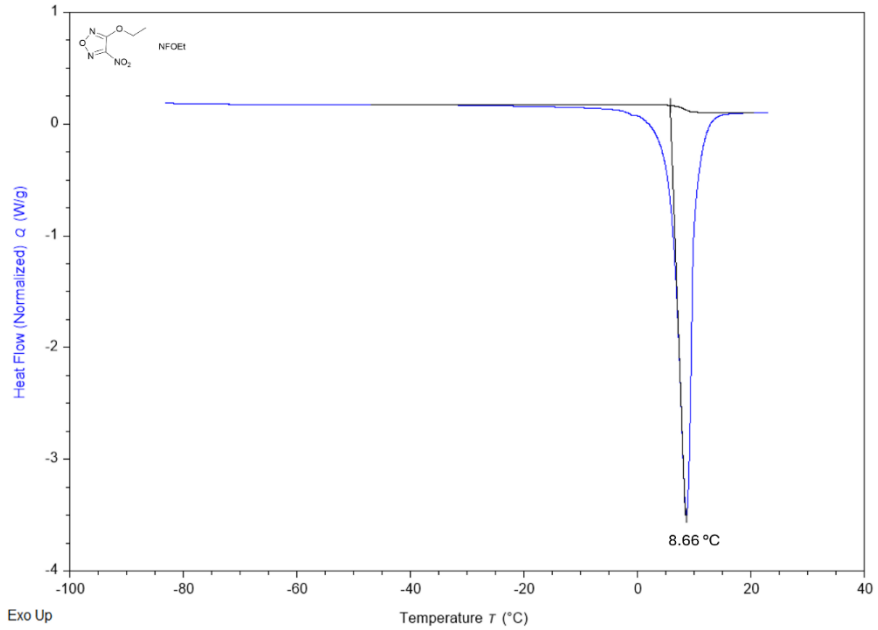

HPLC (S6)

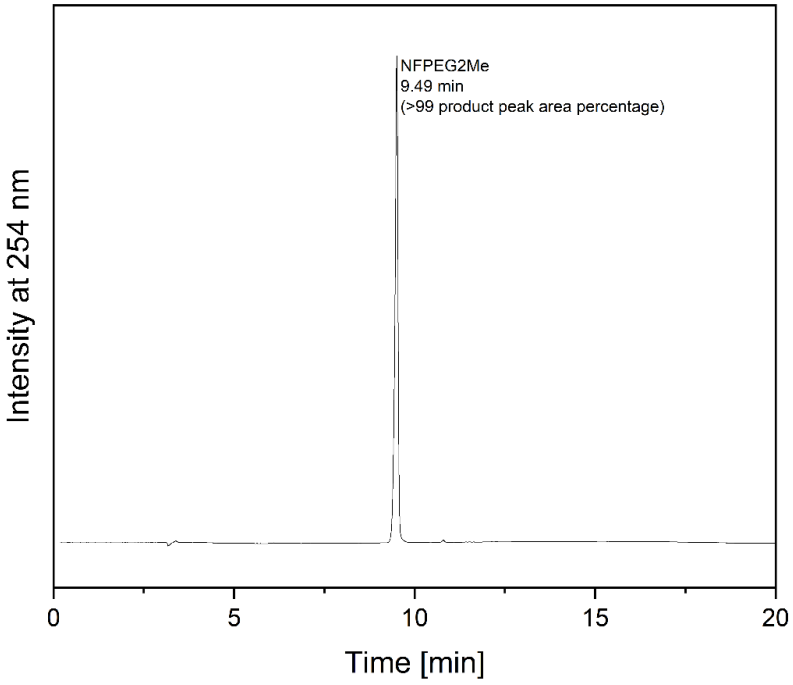
NFPEG2Me
9.49 min
(>99 product peak area percentage)
Intensity at 254 nm
0
5
10
15
20
Time [min]

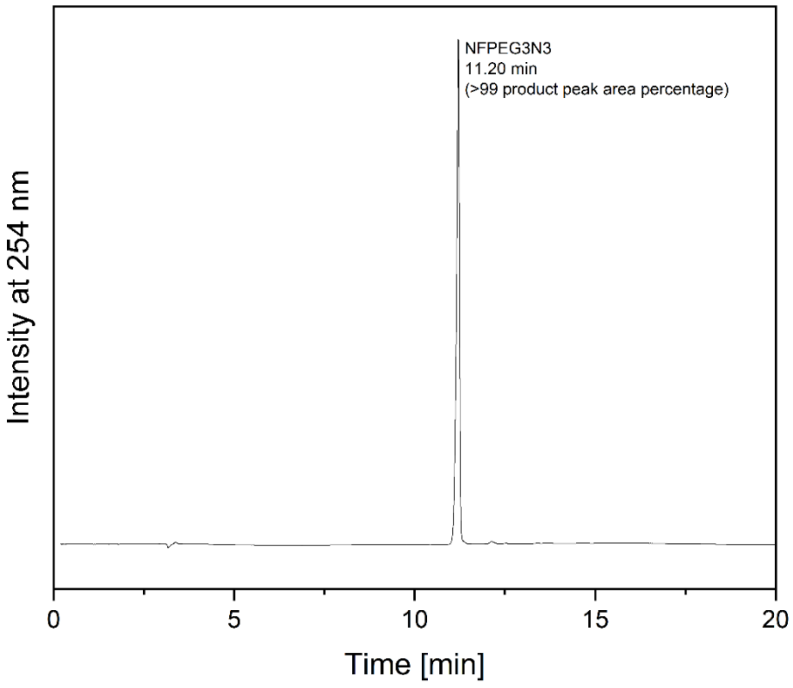
NFPEG3N3
11.20 min
(>99 product peak area percentage)
Intensity at 254 nm
0
5
10
15
20
Time [min]

4 Energetic plasticizers for GAP-based formulations with ADN: compatibility and performance evaluation of a nitrofurazanyl ether

Patrick Lieber*, Uwe Schaller, Thomas M. Klapötke

as published in: *RSC Advances* **2025**, 15, 37006–37011

DOI: 10.1039/D5RA05154A

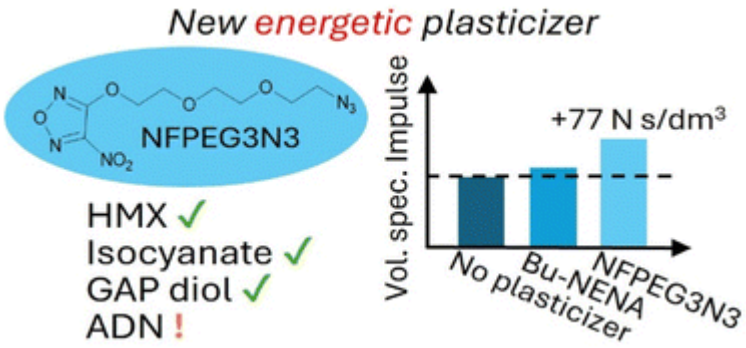

4.1 Abstract

Glycidyl azide polymer (GAP) diol is an energetic binder with azide-functionalized side chains that offer a high enthalpy of formation. When formulated with ammonium dinitramide (ADN), GAP-based systems exhibit promising energetic and ballistic performance. However, GAP suffers from poor mechanical properties compared to inert binders such as hydroxyl-terminated polybutadiene (HTPB). As a result, plasticization is essential to lower the glass transition temperature of GAP. Energetic plasticizers can enhance both mechanical and energetic performance. In this study, we evaluated the compatibility of a novel nitrofurazanyl ether-based energetic plasticizer, NFPEG3N3, with key formulation components: GAP diol, HMX, Desmodur N100, and ADN. Compatibility was assessed using heat-flow microcalorimetry (HFMC) and thermogravimetry (TG), in accordance with STANAG 4147. NFPEG3N3 was found to be compatible with GAP diol, HMX, and N100. Although the NFPEG3N3–ADN mixture passed the HFMC (remaining below the 1% heat of explosion threshold), it failed TG, indicating potential concerns with long-term thermal stability. Performance calculations

showed that replacing 15wt% of GAP with NFPEG3N3 in a composite propellant increased the volume-specific impulse by 77 N·s/dm^3. Additionally, formulations incorporating NFPEG3N3 demonstrated a superior oxygen balance and higher volume-specific impulse compared to those using the widely adopted energetic plasticizer Bu-NENA.

4.2 Introduction

The use of energetic plasticizers is key to the performance of advanced solid propellants and polymer-bonded explosives.[1–3] Plasticizers reduce the glass transition temperature (T_g) of the polymer binder, thereby improving mechanical properties at low temperatures.[4] Unlike inert plasticizers, energetic plasticizers incorporate explosophoric groups, such as nitrate esters, nitramines, azido or nitro functionalities, which contribute to the energetic output of a formulation. Representative energetic plasticizers are shown in the ESI (S1).[5,6] These compounds typically feature a saturated, nearly linear carbon backbone with energetic side groups.[7] Ethylene glycol-based backbones are also common; for example, the thermal properties of BATEG highlight the strong influence of ethylene glycol segments on T_g, which occurs at the remarkably low temperature of -110 °C. However, BATEG suffers from high volatility.[6,8,9] While heterocyclic building blocks have been widely explored in energetic materials, their use as energetic plasticizers remains underrepresented in the literature.[10–12] Among energy-rich heterocycles, oxadiazoles are especially promising due to their favorable oxygen balance compared to triazoles or tetrazoles. Of the four oxadiazole isomers, furazan (1,2,5-oxadiazole) is of particular interest, offering the highest enthalpy of formation and sufficient chemical stability.[13–15] Recently, a novel nitrofurazanyl ether-based plasticizer, NFPEG3N3, was synthesized and evaluated for potential use as a heterocyclic energetic plasticizer (Figure 1). NFPEG3N3 exhibits a low T_g of -72 °C, decomposition onset temperature of 167 °C, and an enthalpy of formation of -41.7 kJ/mol. Compared to conventional energetic plasticizers, NFPEG3N3 significantly lowers the T_g and viscosity of glycidyl azide polymer (GAP) diol.[16] GAP diol is a hydroxyl-terminated polyether containing azide groups in its side chains. When combined with the environmentally friendly oxidizer ammonium dinitramide (ADN), it offers excellent ballistic properties.[17]

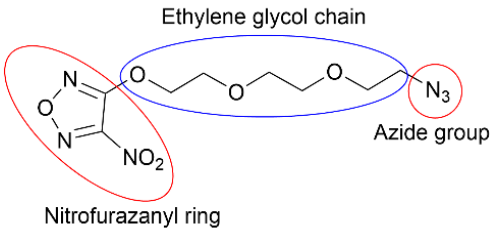

Figure 1 Molecular structure of NFPEG3N3 (3-(2-(2-(2-azidoethoxy)ethoxy) ethoxy)-4-nitro-1,2,5-oxadiazole).

Despite its high density and positive enthalpy of formation, GAP exhibits poor mechanical properties compared to hydroxyl-terminated polybutadiene (HTPB), a widely used inert binder.[18] The molecular structures of GAP and HTPB are compared in the ESI (S2). In addition to favorable thermal and mechanical characteristics, compatibility with formulation components is essential for the safe and effective implementation of new energetic compounds.[19] This is particularly important when manufacturing formulations for the first time. According to STANAG 4147, compatibility should be assessed through complementary test methods. If results remain inconclusive, alternative methods must be used.[20] In this study, we present compatibility and performance data for NFPEG3N3 in combination with GAP diol, HMX, Desmodur N100, and ADN. Figure 2 shows the molecular structure of HDI-biuret, the trifunctional isocyanate component of the commercial hardener N100.[21]

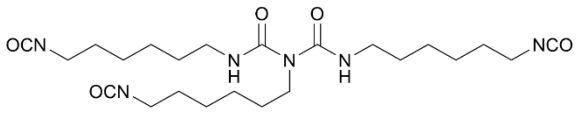

Figure 2 Molecular structure of HDI-biuret (1,3-bis (6-isocyanatohexyl)-1-(6-isocyanatohexylcarbamoyl)urea).

4.3 Results and discussion

4.3.1 Compatibility of NFPEG3N3 with formulation components

The compatibility of NFPEG3N3 with HMX, GAP diol, N100, and ADN was evaluated using dynamic thermogravimetry (TG) and heat-flow microcalorimetry (HFMC) in accordance with STANAG 4147. ADN was used as spherical prills.[22] Images of the ADN prills used, taken with an electron microscope, are included in the ESI (S3). Both methods follow a similar general procedure: a reactivity value (*R*) is calculated based on either

the excess weight loss (TG) or heat generation (HFMC), reflecting interactions that occur between components in the mixture. In the dynamic TG test, the total weight losses of the binary mixture (W_M) is compared with the sum of the weight losses of the individual components ($W_{M,calc}$) at a selected temperature. This temperature corresponds to the lowest temperature at which a derivative peak appears in the TG curve of the mixture. If the weight loss of the mixture exceeds the calculated sum of the individual losses, it indicates potential incompatibility. The percentage of mass loss due to interactions (R_W) was calculated using Equation 1.

Equation 1 Calculation of weight loss-based reactivity.

$$R_W = W_M - W_{M,calc} = W_M - \frac{m_{NFPEG3N3} W_{NFPEG3N3} + m_C W_C}{m_{NFPEG3N3} + m_C}$$

According to STANAG 4147, a weight difference of less than 4% indicates that the materials are compatible. A difference between 4% and 20% suggests potential incompatibility and warrants further testing, while a difference greater than 20% indicates clear incompatibility. Table 1 summarizes the excess weight loss due to interactions in binary mixtures containing NFPEG3N3, along with the corresponding compatibility assessments.

Table 1 Compatibility assessment by dynamic thermogravimetry (ff. = fulfilled).

Component	T_{dTGA} [a] [°C]	$W_{NFPEG3N3}$ [b] [%]	W_C [c] [%]	W_M [d] [%]	R_W [e] [%]	Assmt.
HMX	175	95.7	0.1	37.9	-10.6	ff.
GAP diol	172	95.1	0.3	29.9	-17.5	ff.
N100	183	96.7	6.0	34.3	-19.1	ff.
ADN	158	52.3	20.1	42.1	+5.2	

[a] Mixture derivative peak temperature. [b] Weight loss of NFPEG3N3. [c] Weight loss of component. [d] Weight loss of binary mixture. [e] Reactivity by excess weight loss.

Mixtures of NFPEG3N3 with HMX, GAP diol, and N100 exhibited a lower weight loss than the calculated sum for the individual components, indicating compatibility. In contrast, the mixture with ADN showed an excess weight loss of 5.2%, which exceeds the 4% threshold and therefore requires further investigation. The observed negative reactivity values in some mixtures may be attributed to their elevated viscosity, influenced by the presence of high-viscosity components such as GAP diol and N100, as well as finely dispersed solid HMX. This higher viscosity appears to retard the

evaporation of NFPEG3N3 compared to the single-compound tests. All TG curves are provided in the ESI (S4). The compatibility between NFPEG3N3 and the formulation components was further evaluated using isothermal heat-flow microcalorimetry (HFMC). HFMC is a highly sensitive technique for measuring the heat generation rate of a sample under isothermal conditions. Because it uses larger sample sizes, typically in the gram range, HFMC provides a more representative assessment than screening methods such as TG, which typically use milligram-scale samples. As in the TG study, both pure substances and a binary mixture at a 1:1 weight ratio were analyzed to assess thermal interactions and determine compatibility. The expected heat release for each binary mixture ($Q_{M,calc}$) was calculated from the individual measurements of the two components, as shown in Equation 2.

Equation 2 Calculation of heat flow-based reactivity.

$$R_Q = Q_M - Q_{M,calc} = Q_M - \frac{1}{2}(Q_{NFPEG3N3} + Q_C)$$

It was subtracted from the experimentally measured value of the mixture (Q_M) to determine the heat generated by interactions (R_Q). Figure 3 displays the heat generation profiles of the pure components and their binary mixtures, along with the calculated excess heat generation (R_Q) over the 15-day test period at a constant temperature of 80 °C. In the HFMC test, materials are considered compatible if the heat generated from reactive interactions remains below a threshold during the defined standard assessment period of 10.6 days. Measurements were extended to 15 days to ensure the detection of slow or delayed exothermic reactions. While a general compatibility limit of 30 J/g is widely accepted for nitrocellulose (NC)-based energetic materials, no universal threshold exists for other classes of energetic compounds. More recently, a threshold of 1% of the heat of explosion of the mixture has been proposed and is now included in STANAG 4147.19 Detailed heat flow and reactivity data are provided in the ESI (S5). Based on this criterion, NFPEG3N3 was found to be compatible with HMX and GAP diol, with heat generation well below the threshold. For the ADN, the HFMC threshold was barely met, suggesting borderline compatibility. However, when considered alongside the TG results, the overall findings indicate likely incompatibility according to STANAG 4147.

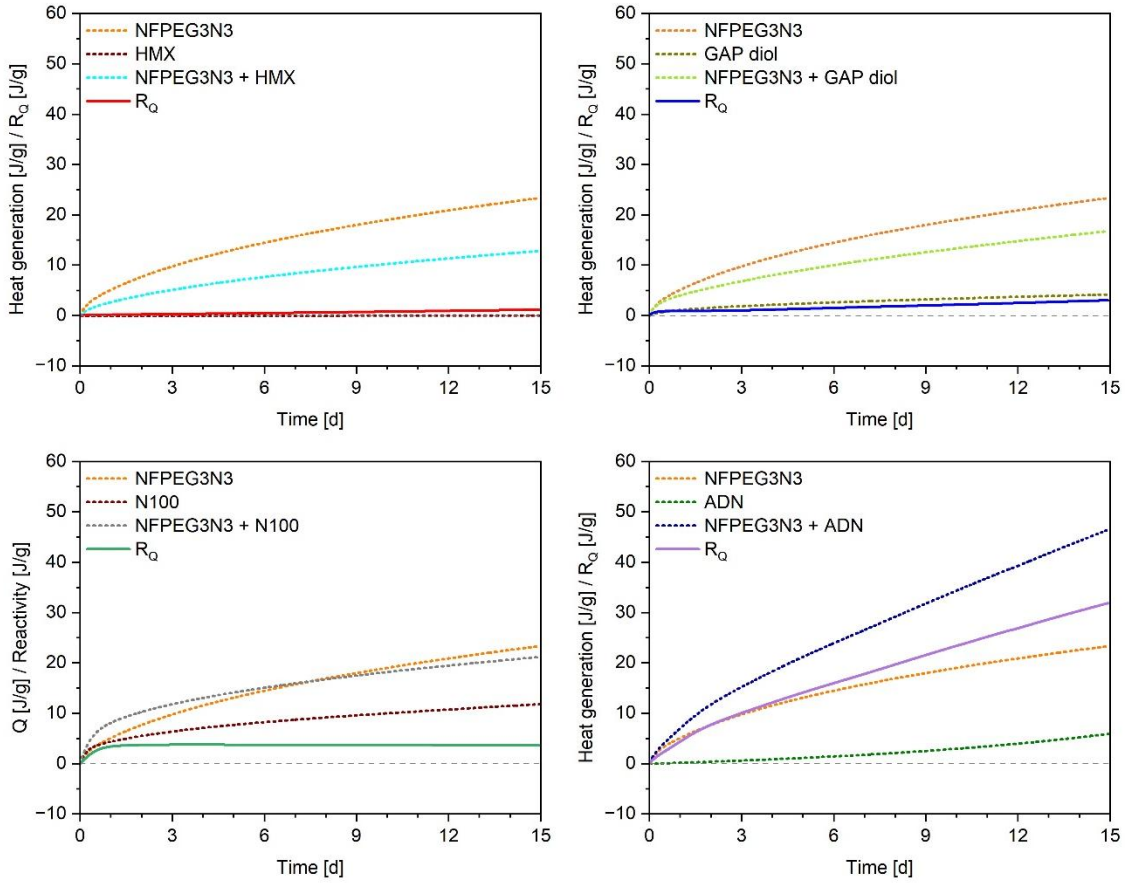

Figure 3 Heat generation data of components and mixtures (1:1 by mass) and the reactivity functions at 80 °C.

One potential solution to this issue could be the use of polymer-coated ADN prills to reduce interactions between the substances.[23,24] In the case of N100, no heat of explosion-based threshold could be calculated due to unavailable thermochemical data. However, the observed heat release was sufficiently low that, when compared with the 30 J/g limit, compatibility can be assumed. Table 2 summarizes the compatibility test results and the corresponding threshold values used in the assessment. The use of untreated ADN with NFPEG3N3 is questionable due to their likely incompatibility. However, NFPEG3N3 has been shown to be suitable for incorporation into high-performance polymer-bonded explosive (PBX) formulations containing GAP diol, N100, and HMX.

Table 2 Summary of compatibility test results and limit values.

Compatibility test	R_Q[a] [J/g] (limit value)[b]	R_W[c] [%] at x °C	Total assessment
Threshold values	-1% of Q_{Ex}< R_Q<1% of Q_{Ex}	R_W<4%	
NFPEG3N3 + HMX	0.80 (38.42)	-10.6 at 175 °C	compatible
NFPEG3N3 + GAP diol	2.24 (32.25)	-17.5 at 172 °C	compatible
NFPEG3N3 + N100	3.67 (30.00[d])	-19.1 at 183 °C	compatible
NFPEG3N3 + ADN	24.46 (41.90)	+5.2 at 158 °C	incompatibility is likely

[a] Reactivity by excess heat generation over 10.6 days at 80 °C measured with HFMC. [b] Limit value of 1% of the heat of explosion of the specified mixture (1:1 weight ratio). [c] Reactivity by excess weight loss at the specified temperature measured with dynamic TG. [d] General limit value for NC-based formulations.[20]

4.3.2 Impact of NFPEG3N3 on the thermodynamic performance of a composite propellant

The impact of NFPEG3N3 on the volume-specific impulse of a GAP-based propellant containing ADN as an environmentally friendly oxidizer was evaluated by theoretical calculations. The performance results were compared with those of commonly used energetic plasticizers BDNPA/F and Bu-NENA, as well as the ethylene glycol compound BATEG (S1). The selected formulation contained a total solid filler content of 70wt%, consisting of 58.7wt% ADN and 11.3wt% HMX. The binder and plasticizer together accounted for 30wt% of the composition. In the thermodynamic calculations, up to 20wt% of the GAP binder was replaced by plasticizer. Figure 4 illustrates the impact of the plasticizers on the volume-specific impulse. Replacing 15wt% of GAP with NFPEG3N3 increased the volume-specific impulse by 77 N·s/dm^3, from 3989 N·s/dm^3 to 4066 N·s/dm^3. This represents a significant performance improvement, especially when considering that substituting the same proportion of GAP with a common inert plasticizer as bis(2-ethylhexyl)adipat (DEHA, sometimes also abbreviated as DOA) reduces the volume-specific impulse by 434 N·s/dm^3. Among the energetic plasticizers studied, NFPEG3N3 provided a greater increase in the volume-specific impulse than BATEG and Bu-NENA. Although BDNPA/F demonstrated slightly higher performance gains in terms of volume-specific impulse, the benefits of NFPEG3N3, particularly in terms of its favorable thermal stability, remain substantial. Tabulated values for all calculated volume and mass-specific impulses are provided in the ESI (S6). Table 3 provides a more detailed comparison of the thermodynamic performance of

formulations containing 10wt% of the evaluated energetic plasticizers. The formulation incorporating NFPEG3N3 exhibits a lower mass-specific impulse compared to those containing BDNPA/F or Bu-NENA, but a higher one than the formulation with BATEG. It also displays a more favorable oxygen balance than those with BATEG or Bu-NENA. Although the BDNPA/F-based formulation shows the highest overall performance parameters, previous studies have indicated that BDNPA/F is relatively ineffective at reducing the glass transition temperature and viscosity of GAP diol.[16,25,26] Because of its greater effect on the volume-specific impulse, the formulation with NFPEG3N3 is better suited for near-surface applications. This is particularly important in scenarios where compact propulsion systems are required to minimize air resistance, and performance per unit volume is a critical design parameter.

Table 3 Calculated thermodynamic performance of composite propellants consisting of 58.7wt% ADN, 11.3wt% HMX, 20wt% GAP and 10wt% energetic plasticizers at an expansion ratio of 70:1.

Plasticizer [Type]	I_{sp}[a] [N s/kg] / [s]	V_{sp}[b] [N·s/dm³]	ϱ[c] [g/cm³]	T_c[d] [°C]	T_a[e] [°C]	OB[f] [%]
BDNPA/F	2490 / 253.8	4081	1.64	2984	1291	-17.3
Bu-NENA	2481 / 252.9	4001	1.61	2880	1218	-22.0
BATEG	2458 / 250.6	3933	1.15	2806	1165	-24.3
NFPEG3N3	2477 / 252.5	4043	1.63	2921	1241	-20.4

[a] Mass-specific impulse. [b] Volume-specific impulse. [c] Formulation density. [d] Chamber temperature. [e] Nozzle temperature. [f] Oxygen balance.

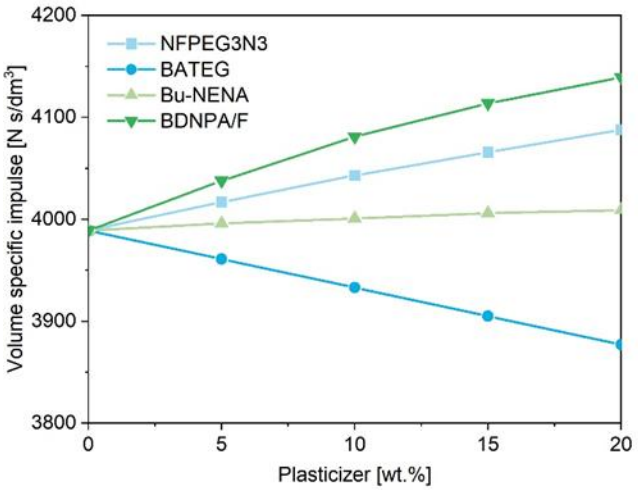

Figure 4 Impact of plasticizers on the volume-specific impulse of GAP-based propellants containing HMX and ADN.

4.4 Conclusion

NFPEG3N3 is compatible with GAP diol, HMX, and Desmodur N100 by HFMC and TG in accordance with STANAG 4147. For N100, a heat of explosion-based threshold could not be defined, but the measured heat release was well below the widely used 30 J/g limit. The NFPEG3N3-ADN pair met the HFMC threshold set at 1% of the mixture's heat of explosion but failed dynamic TG (5.2% excess mass loss), indicating likely long-term thermal incompatibility with untreated ADN. Thermodynamic calculations for a representative ADN/HMX/GAP propellant show that replacing 15wt% of GAP with NFPEG3N3 increases the volume-specific impulse by 77 $N \cdot s/dm^3$ and improves oxygen balance relative to Bu-NENA, identifying NFPEG3N3 as a competitive energetic plasticizer where volume efficiency is critical. These results justify advancing NFPEG3N3 to cured-formulation studies that avoid direct contact with untreated ADN or apply mitigation strategies (e.g., polymer coated ADN prills), alongside extended HFMC and aging at multiple temperatures and mechanical property evaluation. Overall, NFPEG3N3 offers a favorable balance of compatibility with key components and performance potential, warranting further development for GAP-based PBX and propellant applications under appropriately controlled component selections.

4.5 Experimental

4.5.1 Materials

Desmodur N100, a commercial trifunctional isocyanate hardener for polyurethane coating systems, was obtained from Covestro Deutschland AG, Germany. GAP diol (charge 06S15) was purchased from Eurenco, France. HMX Grade B was obtained from Eurenco Bofors AB, Sweden. Prills of ADN (charge P95) were obtained from the Swedish Defense Research Agency (FOI).[22]

4.5.2 Synthesis

NFPEG3N3 was synthesized at Fraunhofer ICT in accordance with the literature.[16]

4.5.3 Characterization methods

Dynamic thermogravimetry (TG) was performed under a nitrogen flow of 25 ml/min using a Discovery 5500 TG system from TA Instruments (subsidiary of Waters

Corporation, USA) and platinum pans. The samples were quickly heated to 50 °C at a rate of 10 °C/min, and then to 500 °C at a rate of 2 °C/min. Samples of 1 mg were measured for pure substances. Mixtures (1:1 ratio by weight) were measured as 2 mg samples. Heat-flow microcalorimetry (HFMC) was performed using a TAM (Thermal Activity Monitor) Type III from TA Instruments (subsidiary of Waters Corporation, USA). The instrument was originally developed by Thermometric AB, Sweden.[27] Samples of 1 g were filled into a glass vial, which was placed inside an air-filled 4 ml stainless-steel ampoule. The steel ampoule was closed tightly and placed into the measuring device, which was submerged in an oil bath under isothermal conditions. The measurements were conducted at 80 °C for a 15-day test period.

4.5.4 Thermodynamic calculations

The heat of explosion of the investigated mixtures was calculated with the ICT thermodynamic code in constant-volume mode.[28] The loading density was set to $\Delta = 0.1$, and the temperature freeze-out threshold for the water-gas equilibrium was set to T = 1500 K. As water is present primarily as vapor at the testing temperature of 80 °C, it was assumed to be in its gaseous state in the calculations. The performance of composite propellant formulations was calculated with the ICT thermodynamic code in constant-pressure mode using an expansion ratio of 70:1 and frozen-equilibrium values. The thermochemical parameters of GAP diol, HMX, ADN, and bis(2-ethylhexyl)adipat (DEHA, sometimes also abbreviated as DOA) were obtained from the ICT thermodynamic code's internal database.

4.6 Data availability

The data supporting this article, including molecular structures, dynamic TG curves, tabulated results of the HFMC compatibility test, tabulated values for the specific impulses, and SEM images of ADN P95 have been included as part of the ESI (S1-S6).

4.7 Acknowledgment

The authors gratefully acknowledge Dr. M. Heil for his valuable guidance and support throughout this study. We thank H. Schuppler for performing the TG measurements, M. Schäfer for assisting with the synthesis of NFPEG3N3 and its precursors, T. Grunwald

for conducting the HFMC measurements, and C. Seidel for providing the scanning electron microscopy (SEM) images. Financial support from WTD91 of the German Ministry of Defense is also gratefully acknowledged.

4.8 References

1 S. Hafner, V. A. Hartdegen, M. S. Hofmayer and T. M. Klapötke, Potential Energetic Plasticizers on the Basis of 2,2-Dinitropropane-1,3-diol and 2,2-Bis(azidomethyl)propane-1,3-diol, Propellants, Explos., Pyrotech., 2016, 41, 806–813.

2 D. Kumari, K. D. B. Yamajala, H. Singh, R. R. Sanghavi, S. N. Asthana, K. Raju and S. Banerjee, Application of Azido Esters as Energetic Plasticizers for LOVA Propellant Formulations, Propellants, Explos., Pyrotech., 2013, 38, 805–809.

3 L. A. Wingard, E. C. Johnson, P. E. Guzmán, J. J. Sabatini, G. W. Drake, E. F. C. Byrd and R. C. Sausa, Synthesis of Biisoxazoletetrakis(methyl nitrate): A Potential Nitrate Plasticizer and Highly Explosive Material, Eur. J. Org. Chem., 2017, 2017, 1765–1768.

4 H. G. Ang and S. Pisharath, Energetic polymers. Binders and plasticizers for enhancing performance, Wiley-VCH-Verl., Weinheim, 1st edn., 2012.

5 Y. Zhao, X. Zhang, W. Zhang, H. Xu, W. Xie, J. Du and Y. Liu, Simulation and Experimental on the Solvation Interaction between the GAP Matrix and Insensitive Energetic Plasticizers in Solid Propellants, J. Phys. Chem. A, 2016, 120, 765–770.

6 M. F. Lemos and M. A. Bohn, DMA of polyester-based polyurethane elastomers for composite rocket propellants containing different energetic plasticizers, J. Therm. Anal. Calorim., 2018, 131, 595–600.

7 T. M. Klapötke, Chemistry of high-energy materials, De Gruyter, Berlin, Boston, 6th edn., 2022.

8 T. Keicher, U. Schaller and V. Gettwert, BATEG - ein vielversprechender neuer Weichmacher, Fraunhofer ICT, 2015.

9 F. Alvarez, N. V. Latypov, E. Holmgren and M. Wanhatalo, New Ingredients for CMDB Propellants, In Proceedings of the 11th Seminar on New Trends in Research of Energetic Materials (NTREM), 2008, 442–447.

10 J. Li, Y. Liu, W. Ma, T. Fei, C. He and S. Pang, Tri-explosophoric groups driven fused energetic heterocycles featuring superior energetic and safety performances outperforms HMX, Nat. Commun., 2022, 13, 5697.

11 M. A. Roux, M. Zeller, E. F. C. Byrd and D. G. Piercey, Synthesis and characterization of the energetic 5,7-diamino-2-nitro-1,2,4-triazolo[1,5-a]-1,3,5-triazine, Propellants, Explos., Pyrotech., 2023, 48. DOI: 10.1002/prep.202300125.

12 Z. Xu, G. Cheng, H. Yang, X. Ju, P. Yin, J. Zhang and J. M. Shreeve, A Facile and Versatile Synthesis of Energetic Furazan-Functionalized 5-Nitroimino-1,2,4-Triazoles, Angew. Chem., 2017, 129, 5971–5975.

13 L. L. Fershtat and N. N. Makhova, 1,2,5-Oxadiazole-Based High-Energy-Density Materials: Synthesis and Performance, ChemPlusChem, 2020, 85, 13–42.

14 T. S. Hermann, T. M. Klapötke, B. Krumm and J. Stierstorfer, Synthesis, Characterization, and Properties of Di- and Trinitromethyl-1,2,4-Oxadiazoles and Salts, Asian J. Org. Chem., 2018, 7, 739–750.

15 W.-L. Cao, Q.-N. Tariq, Z.-M. Li, J.-Q. Yang and J.-G. Zhang, Recent advances on the nitrogen-rich 1,2,4-oxadiazole-azoles-based energetic materials, Def. Technol., 2022, 18, 344–367.

16 P. Lieber, U. Schaller and T. M. Klapötke, Synthesis and characterization of novel nitrofurazanyl ethers as potential energetic plasticizers, RSC Adv., 2025, 15, 12577–12584.
17 K. Menke, T. Heintz, W. Schweikert, T. Keicher and H. Krause, Formulation and Properties of ADN/GAP Propellants, Propellants, Explos., Pyrotech., 2009, 34, 218–230.
18 S. Ek, J. Johansson, M. Brantlind, H. Ellis and M. Skarstind, Synthesis and characterisation of tri- and tetraethyleneglycoldiazide for their use as energetic plasticisers, In Proceedings of the 22nd Seminar on New Trends in Research of Energetic Materials (NTREM), 2019, 81–87.
19 M. A. Bohn, M. Heil, H. Pontius and E.-C. Koch, Insensitive high explosives: VI. experimental determination of the chemical compatibility of nitroguanidine with seven high explosives, Propellants, Explos., Pyrotech., 2024, 49. DOI: 10.1002/prep.202300055.
20 North Atlantic Treaty Organization (NATO) STANAG 4147 Edition 3, Chemical compatibility of ammunition components with explosives (non-nuclear applications), 2023.
21 A. Imiolek, W. Becker, K. Sachsenheimer and V. Weiser, In-situ Characterization of Curing Reaction of GAP and Isocyanates by Near Infrared Spectroscopy, Fraunhofer ICT, 2016.
22 A. Larsson and N. Wingborg, in Advances in Spacecraft Technologies, ed. J. Hall, IntechOpen, Rijeka, Croatia, 2011, pp. 139–156.
23 T. Heintz and M. J. Herrmann, Properties and Structure of ADN-Prills, Propellants, Explos., Pyrotech., 2019, 44, 679–686.
24 T. Heintz, H. Pontius, J. Aniol, C. Birke, K. Leisinger and W. Reinhard, Ammonium Dinitramide (ADN)–Prilling, Coating, and Characterization, Propellants, Explos., Pyrotech., 2009, 34, 231–238.
25 S.-M. Shen, A.-L. Leu, S.-I. Chen and H.-C. Yeh, Thermal characteristics of GAP, GAP/BDNPA/BDNPF and PEG/BDNPA/BDNPF and the energetic composites thereof, Thermochim. Acta, 1991, 180, 251–268.
26 A. Edgar, J. Yang, M. Chavez, M. Yang and D. Yang, Physical characterization of Bis(2,2-dinitropropyl) acetal and Bis(2,2-dinitropropyl) formal, J. Energ. Mater., 2020, 38, 483–503.
27 J. Suurkuusk, M. Suurkuusk and P. Vikegard, A multichannel microcalorimetric system, J. Therm. Anal. Calorim., 2018, 131, 1949–1966.
28 S. Kelzenberg, P.-B. Kempa, S. Wurster, M. Herrmann and T. Fischer, New version of the ICT-thermodynamic code, Fraunhofer ICT, 2014.

4.9 Supporting information

S1 Molecular structures of representative energetic plasticizers used as reference compounds.

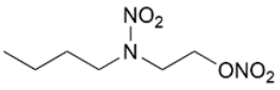

Bu-NENA
N-butyl-N-nitratoethylnitramin

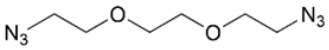

BATEG
1,2-bis(2-azidoethoxy)ethane

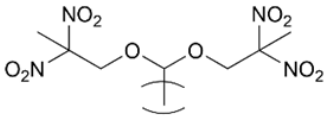

BDNPA/F
bis(2,2-dinitropropyl)acetal/ formal

S2 Repeat units of the prepolymers GAP diol and HTPB.

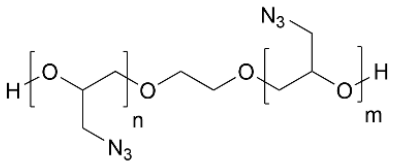

GAP diol
glycidyl azido polymer
diol initiator: ethan-1,2-diol

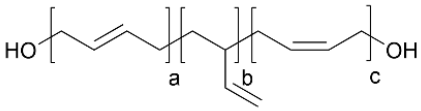

HTPB
hydroxyl-terminated polybutadiene

S3 Scanning electron microscope images of the used spherical prills of ADN.

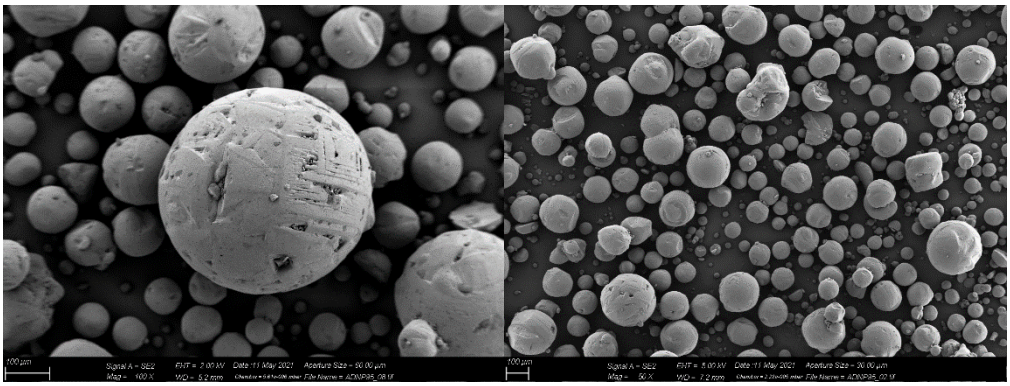

S4 Dynamic thermogravimetry (TG) curves.

Pure compounds

NFPEG3N3, liquid

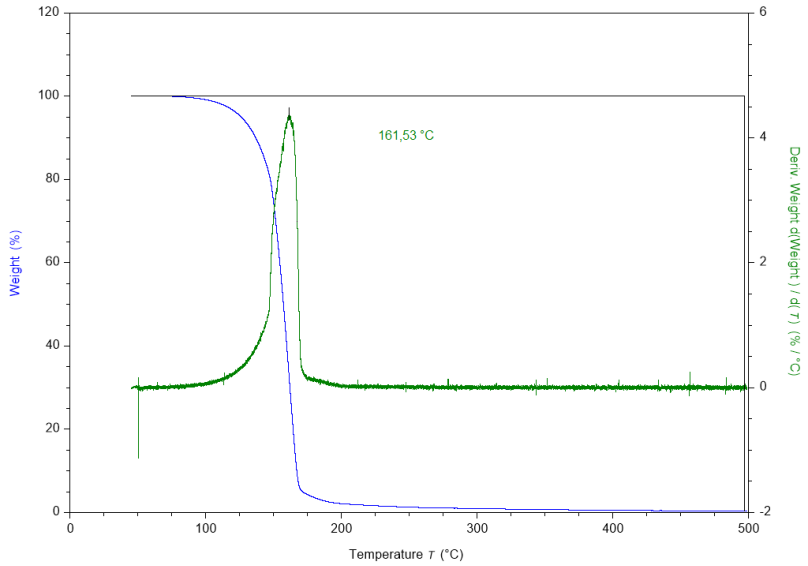

HMX, solid

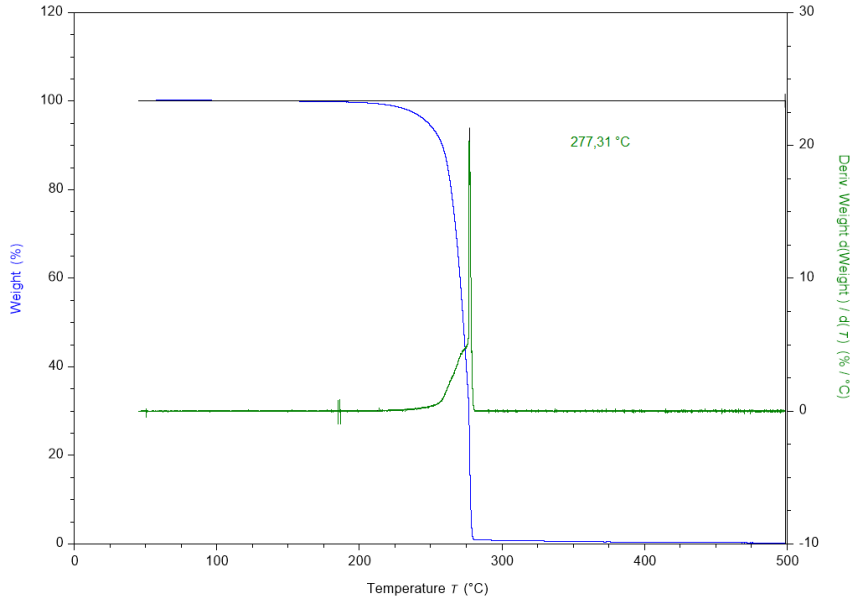

GAP diol, liquid

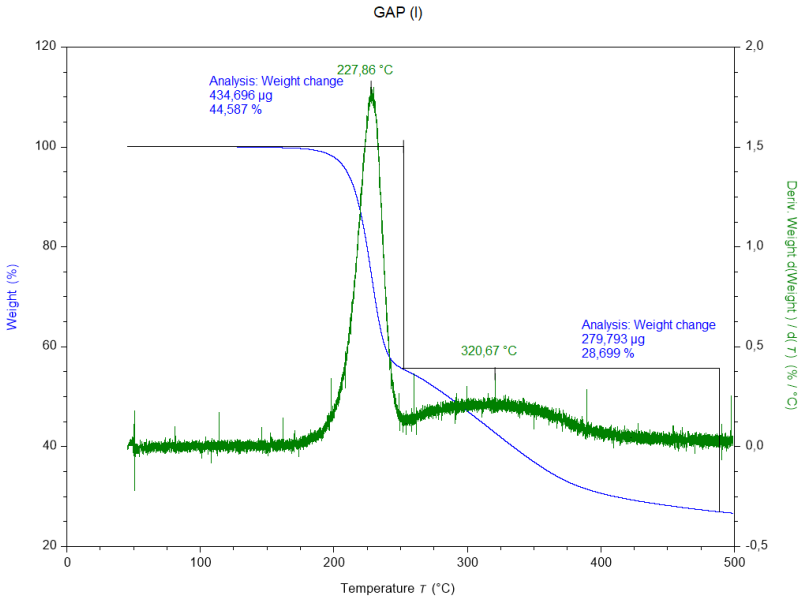

Desmodur N100, liquid

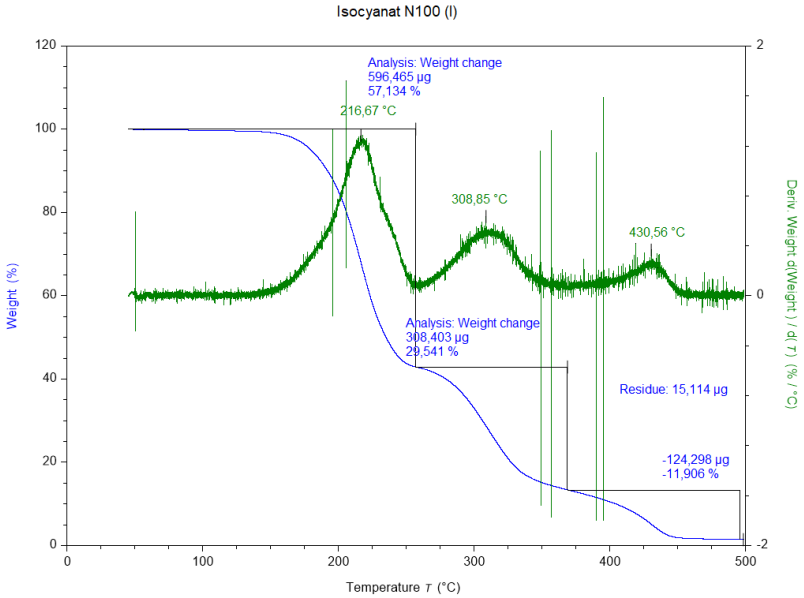

Ammonium dinitramide (ADN), solid

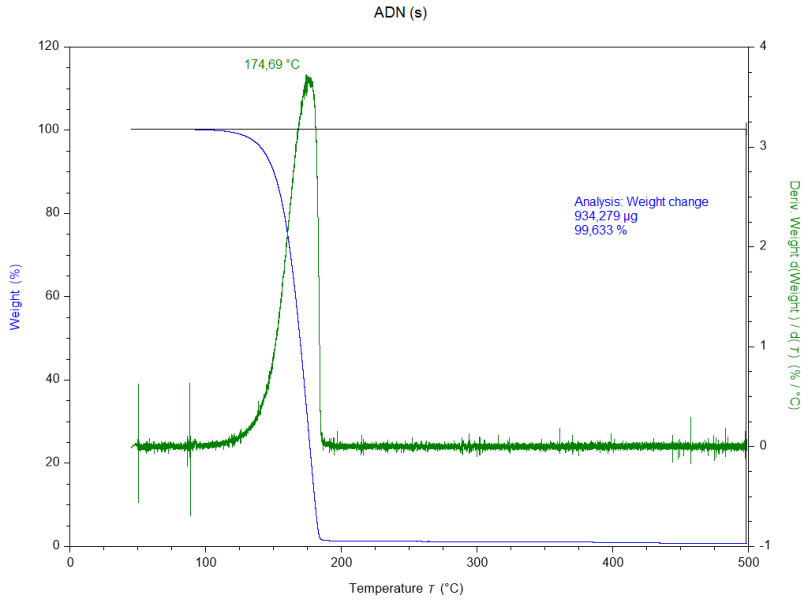

Mixtures

HMX-NFPEG3N3

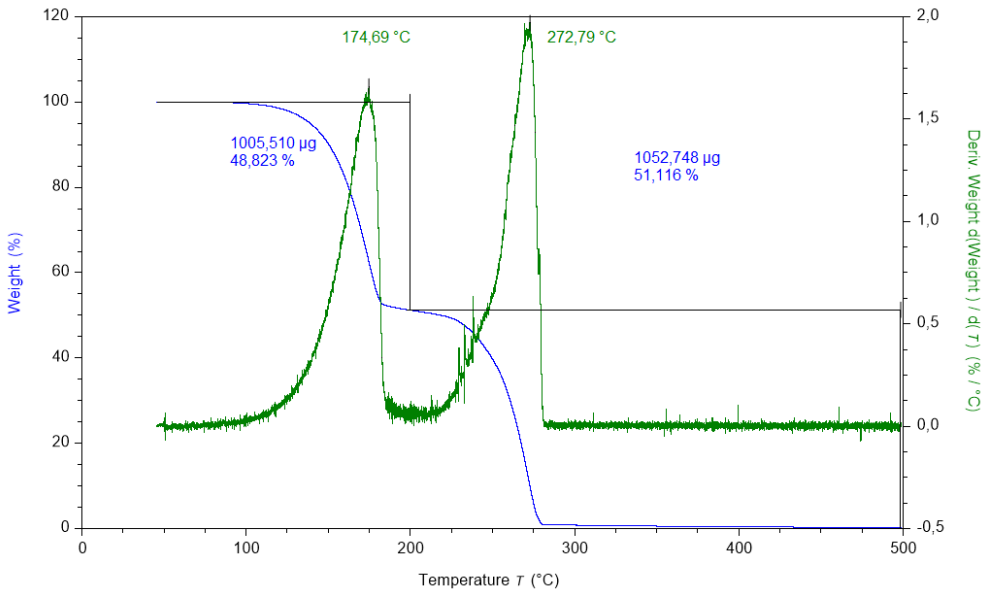

GAP diol-NFPEG3N3

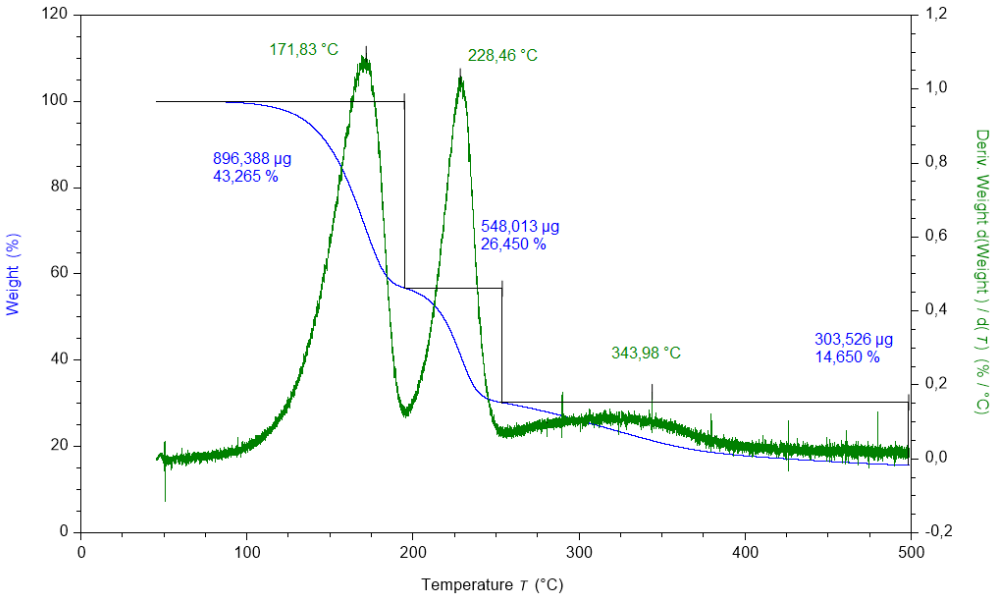

Desmodur N100-NFPEG3N3

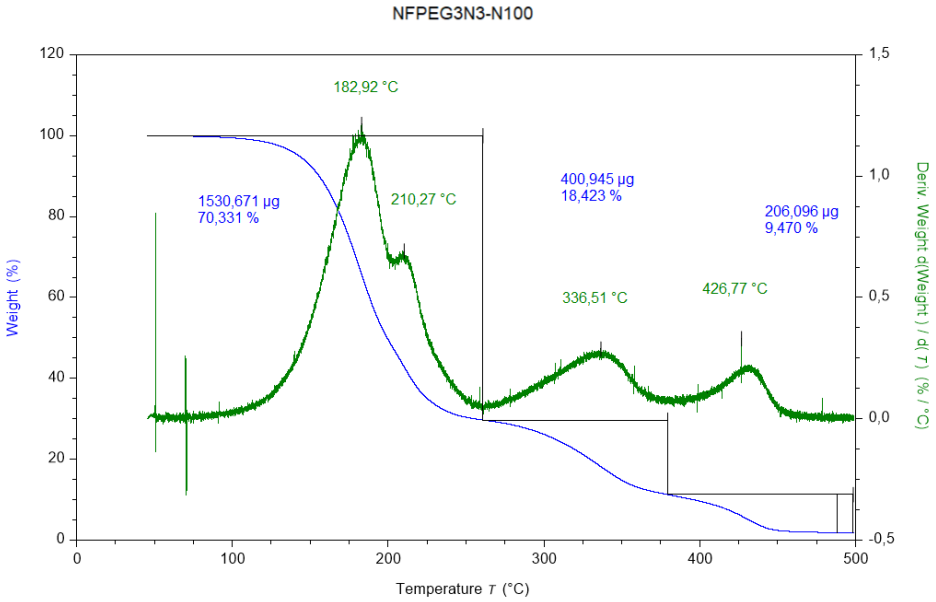

ADN-NFPEG3N3

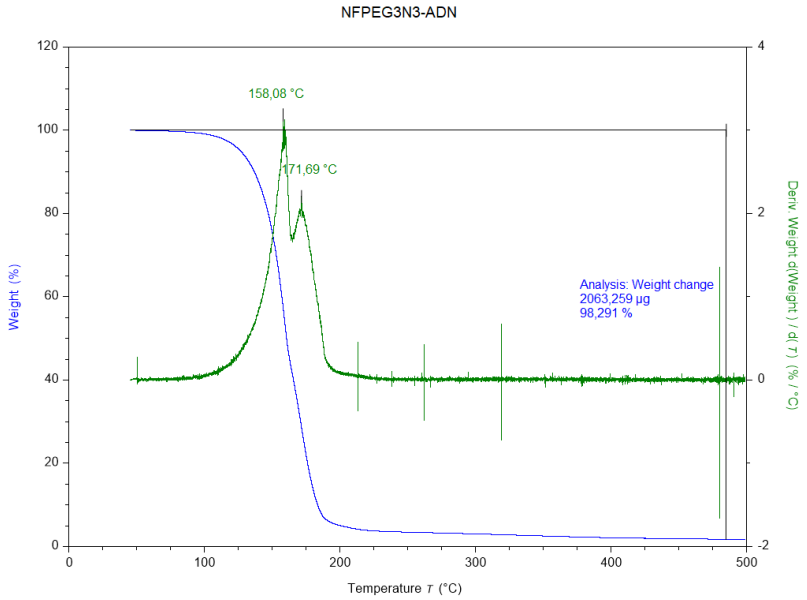

S5 Heat flow and reactivity data of the HFMC compatibility test.

Compound	$Q_{Ex,M}$ [J/g]	1% $Q_{Ex,M}$ [J/g]	Q_C [J/g]	$Q_{NFPEG3N3}$ [J/g]	$Q_{M,calc}$ [J/g]	Q_M [J/g]	Q_R [J/g]	Assmt.
HMX	3842	38.42	-0.03	19.59	9,78	10.57	0.79	ff.
GAP diol	3225	32.25	3.47		11.53	13.77	2.24	ff.
N100	-	30.00*	10.20		14,90	18.57	3.67	ff.
ADN	4190	41.90	3.22		11,41	35.87	24.46	ff.

S6 Mass and volume-specific impulse data of composite propellant formulations (70% filler, 30% binder: GAP + plasticizer) calculated with the ICT thermodynamic code.

Plasticizer content [wt%]	Mass spec. imp. with NFPEG3N3 [N s/Kg]	Mass spec. imp. with BDNPAF [N s/Kg]	Mass spec. imp. with Bu-NENA [N s/Kg]	Mass spec. imp. with BATEG [N s/kg]
0	2456	2456	2456	2456
5	2467	2475	2469	2457
10	2477	2490	2481	2458
15	2486	2499	2493	2459
20	2493	2502	2504	2460

Plasticizer content [wt%]	Volume spec. imp. with NFPEG3N3 [N s/Kg]	Volume spec. imp. with BDNPA/F [N s/Kg]	Volume spec. imp. with Bu-NENA [N s/Kg]	Volume spec. imp. with BATEG [N s/kg]
0	3989	3989	3989	3989
5	4017	4038	3996	3961
10	4043	4081	4001	3933
15	4066	4114	4006	3905
20	4088	4139	4009	3877

5 Comparative assessment of energetic plasticizers including NFPEG3N3 in a GAP/HMX formulation: mechanics, stability, combustion, and performance

Patrick Lieber*, Uwe Schaller, Thomas M. Klapötke

as accepted for publication in: *Propellants, Explosives, Pyrotechnics*

DOI: 10.1002/prep.70095

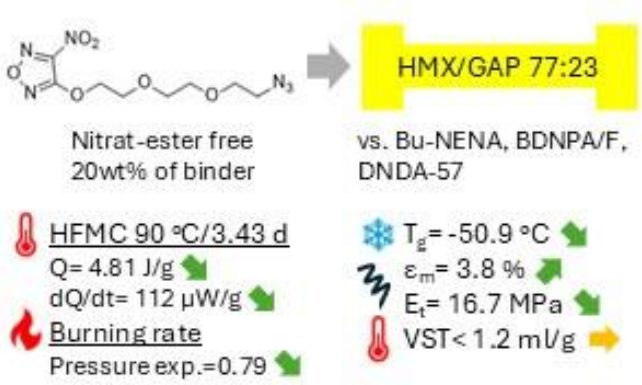

5.1 Abstract

We examine the new energetic plasticizer 3-(2-(2-(2-azidoethoxy)ethoxy)ethoxy)-4-nitro-1,2,5-oxadiazole NFPEG3N3, three reference compounds (BDNPA/F, Bu-NENA and DNDA-57) and a plasticizer-free control in a fixed HMX/GAP composite. NFPEG3N3 provides the strongest low-temperature properties, yielding the lowest formulation glass transition temperature of -50.9 °C. In tensile testing, NFPEG3N3, Bu-NENA, and DNDA-57 show comparable peak strengths (0.36-0.38 MPa), while BDNPA/F is higher (0.50 MPa). NFPEG3N3 achieves the highest ductility (3.8% strain at maximum stress) and the lowest elastic modulus (16.7 MPa), indicating superior compliance without a penalty in peak load capacity relative to the other energetic plasticizers. All formulations meet STANAG referenced stability criteria in vacuum stability, heat-flow microcalorimetry and mass loss. Consistent with its nitrate ester-free structure, NFPEG3N3 exhibits distinctly lower heat release and mass loss than BDNPA/F and Bu-NENA. Burning rate regression shows NFPEG3N3 does not significantly change the

burn rate at 7 MPa, while reducing the Vieille pressure exponent by 16.5% to 0.792. As polymer-bonded explosives DNDA-57 and BDNPA/F yield the highest detonation velocity and pressure, while NFPEG3N3 is slightly above the control in detonation velocity and notably higher in pressure and temperature of detonation. As composite propellants, NFPEG3N3 matches Bu-NENA in mass-specific impulse and exceeds it in volume-specific impulse. Overall, NFPEG3N3 has balanced properties: enhanced toughness, acceptable strength, favorable stability, and improved combustion characteristics. These properties make it a promising alternative to nitrate ester plasticizers in GAP/HMX systems.

5.2 Introduction

Polymer-bonded energetic materials pair crystalline oxidizers, metallic fuels or explosives with a polymeric binder to balance energy, processability, and mechanical integrity. [1] Glycidyl azide polymer (GAP) is a widely used energetic binder whose high nitrogen content and positive heat of formation can enhance performance relative to inert matrices such as hydroxyl-terminated polybutadiene (HTPB). [2] A well-known limitation, however, is GAP's brittleness, especially at low temperatures, which promotes microcracking, debonding, and defect growth under thermal or mechanical loads. [3] Achieving a sufficiently low glass transition temperature (T_g) and adequate strain capacity is therefore essential to preserve structural integrity and predictable ballistic or detonation behavior. Plasticizers are routinely employed to tune the viscoelastic response of cured GAP networks by increasing chain mobility and lowering T_g, thereby improving ductility. [4,5] Plasticizers can contribute to energy release, oxygen balance, and combustion characteristics when they are energetic. Their selection entails trade-offs spanning curing behavior, filler-binder interactions, thermal stability and aging, sensitivity, and effects on burning rate and pressure dependence. Although legacy energetic plasticizers such as BDNPA/F [5,6], Bu-NENA [7], and DNDA-57 [8] have extensive histories of research, nitrate ester functionalities can raise concerns about thermally driven aging and compatibility margins in certain systems. This has motivated interest in nitrate-ester-free energetic plasticizers that provide robust mechanical compliance and storage stability without sacrificing performance. [9]

3-(2-(2-(2-azidoethoxy)ethoxy)ethoxy)-4-nitro-1,2,5-oxadiazole (NFPEG3N3) is a novel energetic plasticizer featuring a nitrofurazanyl and an azide moiety. [10] It has demonstrated compatibility with GAP diol, isocyanate, and Octogen (HMX), suggesting chemical stability in GAP/HMX composites. [11] Despite the central role of plasticizers in GAP-based systems, there are limited comprehensive, side-by-side comparisons that integrate mechanical, thermal, stability, and combustion metrics within a single, fixed formulation. To our knowledge, NFPEG3N3 has not been benchmarked against other energetic plasticizers using this framework.

5.3 Experimental section

5.3.1 Safety statement

All work with energetic materials (HMX, GAP, BDNPA/F, Bu-NENA, DNDA-57, NFPEG3N3) was performed by trained personnel in facilities authorized for explosives handling. Some of the procedures described in this publication, particularly those involving the mixing and curing of formulations, require the use of protective equipment and remote control.

5.3.2 Materials

Desmodur N100 was purchased from Covestro Deutschland AG, Germany. GAP diol (charge 06S15, MW 1814 g/mol, EQ 1228 g/mol, functionality 1.5) was purchased from Eurenco, France. HMX was supplied by Eurenco Bofors AB, Sweden. Dibutyltin dilaurate (D22) was purchased from Sigma-Aldrich. Bu-NENA and BDNPA/F were purchased from Chemring, Sweden. DNDA-57 was obtained from N. D. Zelinsky Institute of Organic Chemistry, Russia.

5.3.3 Synthesis

NFPEG3N3 was synthesized at Fraunhofer ICT according to literature. [10]

5.3.4 Composition

Table 1 shows the detailed composition of the plasticized formulations investigated in this study: NFPEG3N3 (GHX213), BDNPA/F (GHX193), Bu-NENA (GHX196), and DNDA-57 (GHX197), as well as the control formulation without plasticizer (GHX192). After curing the mass of GAP is considered as sum of GAP diol and Desmodur N100.

Table 1 Composition of plasticized and non-plasticized formulations.

Compound	GHX193, 196, 197, 213 Mass [wt%]	GHX192 Mass [wt%]
HMX Grade B Class 3	53.90	53.90
HMX Grade B Class 5	23.10	23.10
Gap Diol 06S15	15.96	19.95
Energetic plasticizer	4.60	-
Desmodur N100	2.44	3.05
D22 (Catalyst)	0.000575	0.000345

5.3.5 Processing

A total of 200 g of all compounds were weighed and mixed in a Resodyne (Butte, MT 59701, USA) LabRAM acoustic mixer at a g-force of 70 g for 750 seconds in a 250 ml vessel. Then, the mixture was degassed at 15 mbar for 180 seconds. During the mixing process, the temperature of the material increased from 22.7 °C to 45.1 °C. The mixture was then poured into molds on a vibrating table. The material was then cured for seven days at 50 °C.

5.3.6 Instruments and methods

Glass transition temperature was determined using a TA Instruments Q1000 differential scanning calorimeter (DSC) and perforated aluminum crucibles. The sample was first cooled to –90 °C and then heated at a rate of 10 °C/min under a nitrogen flow of 25 ml/min. The glass transition temperature was taken as the inflection point of the heat flow curve during the heating cycle.

Mechanical properties of the cured formulations were determined with a ZWICK-Roell UPM 1476 tensile test machine. The mini-dog bone specimens [12] were punched from plates and stored over silica gel desiccant. The measurements were performed at 20 to 23 °C and atmospheric pressure in uniaxial tensile mode with a crosshead speed of 50 mm/min. The effective gauge length of the specimen was 16 mm. The following numbers of specimens could be tested: Thirteen specimens for NFPEG3N3, six for the unplasticized control, six for BDNPA/F, six for Bu-NENA, and seven for DNDA-57. The difference in the number of specimens is due to losses caused by damage during sample preparation.

Burning rates were measured under nitrogen atmosphere. Test samples, in the form of strands measuring 5 × 5 × 120 mm^3, were cut from plates. These samples were burned

in the optical bomb, a high-pressure autoclave equipped with glass windows, allowing for non-intrusive combustion measurements. A detailed outline of the approach is published elsewhere. [13] In this study, a color high-speed camera (Redlake MotionPro X3) and an emission spectrometer (ZEISS MCS 611 NIR 2.2) were employed. The ignition was carried out using ignition paste. Burning rates were derived from video recordings through image post-processing. A total of 9 measurements were performed for the formulation with NFPEG3N3 (three measurements at 3 MPa, one measurement at 5 MPa and 13 MPa and two measurements each at 7 MPa and 10 MPa). Ten measurements were taken for each reference formulation (two measurements each at 3 MPa, 5 MPa, 7 MPa, 10 MPa, and 13 MPa).

Heat-flow microcalorimetry (HFMC) was performed using a TAM (Thermal Activity Monitor) Type III from TA Instruments (subsidiary of Waters Corporation, USA). The instrument was originally developed by Thermometric AB, Sweden. Samples of 1 g were filled into a glass vial, which was placed inside an air-filled 4 ml stainless-steel ampoule. Testing under air conditions is specified in STANAG 4147 to simulate realistic conditions. It introduces oxygen into the test environment, which for example can influence oxidation or corrosion reactions between the explosive and the metal. The steel ampoule was closed tightly and placed into the measuring device, which was submerged in an oil bath under isothermal conditions. The measurements were conducted at 90 °C for a 20-day test period.

Vacuum stability (VST) was estimated by glass sample tubes that were filled with 2.5 g of the test material and connected to a mercury-filled manometer. The mercury served both as a measuring medium and as a seal for the apparatus. The sample tube and the manometer were evacuated, and the ambient temperature and atmospheric pressure were recorded. The sample was then heated to 100 °C and maintained at this temperature for 40 hours. After the heating period, the system was allowed to cool to room temperature. The volume of gas released during the test was determined by measuring the displacement of the mercury column in the manometer. Final ambient temperature and pressure were again recorded. Based on the measured gas volumes and the recorded environmental conditions, the gas volumes were corrected to standard temperature (0 °C) and pressure (1 atm).

Mass loss (ML) samples of 2 g each were stored in glass vials with a diameter of 17 mm (two replicates per formulation). The vials were closed with loosely inserted ground stoppers that were not greased or clamped. The samples were stored in PID-controlled aluminum block ovens. Vial masses were recorded using an analytical balance with a precision of 0.1 mg.

Propulsion performance of the formulations as composite propellants was evaluated using the ICT Thermodynamic Code V2017.1.1 [14] under idealized conditions with a nozzle expansion ratio of 70:1 in the frozen equilibrium mode. During the calculations water was treated as gaseous. Unless otherwise specified, the thermochemical properties of the components were obtained from the ICT database.

Detonation performance of the formulations as PBX was evaluated using Explo5 V6.06 [15] and the BKW EOS at an initial guess temperature of 3600 °C and an initial pressure of 0.1 MPa.

Mechanical sensitivity was estimated with a BAM drop hammer and BAM friction device, in accordance with DIN EN 13631.

5.4 Results and discussion

5.4.1 Composition and processing

To investigate the impact of NFPEG3N3 on an actual energetic formulation for the first time, a GAP-based formulation containing 77wt% HMX filler and 23wt% binder was selected. The HMX consisted of a bimodal mixture of 53.9wt% Grade B Class 3 and 23.1wt% Grade B Class 5. The binder cures to a polyurethane network through the reaction of GAP diol with the trifunctional isocyanate Desmodur N100. The binder comprised 18.4wt% GAP and 4.6wt% plasticizer, with the plasticizer accounting for 20% of the binder content by weight. The composition of the plasticized formulations is shown graphically in Figure 1. This formulation could serve as a weaker explosive charge or as a sustainer stage in a solid rocket motor. It was chosen primarily for its robustness and exemplary nature. In addition to the new nitrofurazanyl plasticizer NFPEG3N3, the well-known energetic plasticizers Bu-NENA, DNDA-57, and BDNPA/F were used to create the reference formulations. A control formulation without plasticizer was also prepared, in which the plasticizer fraction was replaced by GAP. All

formulations were prepared by acoustic mixing and cured at 50 °C. The cured NFPEG3N3 formulation had an impact sensitivity of 15 J and a friction sensitivity of 324 N, enabling the new material to be stamped, cut, or otherwise processed to produce the necessary test specimens for the tensile tests shown in Figure 2.

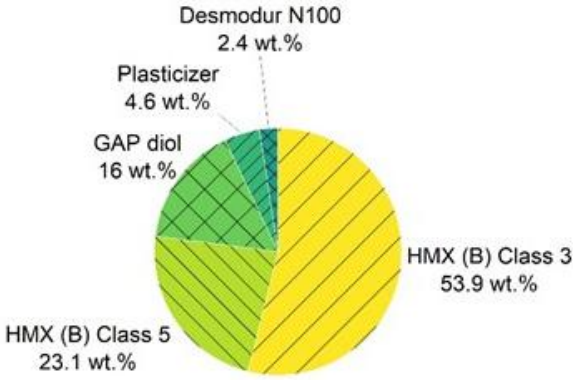

Figure 1 Composition of plasticized formulations investigated.

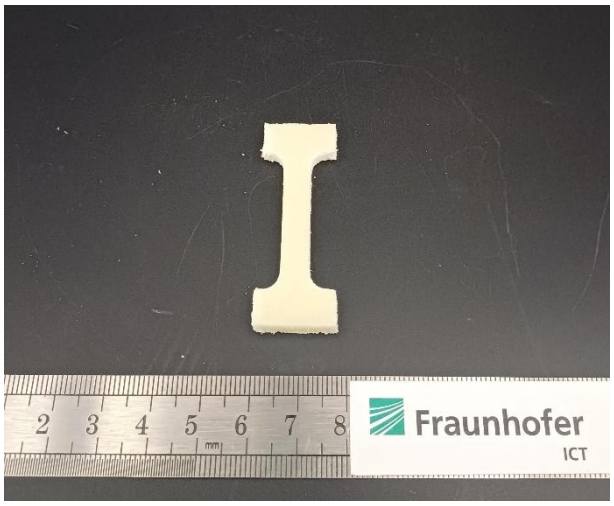

Figure 2 Dog bone specimen of the NFPEG3N3 plasticized formulation.

5.4.2 Mechanical properties

Glass transition temperature

The glass transition temperature (T_g) of the formulation with NFPEG3N3 was measured by DSC to –50.9 °C. The control without plasticizer exhibited a T_g of –36.8 °C. References containing DNDA-57, BDNPA/F, and Bu-NENA showed T_g values of –39.7 °C, –40.3 °C, and –49.3 °C, respectively. Among the tested plasticizers, the formulation with NFPEG3N3 exhibited the lowest T_g, indicating a superior low-temperature plasticization capability of the novel compound. Figure 3 shows a comparison of the measured T_g.

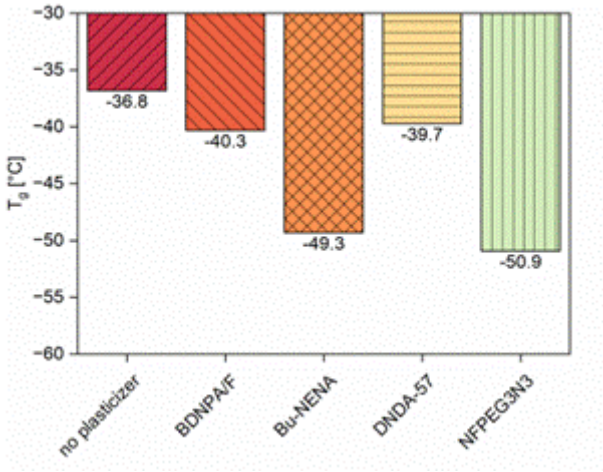

Figure 3 Glass transition temperatures of the investigated formulations.

Tensile test

The mechanical properties of the formulations were evaluated using a tensile testing machine. As expected, the presence of plasticizers led to a reduction in maximum stress compared to the unplasticized formulation (Figure 4). The formulations containing NFPEG3N3, Bu-NENA, and DNDA-57 exhibited similar maximum stress values, ranging from 0.36 to 0.38 MPa. In contrast, the BDNPA/F-containing formulation showed a higher value of 0.50 MPa, indicating it can withstand a greater load before undergoing plastic deformation. All stress-strain curves and detailed data have been added to the supporting information (SI). The strain at maximum stress provides insight into the ductility of a material (Figure 5). A higher value indicates that the material can elongate more before reaching its peak strength. The increase in this parameter reflects the effectiveness of the plasticizer. Among the plasticizers tested, NFPEG3N3 exhibited the strongest plasticizing effect, with an elongation at maximum stress of 3.8%, followed by DNDA-57 (2.9%), Bu-NENA (2.6%), and BDNPA/F (2.1%). The unplasticized sample showed the lowest elongation at only 1.9%. NFPEG3N3 thus demonstrates superior plasticizing performance, enabling greater elongation at comparable maximum stress. Figure 6 shows a plot of these two properties against each other. This is further supported by the formulation's lowest elastic (Young's) modulus of 16.7 MPa, indicating to be the overall most flexible material in the study (Figure 7).

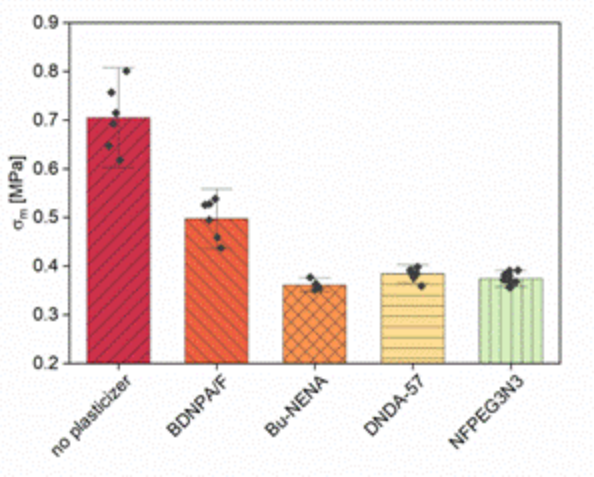

Figure 4 Maximum stress.

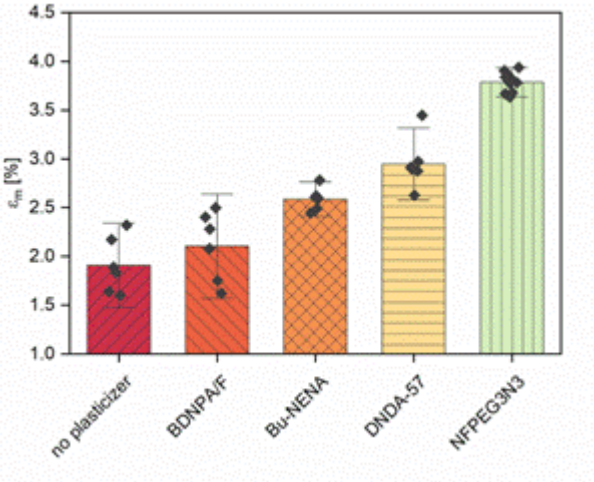

Figure 5 Strain at maximum stress.

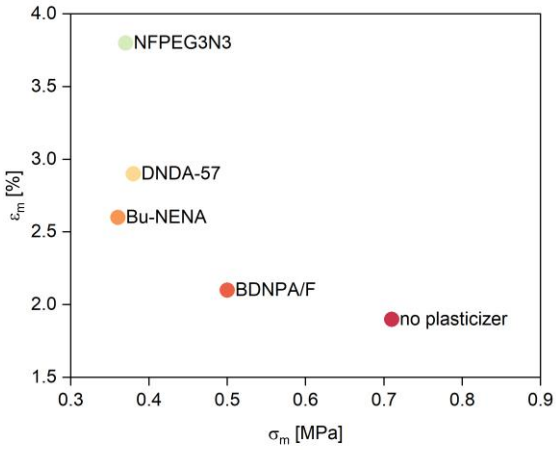

Figure 6 Maximum stress against strain at maximum stress.

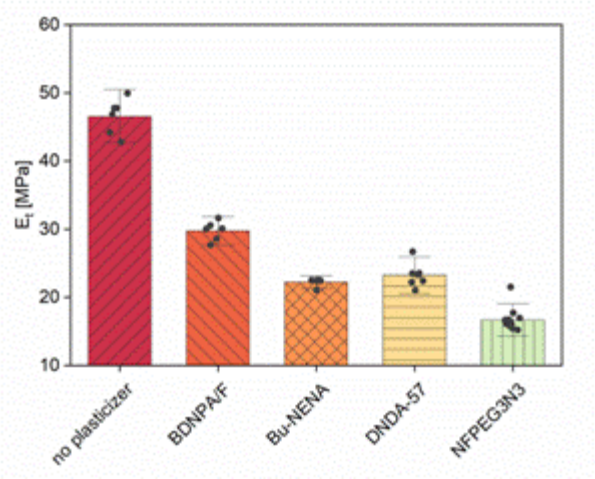

Figure 7 Elastic (Young's) modulus.

5.4.3 Stability

We evaluated the stability of the formulation with NFPEG3N3, as well as references with BDNPA/F and Bu-NENA, and a control without plasticizer, using vacuum stability testing (VST), heat-flow microcalorimetry (HFMC), and mass loss (ML) testing. VST was performed according to STANAG 4556 Ed. 2 [16]. A gas generation limit of 1.2 ml/g over 40 hours at 100 °C was applied, as specified in TL 1376-800 by the German military. HFMC was performed according to STANAG 4582 Ed. 1 [17] with a heat generation limit of 103.8 J/g and a heat flow limit of 350 µW/g over 3.43 days, respectively. [18] For ML the frequently cited limit of 3% over 18 days was used as the basis. [19] It originates from the German military's technical delivery conditions for gun propellants. For the longer investigation period of 21 days in this study, it was extrapolated linearly to 3.5%. An extended measurement period helps to detect slow or delayed gas-forming reactions. As shown in Table 2, all formulations meet the stability requirements in the respective tests.

Table 2 Summary of stability results and limits.

	VST[a]	HFMC[b]		ML[c]
T/ t	100 °C/ 40 h	90 °C/ 3.43 d		90 °C/21 d
Limit	V<1.2 ml/g	Q<103.8 J/g	Max dQ/dt<350 µW/g	ML<3.5%
No plasticizer	0.330	2.04	20	0.13
BDNPA/F	0.450	5.95	140	0.17
Bu-NENA	0.780	20.39	179	0.87
NFPEG3N3	0.630	4.81	112	0.16

[a] Vacuum stability test. [b] Heat-flow microcalorimetry. [c] Mass loss.

The formulation without plasticizers shows the best stability values, as GAP has been replaced by more energy-rich but also more unstable components in the other formulations. In HFMC and ML, NFPEG3N3 performs significantly better than the comparative plasticizers. One advantage could be that, unlike the reference substances, NFPEG3N3 does not contain any aliphatic nitro or nitrate ester groups. In the case of VST, the new formulation is in the area of comparative plasticizers. The heat generation and heat flow curves are shown in Figure 8. HFMC measurements were extended to 20 days to ensure the detection of slow or delayed exothermic reactions. The curve for the formulation with Bu-NENA shows a sharp increase at the beginning and flattens out significantly after one day. It is possible that decomposition products of the nitrate ester compound have already accumulated during the seven-day curing period at 50 °C, which react at the start of the measurement at 90 °C. In all cases, the heat flow is nearly constant and without abnormalities after a short period of time. Figure 9, showing the mass loss over 21 days also reveals the significantly steeper increase in the Bu-NENA-containing formulation.

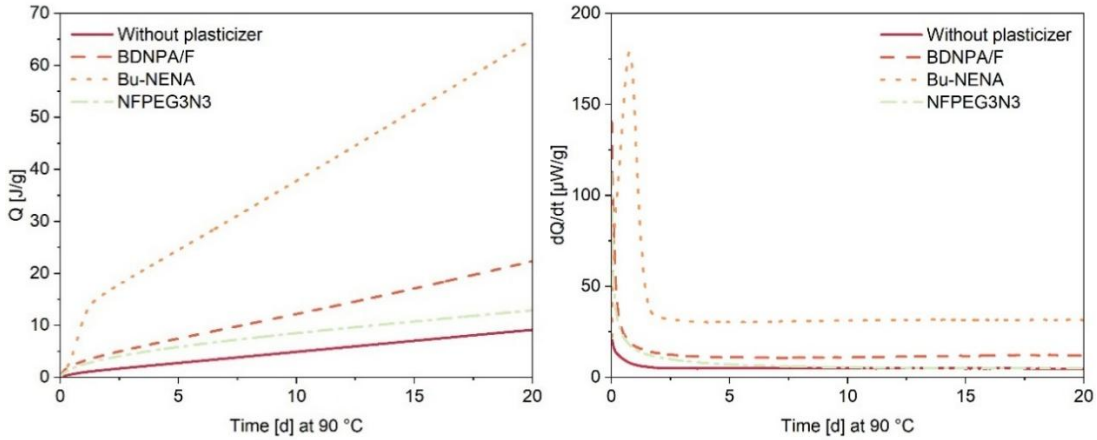

Figure 8 Heat generation (left) and heat flow curves (right) of investigated formulations.

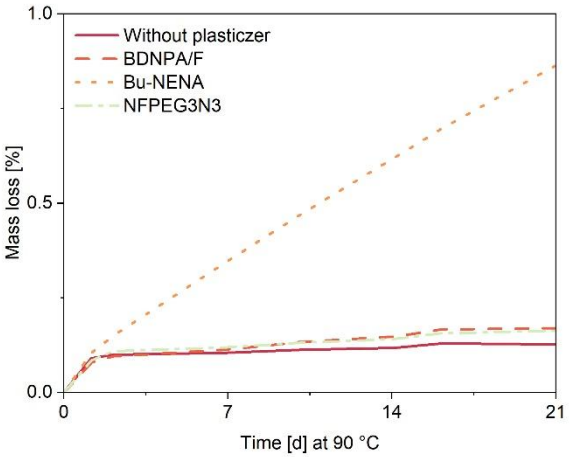

Figure 9 Mass loss curves of investigated formulations.

The results indicate that GAP-based formulations containing NFPEG3N3 and HMX meet the standard thermal stability criteria and are highly likely to be suitable for long-term storage. Additionally, the formulation investigated in this study demonstrates higher thermal stability than the reference samples containing Bu-NENA and BDNPA/F in HFMC and ML investigations.

5.4.4 Performance evaluation

Burning rate

Burning rate measurements were carried out of the formulation with NFPEG3N3 and three reference formulations. The burning rate behavior at a pressure range from 3 MPa to 13 MPa was characterized by the empirical Vieille's law (Equation 1), where n is the dimensionless pressure exponent, r is burn rate, p is pressure, and a is a pre-exponential coefficient. Results are presented in Table 3.

Equation 1 Vieille's burning-rate law.

$$r = a \cdot p^n$$

Table 3 Results of burning rate regression by Vieille's law.

Formulation	r[a] [mm/s] at 7 MPa	n[b]	a[c] [mm/s]	R^{2} [d]
No plasticizer	9.56 ± 1.53	0.948 ± 0.031	0.141 ± 0.020	0.994
BDNPA/F	7.09 ± 0.77	0.859 ± 0.017	0.185 ± 0.015	0.998
Bu-NENA	7.27 ± 1.55	0.940 ± 0.034	0.134 ± 0.021	0.993
NFPEG3N3	9.24 ± 3.12	0.792 ± 0.055	0.319 ± 0.078	0.976

[a] Burn rate from the estimated Vieille parameters at a given pressure. [b] pressure exponent. [c] pre-exponential coefficient. [d] coefficient of determination (COD).

NFPEG3N3 reduced the pressure exponent by 16.5% relative to the control, a larger reduction than BDNPA/F (9%). Bu-NENA has no significant effect on the pressure exponent. BDNPA/F and Bu-NENA reduce the burn rate at 7 MPa, whereas NFPEG3N3 does not cause a significant change. A lower pressure exponent positively impacts stability, robustness, and predictability of performance by making the propellant less sensitive to pressure fluctuations.

Polymer-bonded explosive

Detonation performance of the GAP/HMX formulations was computed using Explo5 V6.06. The calculated parameters are summarized in Table 4. In general, energetic plasticization raises detonation pressure and temperature relative to the inert plasticizers bis(2-ethylhexyl)adipat (DEHA, sometimes also abbreviated as DOA) and the plasticizer-free control. It also shifts the oxygen balance towards neutrality.

Table 4 Detonation performance parameters calculated by Explo5 (PBX composition: 77wt% HMX, 18.4wt% GAP, 4.6wt% plasticizer).

Plasticizer	p[a] [g/cm^3]	D[b] [m/s]	P[c] [GPa]	T[d] [°C]	Q_{CJ}[e] [kJ/Kg]	OB_{CO2}[f] [%]
DEHA	1.68	8037	25.36	3276	-4999	-51.0
without	1.72	8284	27.42	3394	-5180	-44.5
BDNPA/F	1.73	8324	28.14	3438	-5247	-41.6
Bu-NENA	1.71	8268	27.49	3405	-5207	-43.7
DNDA-57	1.72	8330	28.13	3422	-5229	-42.3
NFPEG3N3	1.72	8293	27.79	3413	-5195	-43.0

[a] Theoretical maximum density (TMD). [b] Detonation velocity. [c] Detonation pressure. [d] Detonation temperature. [e] Heat of detonation. [f] Oxygen balance assigned to CO_2.

Among the energetic set, DNDA-57 and BDNPA/F have the highest detonation velocity (8330–8324 m/s) and detonation pressure (approximately 28.13 GPa). This is consistent with their favorable oxygen balance and energy content. NFPEG3N3 yields detonation performance above DEHA and the control in detonation pressure (+0.37 GPa vs control) and temperature of detonation (+19 °C vs control), with detonation velocity slightly above the control (8293 vs 8284 m/s). Bu-NENA is close to the control in detonation velocity and pressure. The magnitude of the heat of detonation Q_{CJ} increases for all energetic plasticizers relative to DEHA and the control, with BDNPA/F showing the largest value. Collectively, these results indicate that NFPEG3N3 delivers appropriate

PBX detonation performance while complementing the mechanical and stability advantages demonstrated elsewhere in this work.

Solid rocket propellant

We calculated the performance of the formulation as a solid rocket propellant using the ICT Thermodynamic Code V2017.1.1. The results are displayed in Table 5. Compared to a formulation without or with an inert plasticizer, NFPEG3N3 increases the mass and volume-specific impulse. Among the energetic plasticizers, mass-specific impulse ranks DNDA-57 ≈ BDNPA/F > Bu-NENA ≈ NFPEG3N3. Volume-specific impulse ranks BDNPA/F ≈ DNDA-57 > NFPEG3N3 > Bu-NENA. Accordingly, NFPEG3N3 matches Bu-NENA in mass-specific impulse, while in volume-specific impulse it clearly surpasses Bu-NENA but remains below BDNPA/F and DNDA-57. Examining the calculated reaction products revealed that none of the evaluated formulations produced condensed reaction products, particularly solid carbon.

Table 5 Propulsion performance parameters calculated by ICT thermodynamic code (propellant composition: 77wt% HMX, 18.4wt% GAP, 4.6wt% plasticizer).

Plasticizer	p[a] [g/cm³]	I_{sp}[b] [s]	V_{sp}[c] [N·s/dm³]	T_c[d] [°C]	T_a[e] [°C]
DEHA	1.68	232.8	3835	2325	851
without	1.72	241.5	4075	2578	975
BDNPA/F	1.73	244.2	4138	2667	1028
Bu-NENA	1.71	243.1	4087	2610	995
DNDA-57	1.72	244.4	4134	2654	1018
NFPEG3N3	1.72	243.0	4110	2630	1004

[a] Theoretical maximum density (TMD). [b] Mass-specific impulse. [c] Volume-specific impulse. [d] Chamber temperature. [e] Nozzle temperature.

5.5 Conclusion

Among the plasticizers investigated, NFPEG3N3 delivered the strongest overall plasticization. It produced the lowest glass transition temperature (–50.9 °C) and the highest ductility (3.8% strain at maximum stress) at comparable strength to Bu-NENA and DNDA-57. These results indicate superior low-temperature compliance and reduced brittleness relative to other energetic plasticizers. As expected, the plasticizer-free control was the most stable. However, NFPEG3N3 showed distinctly lower heat release and mass loss than BDNPA/F and Bu-NENA. The stability advantages of a plasticizer that does not contain aliphatic nitro or nitrate ester groups are evident. All

formulations met the German military standards for gun propellants in terms of VST performance. Combustion testing showed NFPEG3N3 did not significantly change the 7 MPa burn rate versus the plasticizer-free control while reducing the pressure exponent significantly. Relative to BDNPA/F and Bu-NENA, NFPEG3N3 exhibited with approximately 9 mm/s a higher 7 MPa burn rate. The reduced pressure sensitivity with maintained burn rate is favorable for propellant robustness and controllability. Thermochemical modeling indicated that NFPEG3N3 is competitive in mass- and volume-specific impulse with Bu-NENA, though DNDA-57 and BDNPA/F retain an advantage in mass-specific impulse. Overall, NFPEG3N3 offers enhanced low-temperature toughness and favorable aging behavior while maintaining or improving combustion characteristics. This positions NFPEG3N3 as a promising alternative when storage stability and low-temperature handling are priorities.

5.6 Acknowledgment

We thank A. Happ for formulation processing, G. Kronis for specimen preparation and tensile testing, H. Schuppler for DSC measurements, D. Bieroth and P. E. Pietrek for burn rate measurements, C. Müller and T. Grunwald for stability tests and, M. Jung for mechanical sensitivity testing. Financial support from WTD91 of the German Ministry of Defense is also gratefully acknowledged.

5.7 Conflict of Interest

There are no conflicts to declare.

5.8 Data availability statement

The data supporting this article, including detailed tensile test results and DSC curves, have been included as part of the Supporting information (SI).

5.9 References

[1] [1a] R. Meyer, J. Köhler, A. Homburg, Explosives, 7th ed., Wiley-VCH, Weinheim 2016; [1b] J. P. Agrawal, R. D. Hodgson, Organic chemistry of explosives: Theory and evidence, Wiley, West Sussex 2007; [1c] Klapötke, Chemistry of High-Energy Materials, 7th ed.;

[2] H. G. Ang, S. Pisharath, Energetic polymers: Binders and plasticizers for enhancing performance, 1st ed., Wiley-VCH-Verl., Weinheim 2012.

[3] S. Ek, J. Johansson, M. Brantlind, H. Ellis, M. Skarstind, Synthesis and characterisation of tri- and tetraethyleneglycoldiazide for their use as energetic plasticisers, in: Proceedings of the 22nd Seminar on New Trends in Research of Energetic Materials (NTREM) 2019, pp. 81–87.

[4] K. Menke, T. Heintz, W. Schweikert, T. Keicher, H. Krause, Formulation and Properties of ADN/GAP Propellants, Propellants Explos. Pyrotech. 2009, 34, 218–230, https://doi.org/10.1002/prep.200900013.

[5] K. Selim, S. zkar, L. Yilmaz, Thermal characterization of glycidyl azide polymer (GAP) and GAP-based binders for composite propellants, J. Appl. Polym. Sci. 2000, 77, 538–546, https://doi.org/10.1002/(SICI)1097-4628(20000718)77:3<538:AID-APP9>3.0.CO;2-X.

[6] V. Grakauskas, Polynitroalykyl ethers, J. Org. Chem. 1973, 38, 2999–3004, https://doi.org/10.1021/jo00957a017.

[7] K. P. C. Rao, A. K. Sikder, M. A. Kulkarni, M. M. Bhalerao, B. R. Gandhe, Studies on n-Butyl Nitroxyethylnitramine (n-BuNENA): Synthesis, Characterization and Propellant Evaluations, Propellants Explos. Pyrotech. 2004, 29, 93–98, https://doi.org/10.1002/prep.200400035.

[8] R. Vijayalakshmi, N. H. Naik, G. M. Gore, A. K. Sikder, Linear Nitramine (DNDA-57): Synthesis, Scale-Up, Characterization, and Quantitative Estimation by GC/MS, Journal of Energetic Materials 2015, 33, 1–16, https://doi.org/10.1080/07370652.2013.853710.

[9] D. Kumari, K. D. B. Yamajala, H. Singh, R. R. Sanghavi, S. N. Asthana, K. Raju, S. Banerjee, Application of Azido Esters as Energetic Plasticizers for LOVA Propellant Formulations, Propellants Explos. Pyrotech. 2013, 38, 805–809, https://doi.org/10.1002/prep.201300070.

[10] P. Lieber, U. Schaller, T. M. Klapötke, Synthesis and characterization of novel nitrofurazanyl ethers as potential energetic plasticizers, RSC Adv. 2025, 15, 12577–12584, https://doi.org/10.1039/D5RA01282A.

[11] P. Lieber, U. Schaller, T. M. Klapötke, Energetic plasticizers for GAP-based formulations with ADN: compatibility and performance evaluation of a nitrofurazanyl ether, RSC Adv. 2025, 15, 37006–37011, https://doi.org/10.1039/D5RA05154A.

[12] North Atlantic Treaty Organization, AOP-7 Edition 2: Manual of data requirements and tests for the qualification of explosive materials for military use 2003.

[13] [13a] N. Eisenreich, T. S. Fischer, G. Langer, S. Kelzenberg, V. Weiser, Burn Rate Models for Gun Propellants, Propellants Explos. Pyrotech. 2002, 27, 142, https://doi.org/10.1002/1521-4087(200206)27:3<142:AID-PREP142>3.0.CO;2-8; [13b] W. Eckl, N. Eisenreich, Determination of the Temperature in a Solid Propellant Flame by analysis of emission spectra, Propellants, Explos., Pyrotech. 1992, 17, 202–206, https://doi.org/10.1002/prep.19920170411; [13c] W. Eckl, V. Weiser, G. Langer, N. Eisenreich, Burning Behaviour of Nitramine Model Formulations, Propellants, Explos., Pyrotech. 1997, 22, 148–151, https://doi.org/10.1002/prep.19970220309; [13d] N. Eisenreich, H. P. Kugler, F. Sinn, An Optical System for Measuring the Burning Rate of Solid Propellant Strands, Propellants, Explos., Pyrotech. 1987, 12, 78–80, https://doi.org/10.1002/prep.19870120304;

[14] S. Kelzenberg, P. B. Kempa, S. Wurster, M. Herrmann, T. S. Fischer, New Version of the ICT-Thermodynamic Code 2014.

[15] [15a] M. Suceska, M. Dobrilovic, V. Bohanek, B. Stimac, Estimation of Explosive Energy Output by EXPLO5 Thermochemical Code, Anorg. Allg. Chem. 2021, 647, 231–238, https://doi.org/10.1002/zaac.202000219; [15b] M. Sućeska, EXPLO5 V6.06, Zagreb, Croatia 2013;

[16] North Atlantic Treaty Organization, STANAG 4556 Edition 2: Energetic Materials, Vacuum stability test 2024.

[17] North Atlantic Treaty Organization, STANAG 4582 Edition 1: Explosives, nitrocellulose based propellants, stability test procedure and requirements using heat flow calorimetry 2007.
[18] M. A. Bohn, M. Heil, H. Pontius, E.-C. Koch, Insensitive high explosives: VI. experimental determination of the chemical compatibility of nitroguanidine with seven high explosives**, Propellants Explos. Pyrotech., in press, https://doi.org/10.1002/prep.202300055#prep202300055-bib-0025.
[19] M. A. Bohn, Prediction of In-Service Time Period of Three Differently Stabilized Single Base Propellants, Propellants Explos. Pyrotech. 2009, 34, 252–266, https://doi.org/10.1002/prep.200900007.

5.10 Supporting information

Supporting Information

Tensile testing

NFPEG3N3

NFPEG3N3	b	h	A_0	F_{max}	s_m	e_m	s_b	e_b	E_t
	mm	mm	mm²	N	MPa	%	MPa	%	MPa
GHX 213_1	6	5.38	32.280	11.996	0.372	3.666	0.286	6.822	16.251
GHX 213_2	6.02	5.38	32.388	12.377	0.382	3.634	0.305	6.289	21.530
GHX 213_3	6.07	5.34	32.414	12.049	0.372	3.860	0.275	7.783	15.976
GHX 213_4	6.01	5.23	31.432	12.316	0.392	3.936	0.304	7.488	16.949
GHX 213_5	6.03	5.22	31.477	11.904	0.378	3.775	0.293	6.316	15.695
GHX 213_6	6.03	5.34	32.200	11.495	0.357	3.648	0.242	7.406	16.331
GHX 213_7	6.01	5.41	32.514	11.912	0.366	3.679	0.259	7.338	17.695
GHX 213_8	6.05	5.39	32.610	11.994	0.368	3.782	0.314	5.205	15.200
GHX 213_9	6.01	5.15	30.952	11.843	0.383	3.839	0.294	7.785	16.121
GHX 213_10	6.01	5.3	31.853	12.461	0.391	3.830	0.298	6.970	16.129
GHX 213_11	6.02	5.52	33.230	12.382	0.373	3.903	0.312	6.103	16.690
GHX 213_12	6.01	5.12	30.771	11.546	0.375	3.840	0.275	9.010	16.747
GHX 213_13	6.06	5.12	31.027	11.092	0.357	3.808	0.314	5.435	15.450

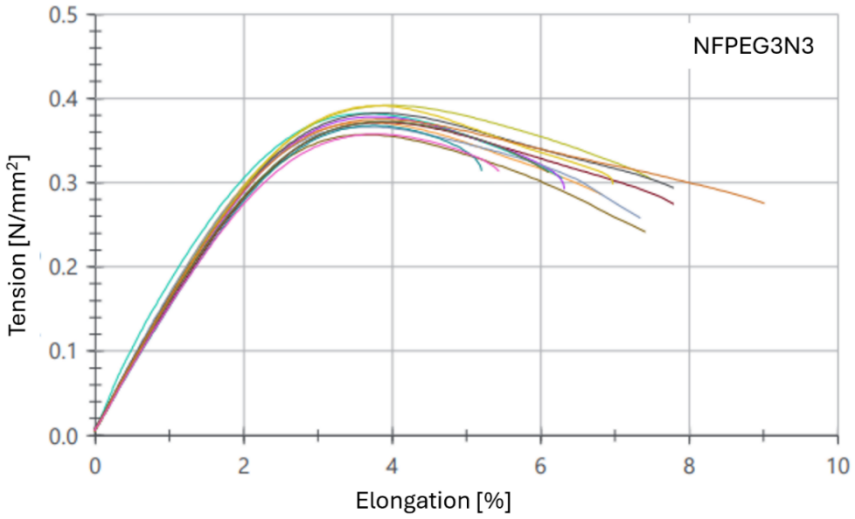

No plasticizer

No plasticizer	b	h	A_0	F_{max}	s_m	e_m	s_b	e_b	E_t
	mm	mm	mm²	N	MPa	%	MPa	%	MPa
GHX192_1	6.01	5.91	35.519	26.884	0.757	2.173	0.740	2.242	46.864
GHX192_2	5.97	5.72	34.148	24.410	0.715	1.833	0.715	1.833	47.752
GHX192_3	5.95	5.7	33.915	23.483	0.692	1.888	0.673	1.943	47.760
GHX192_4	5.99	6.04	36.180	28.994	0.801	2.321	0.779	2.432	49.952
GHX192_5	5.92	6.8	40.256	26.046	0.647	1.640	0.644	1.664	44.196
GHX192_6	6	6.67	40.020	24.726	0.618	1.601	0.618	1.601	42.786

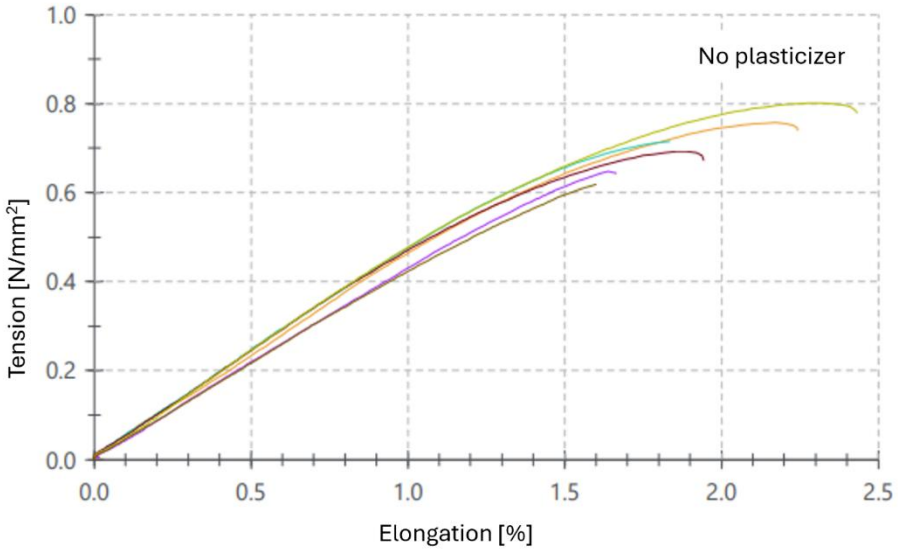

BDNPA/F

BDNPA/F	b	h	A_0	F_{max}	s_m	e_m	s_b	e_b	E_t
	mm	mm	mm^2	N	MPa	%	MPa	%	MPa
GHX193_1	6.05	6.16	37.268	20.067	0.538	2.498	0.496	2.788	28.561
GHX193_2	5.98	5.86	35.043	17.341	0.495	2.079	0.467	2.240	30.538
GHX193_3	5.99	6.05	36.240	16.644	0.459	1.751	0.459	1.751	31.637
GHX193_4	5.98	6.14	36.717	16.077	0.438	1.622	0.429	1.659	30.091
GHX193_5	6.02	6.05	36.421	19.231	0.528	2.282	0.491	2.502	27.698
GHX193_6	5.98	6.06	36.239	19.069	0.526	2.403	0.505	2.569	30.044

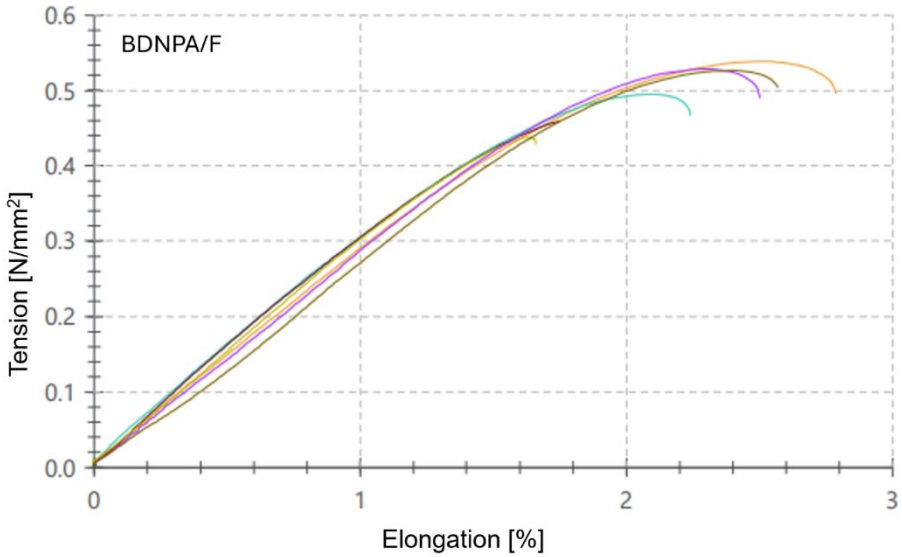

Bu-NENA

Bu-NENA	b	h	A_0	F_{max}	s_m	e_m	s_b	e_b	E_t
	mm	mm	mm²	N	MPa	%	MPa	%	MPa
GHX196_1	5.94	5.07	30.116	10.799	0.359	2.595	0.296	3.776	22.530
GHX196_2	5.93	5.2	30.836	10.952	0.355	2.781	0.274	5.373	22.447
GHX196_3	5.93	5.8	34.394	12.961	0.377	2.447	0.292	3.673	22.505
GHX196_4	5.98	5.23	31.275	10.979	0.351	2.603	0.276	4.612	21.036
GHX196_5	5.93	5.42	32.141	11.694	0.364	2.484	0.277	4.064	22.439
GHX196_6	5.95	5.45	32.428	11.783	0.363	2.622	0.278	4.833	22.498

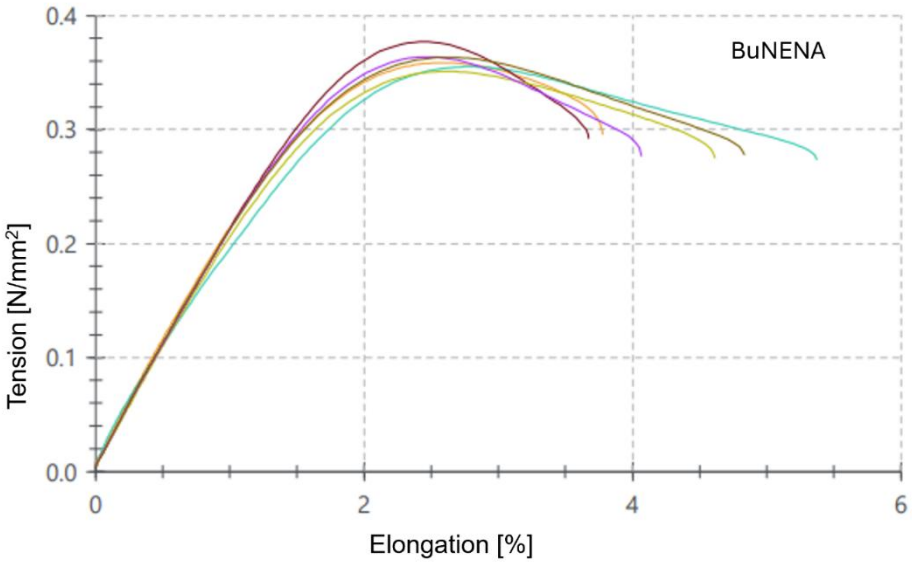

DNDA-57

DNDA-57	b	h	A_0	F_{max}	s_m	e_m	s_b	e_b	E_t
	mm	mm	mm²	N	MPa	%	MPa	%	MPa
GHX197_1	5.95	5.1	30.345	11.676	0.385	2.877	0.353	3.421	23.324
GHX197_2	5.96	5.14	30.634	12.012	0.392	2.914	0.333	4.478	22.220
GHX197_3	5.95	5.28	31.416	12.297	0.391	2.898	0.352	3.774	23.516
GHX197_4	5.98	5.71	34.146	12.864	0.377	2.628	0.358	2.901	21.007
GHX197_5	5.96	5.58	33.257	13.246	0.398	2.971	0.325	4.482	23.539
GHX197_6	5.97	5.48	32.716	11.764	0.360	3.445	0.296	5.960	22.400
GHX197_7	5.94	5.44	32.314	12.467	0.386	2.898	0.330	3.867	26.710

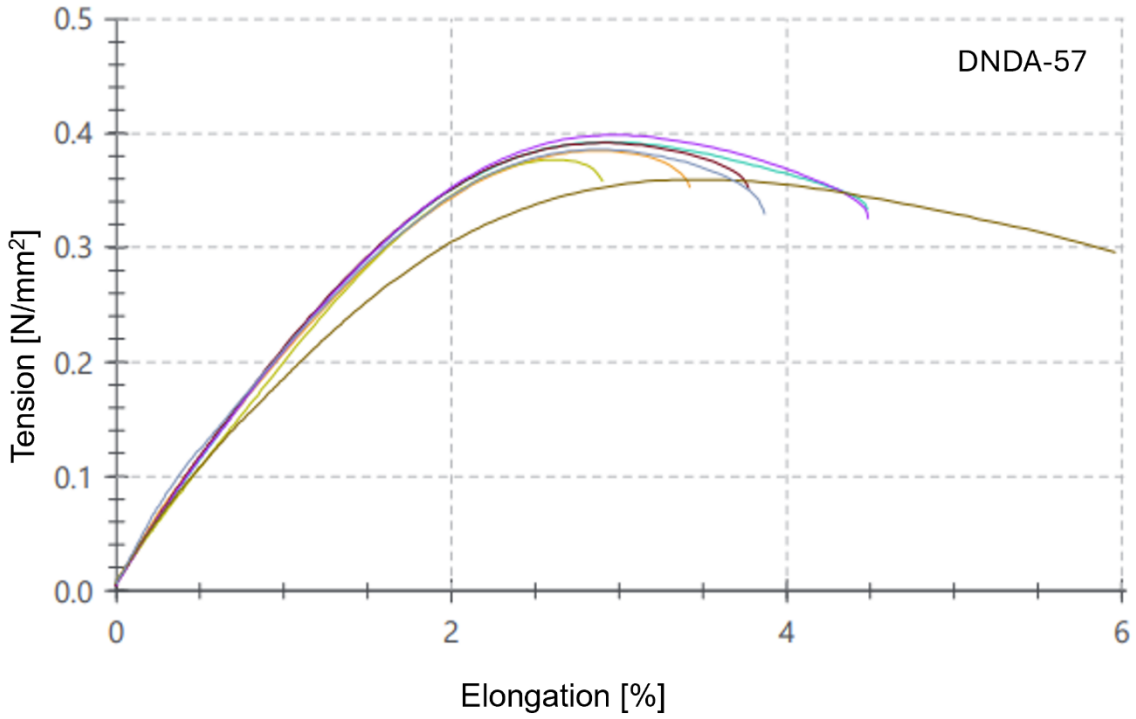

DSC of cured formulations

NFPEG3N3

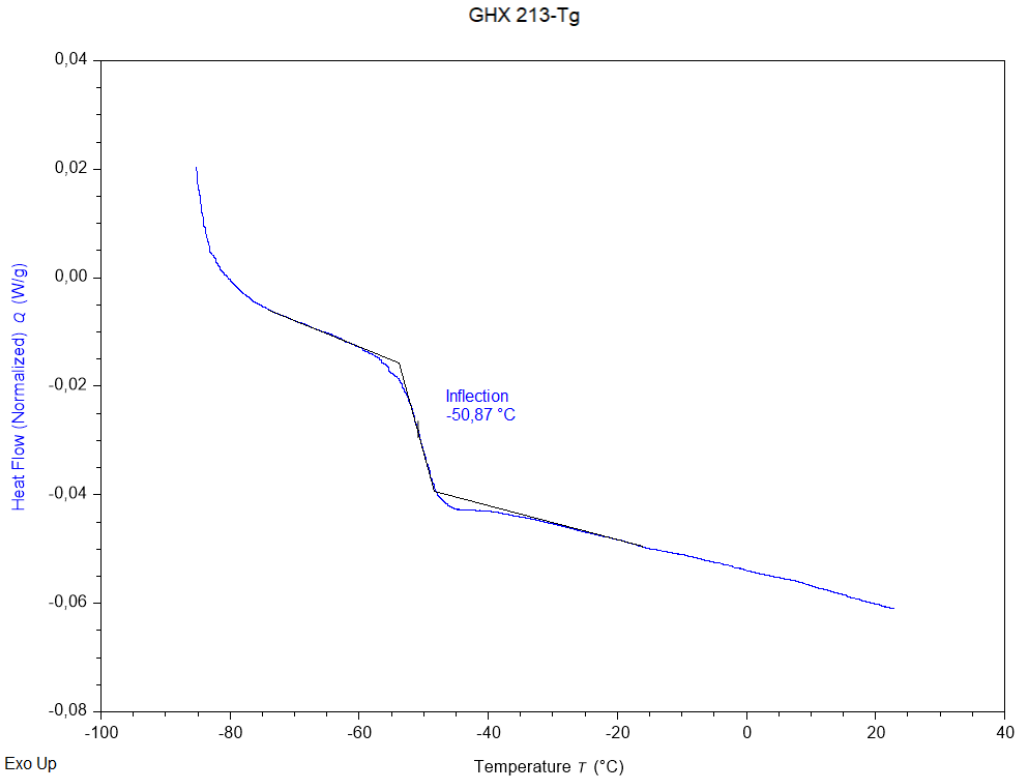

No plasticizer

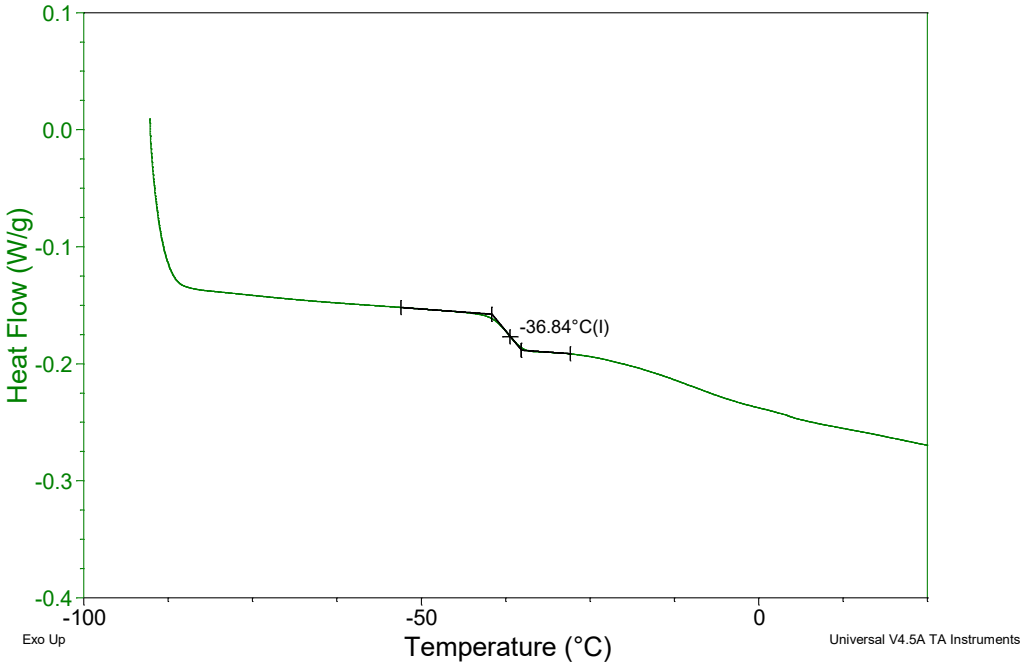

BDNPA/F

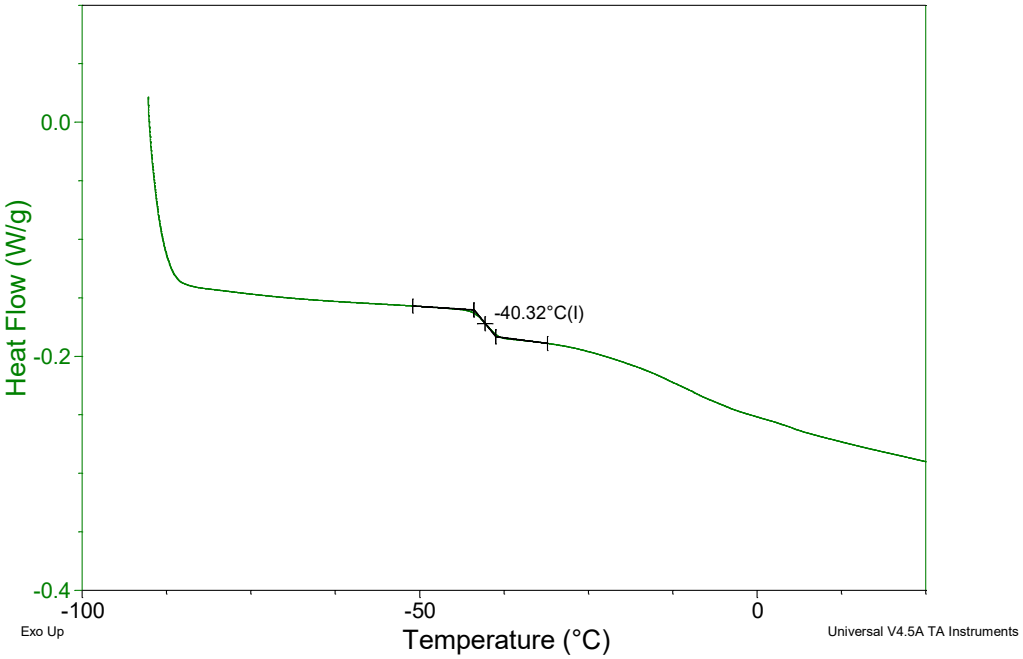

Bu-NENA

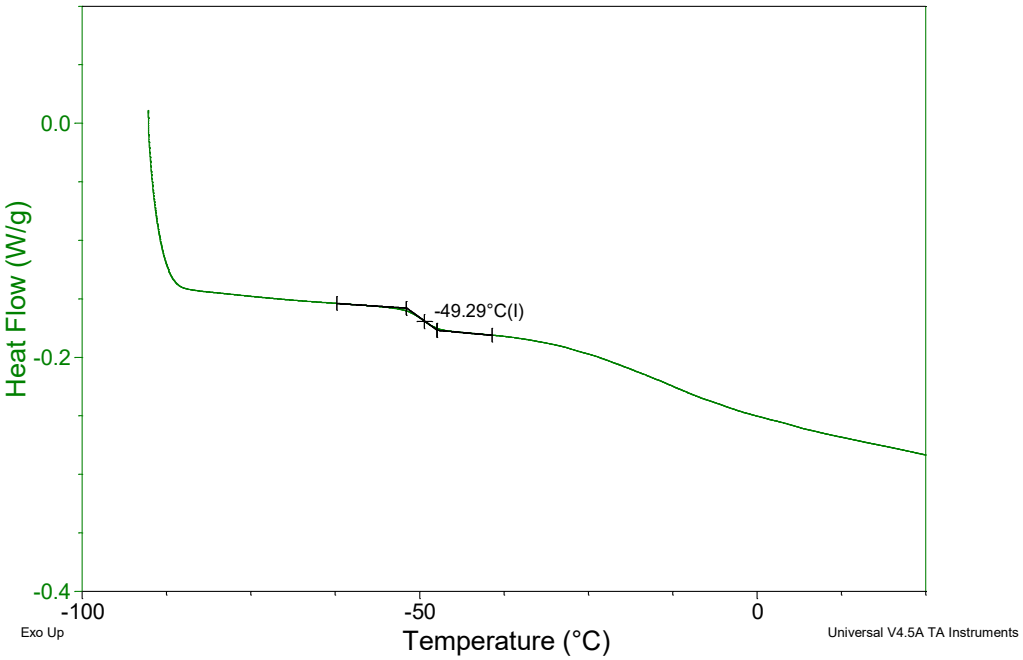

DNDA-57

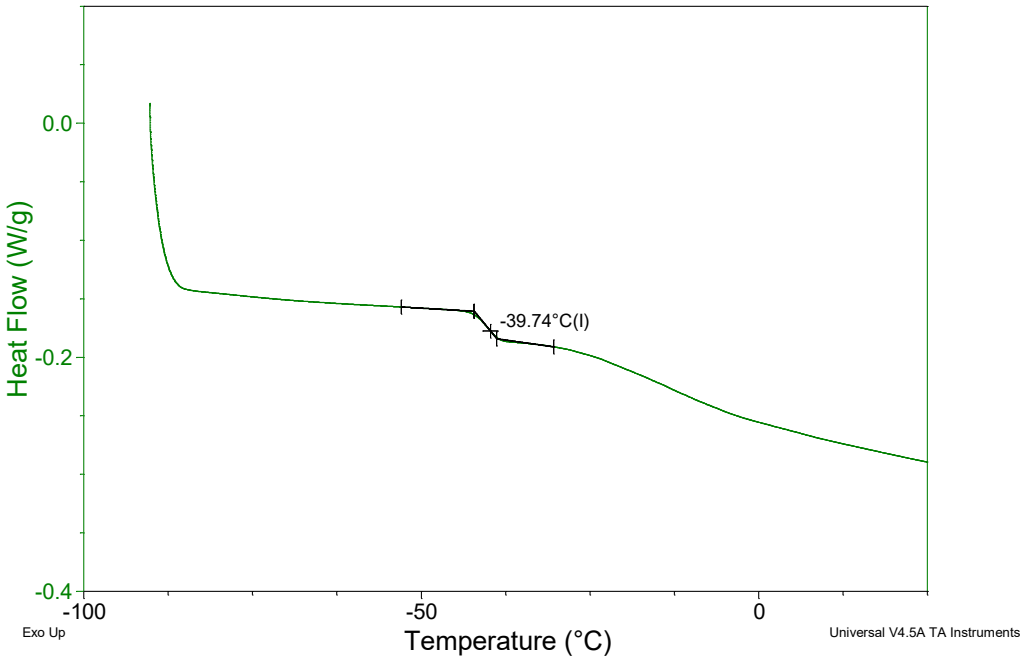
0.0
-0.2
-0.4
Heat Flow (W/g)
-39.74°C(I)
-100
-50
0
Exo Up
Temperature (°C)
Universal V4.5A TA Instruments

6 Synthesis and characterization of an azido nitrofurazanyl ether as energy-rich heterocyclic plasticizer with a low glass transition temperature for GAP and NC formulations

Patrick Lieber*, Andreas Omlor, Uwe Schaller, Thomas M. Klapötke

as submitted to: *Propellants, Explosives, Pyrotechnics*

Manuscript ID 4150638

6.1 Abstract

We report on the synthesis and characterization of 3-(2-(2-azidoethoxy)ethoxy)-4-nitro-1,2,5-oxadiazole (NFPEG2N3), which is a liquid nitrofurazanyl ether that was designed to be an energy-rich plasticizer for GAP- and NC-based formulations. NFPEG2N3 was obtained from 3,4-dinitrofurazan via nucleophilic substitution with lithium 2-(2-azidoethoxy)ethanolate. It was then characterized using ^{1}H and ^{13}C NMR, IR, Raman, elemental analysis, and density measurement (ϱ = 1.375 g/cm^3). The experimental IR bands were assigned with the help of DFT (B3LYP/6-31G*) calculations. Composite methods (CBS-QB3, G4MP2, and G4) were used to determine the enthalpy of formation. NFPEG2N3 exhibits a glass transition temperature (T_g) of -74.9 °C, a thermogravimetric analysis mass-loss midpoint of 156 °C, and a closed-crucible differential scanning calorimetry exotherm onset at 186 °C. Among the comparators Bu-NENA and BDNPA/F, it shows the highest enthalpy of formation (164 kJ mol^{-1}) and heat of explosion (4024 J g^{-1}). Blending with GAP diol significantly improves processability. Viscosity at 20 °C decreases from 4560 mPa·s (pure GAP) to 1369 mPa·s at a 20wt% NFPEG2N3 content. Meanwhile, the mixtures T_g decreases from -49.4 °C to -53.5 °C at a 10wt% NFPEG2N3 content. Thermodynamic analyses indicate that NFPEG2N3 in NC systems raises the specific energy while keeping the temperature of explosion moderate with an optimum near 20wt% plasticizer content. In GAP/AP/HMX composite propellants, NFPEG2N3 increases the volume-specific impulse and delivers the highest mass-specific impulse at 5-10wt% compared to Bu-NENA and BDNPA/F. These results

identify NFPEG2N3 as a promising energetic plasticizer that combines effective rheological modification with enhanced energetic performance.

6.2 Introduction

Plasticizers are essential components in modern polymer-bonded energetic materials, including composite propellants and polymer-bonded explosives [1]. Their primary role is to enhance the mechanical performance, particularly at low temperatures. A key parameter for evaluating this effect is the glass transition temperature (T_g), which represents the temperature at which an amorphous polymer transitions from a flexible, rubber-like state to a rigid and brittle form due to a substantial reduction in molecular mobility [2]. In addition to improving low-temperature mechanical properties, plasticizers also reduce the viscosity of the uncured mixture, thereby facilitating improved processability during manufacturing [3]. Energetic plasticizers serve a dual function in this context: they not only lower the Tg but also contribute to the overall energy content of the formulation. Figure 1 shows a selection of energetic plasticizers. In contrast, inert plasticizers such as bis(2-ethylhexyl) adipate (DEHA, sometimes also abbreviated as DOA) lower the overall energy of a formulation [4]. The combination of an energetic binder, such as glycidyl azide polymer (GAP), with an energetic plasticizer enables the development of advanced formulations with superior energy content. In such systems, the plasticizing effect of the energetic plasticizer is particularly important. Energetic binders such as GAP have beneficial ballistic properties but poor mechanical properties compared to inert binders, like the common hydroxyl-terminated polybutadiene (HTPB) [5]. Nitrofurazans, such as dinitrofurazan (DNF) and nitrofurazanyl ethers, exhibit notable thermal properties, most remarkably their liquid state and low viscosity at room temperature [6,7]. More importantly, the furazan ring is recognized as an energy-rich structural motif, owing to its high enthalpy of formation and favorable oxygen balance [8]. Recently, 3-amino-4-azidoethoxyfurazan was characterized as an insensitive and temperature-stable energetic material, but it is a solid at room temperature [9]. Our approach aims to leverage the advantageous characteristics of the nitrofurazanyl ring by introducing a flexible, energy-dense side chain to optimize the balance between energetic performance and mechanical properties. Since 3-(2-(2-(2-

azidoethoxy)ethoxy)ethoxy)-4-nitro-1,2,5-oxadiazole (NFPEG3N3) is compatible with GAP and Octogen (HMX) and has a competitive energy content [6,10], this study aims to introduce a shorter ethyl ether chain to improve the oxygen balance and achieve an even higher energy content.

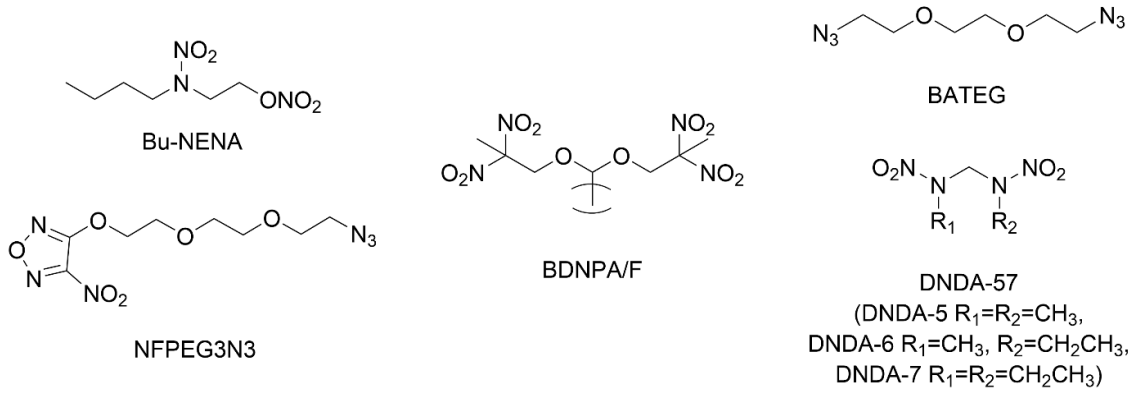

Figure 1 Molecular structures of selected energetic plasticizers N-nitratoethyl nitramine (Bu-NENA), bis-(2,2-dinitropropyl)acetal/ formal (BDNPA/F), 3-(2-(2-(2 azidoethoxy)ethoxy)ethoxy)-4-nitro-1,2,5-oxadiazole (NFPEG3N3), bisazidotriethylene glycol (BATEG), and dinitro-diaza-alkanes mixture (DNDA-57).

6.3 Experimental section

6.3.1 Safety statement

Although no accidents occurred during the work described here, caution should always be exercised when handling new explosives. All work with energetic materials (DNF, NFPEG2N3, GAP diol) was performed by trained personnel in facilities authorized for explosives handling. Some of the procedures described in this publication, particularly those involving the handling of the highly impact sensitive energetic liquids DNF and NFPEG2N3, require the use of protective equipment. Although both liquids could be stored in the refrigerator for several months without decomposition, energetic liquids should be stored in small quantities and away from heat sources and direct sunlight.

6.3.2 Materials

2-(2-Azidoethoxy)ethanol was purchased from ABCR (Karlsruhe, Germany). GAP diol charge 03S19 (MW 1814 g mol−1, EQ 1228 g mol−1, functionality 1.5) was supplied from Eurenco (France).

6.3.3 Methods

Infrared (IR) spectra were recorded on a Thermo Scientific iS 50 FTIR spectrometer using attenuated total reflection (ATR). Raman spectra were recorded on a Bruker FT MultiRAM spectrometer at 1064 nm (Neodymium-YAG laser). Elemental analysis (EA) was performed using a Thermo Flash EA apparatus. A triple determination was performed. To determine the CHN content, a tin sleeve was used at 900 °C in a helium-oxygen stream. To determine the oxygen content, a silver sleeve was used at 1090 °C in a helium stream. Glass transition temperature was determined using a TA Instruments Q1000 differential scanning calorimeter (DSC) and perforated aluminum crucibles. The sample was first cooled to –90 °C and then heated at a rate of 10 °C/min under a nitrogen atmosphere. The glass transition temperature was taken as the inflection point of the heat flow curve during the heating cycle. The thermal decomposition temperature was measured by DSC on the same apparatus at a heat rate of 5 °C/min in pressure-tight closed steel crucibles (type F20) purchased from the Swiss Institute for the Promotion of Safety. Thermogravimetric analysis (TGA) was determined using a TA Instruments Q500 thermogravimetric analyzer. Samples were heated at a rate of 5 °C/min in a 100 µL platinum pan under a nitrogen atmosphere. TGA temperatures are reported as the central points of the thermal events, in accordance with DIN EN ISO 11358. The density of NFPEG2N3 was determined using a Krüss DS7800 density meter based on the bending oscillator principle. ^{1}H NMR and ^{13}C NMR spectra were recorded on a 400 MHz Bruker AV-400 spectrometer at ambient temperature. The viscosity was determined using an Anton Paar Physica MCR 501 apparatus. The impact sensitivity (IS) was estimated by a BAM drop hammer according to DIN EN 13631-4 and Council Regulation (EC) No 440/2008 using 40 mm^3 of sample volume. The evaluation was performed using the six-without-ignition method with a minimum energy load of 1 J. The liquid was applied to the inner edge of the lower steel stamp using a micropipette in a circular motion. The gap between the cylinders was adjusted with a depth gauge and secured with a rubber ring.

6.3.4 Synthesis

Synthesis of 3,4-dinitrofurazan (DNF):

DNF was prepared according to the literature [11].

Synthesis of 3-(2-(2-Azidoethoxy)ethoxy)-4-nitro-1,2,5-oxadiazole (NFPEG2N3):

2-(2-Azidoethoxy)ethan-1-ol (3.44 g, 26.24 mmol, 1.00 equiv.) was dissolved in 15 ml of dry tetrahydrofuran (THF). The solution was cooled to –94 °C in a nitrogen–acetone bath. A solution of n-butyllithium (16.40 ml, 1.6 M in hexanes, 26.24 mmol, 1.00 equiv.) was added dropwise via syringe under a nitrogen atmosphere. The reaction mixture was stirred at –94 °C for 15 minutes, then allowed to warm to room temperature. Meanwhile, dinitrofurazan (DNF, 4.20 g, 26.24 mmol, 1.00 equiv.) was dissolved in 15 ml of THF and cooled to –94 °C. The alcoholate solution was added dropwise to the cooled DNF solution. Upon completion of the addition, the cooling bath was removed, and the reaction mixture was allowed to warm to room temperature. The solvent was removed under reduced pressure using a rotary evaporator. The residue was dissolved in 20 ml of ethyl acetate and washed four times with 60 ml of half-saturated aqueous NaCl solution, or until phase separation occurred quickly and the aqueous layer was colorless. The organic layer was dried over sodium sulfate, filtered, and the solvent was removed under reduced pressure. The crude product was purified by column chromatography on silica gel using 30% n-hexane in ethyl acetate as the eluent, yielding 3.69 g of a yellow oil (56%). T_g –74.9 °C. TGA 156 °C. DSC (closed crucible) 186 °C. Found: C, 30.6; H, 3.5; N, 33.8; O, 32.6%. $C_6H_8N_6O_5$ requires C, 29.5; H, 3.3; N, 34.4; O, 32.8%. IR (ATR, cm^{-1}): 2927, 2875, 2098, 1599, 1547, 1498, 1446, 1431, 1355, 1285, 1202, 1132, 1084, 1032, 922, 891, 872, 851, 828, 765, 743, 698, 645, 591, 557, 534, 502. Raman (1064 nm, cm^{-1}): 2946, 2878, 2823, 2762, 2112, 1604, 1550, 1501, 1474, 1431, 1369, 1287, 1249, 1120, 1034, 990, 925, 873, 832, 766, 743, 647, 599, 440, 377. 1H NMR (400 MHz, $CDCl_3$) δ [ppm] = 4.61 – 4.55 (m, 2H), 3.90 – 3.84 (m, 2H), 3.68 (m, J = 4.7 Hz, 2H), 3.32 (t, J = 5.0 Hz, 2H). 13C NMR (101 MHz, $CDCl_3$) δ [ppm] = 158.24, 151.48, 73.42, 70.56, 68.47, 50.60. Impact sensitivity < 1 J. Friction sensitivity > 360 N. ϱ 1.375 g cm^{-3}.

6.3.5 Quantum chemical calculations to determine the standard enthalpy of formation

Quantum chemical calculations were performed using the Gaussian 16 software [12]. To find the most stable isomers, precise yet cost-efficient quantum mechanics (QM) calculations based on density functional theory (DFT) [13] are performed. The functionals B3LYP [14] and B3PW91 [15] are used in combination with the basis sets 6-31G* and 6-31G** [16], as well as AUG-cc-PVTZ [17]. These combinations were also used because Politzer [18] and Rice's [19] empirical methods were developed with them. However, more accurate and complex calculations than the aforementioned DFT methods are needed to calculate the standard enthalpies of formation in the gas phase. To this end, "composite" or "compound" calculations are performed on the molecular structures to be investigated [20]. These calculations involve a fixed protocol of diverse QM calculations with different parameters. To obtain the most accurate thermodynamic data possible, calculations are performed using the Gaussian™ "composite" methods CBS-QB3 [21], G4MP2 [22] and, G4 [23]. The standard gas-phase enthalpy of formation was obtained via the atomization method [24] using the three composite methods (CBS-QB3, G4MP2, G4). The mean values from ΔH_{vap}^{0} and ΔH_{sub}^{0}, as determined according to Politzer and Rice, are taken as the vaporization enthalpy and sublimation enthalpy, respectively. The corresponding differences (standard enthalpy of formation in the gas phase – vaporization enthalpy) or (standard enthalpy of formation in the gas phase – sublimation enthalpy) provide the values for the standard enthalpy of formation in the condensed phases ($\Delta_f H_M^0(l)$, $\Delta_f H_M^0(s)$).

6.3.6 Thermodynamic calculations to determine performance in propellant applications

The heat of explosion of energetic plasticizers was calculated using the ICT Thermodynamic Code [25] in the constant-volume mode at a loading density of 0.10 g/cm^3. Products were cooled to 298 K with water condensed (liquid), following closed-bomb convention. Specific energy and explosion temperature for nitrocellulose (12.6wt% N)–plasticizer mixtures were computed in constant-volume mode at a loading density of 0.20 g/cm^3, using equilibrium composition. The water was treated as gaseous at the adiabatic constant-volume equilibrium state; condensed carbon was allowed when

oxygen balance was negative. Stabilizers and additives were neglected. Mass- and volume-specific impulse of polymer-bound propellants were calculated with the ICT Thermodynamic Code in constant-pressure mode using frozen-composition nozzle expansion (equilibrium in the chamber, frozen through the nozzle) to an area expansion ratio of 70:1. Water was treated as gaseous at chamber conditions and throughout expansion.

6.4 Results and discussion

6.4.1 Synthesis

NFPEG2N3 was synthesized from DNF via nucleophilic substitution of a nitro group with the corresponding alcoholate (Figure 2).

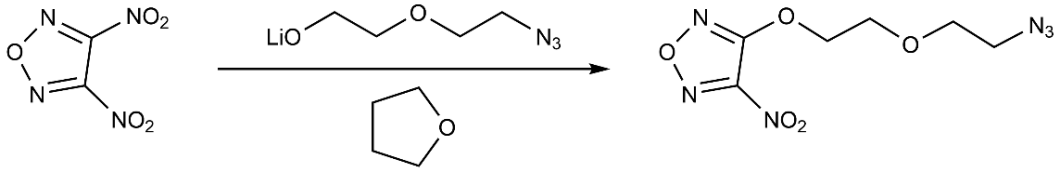

Figure 2 Synthesis of NFPEG2N3 by nucleophilic substitution of a nitro group.

Since a 2-(2-azidoethoxy)ethan-1-olate is not commercially available, lithium 2-(2-azidoethoxy)ethan-1-olate was prepared from 2-(2-azidoethoxy)ethanol by deprotonation using n-butyllithium. The resulting alcoholate solution was used directly without further purification. Both synthetic steps were conducted in THF at -94 °C using a nitrogen-acetone cooling bath. The molecular structure of the product was confirmed by ^{1}H and ^{13}C NMR spectroscopy (Figure 3) and elemental analysis (EA). The detailed results of the EA can be found in the Supporting Information (S1). The azidomethylene (–CH2–N3) exhibits a ^{1}H signal at 3.32 ppm as a triplet (J = 5 Hz, 2H), consistent with vicinal coupling to a neighboring methylene and typical for aliphatic azides. NFPEG2N3 is a liquid at room temperature.

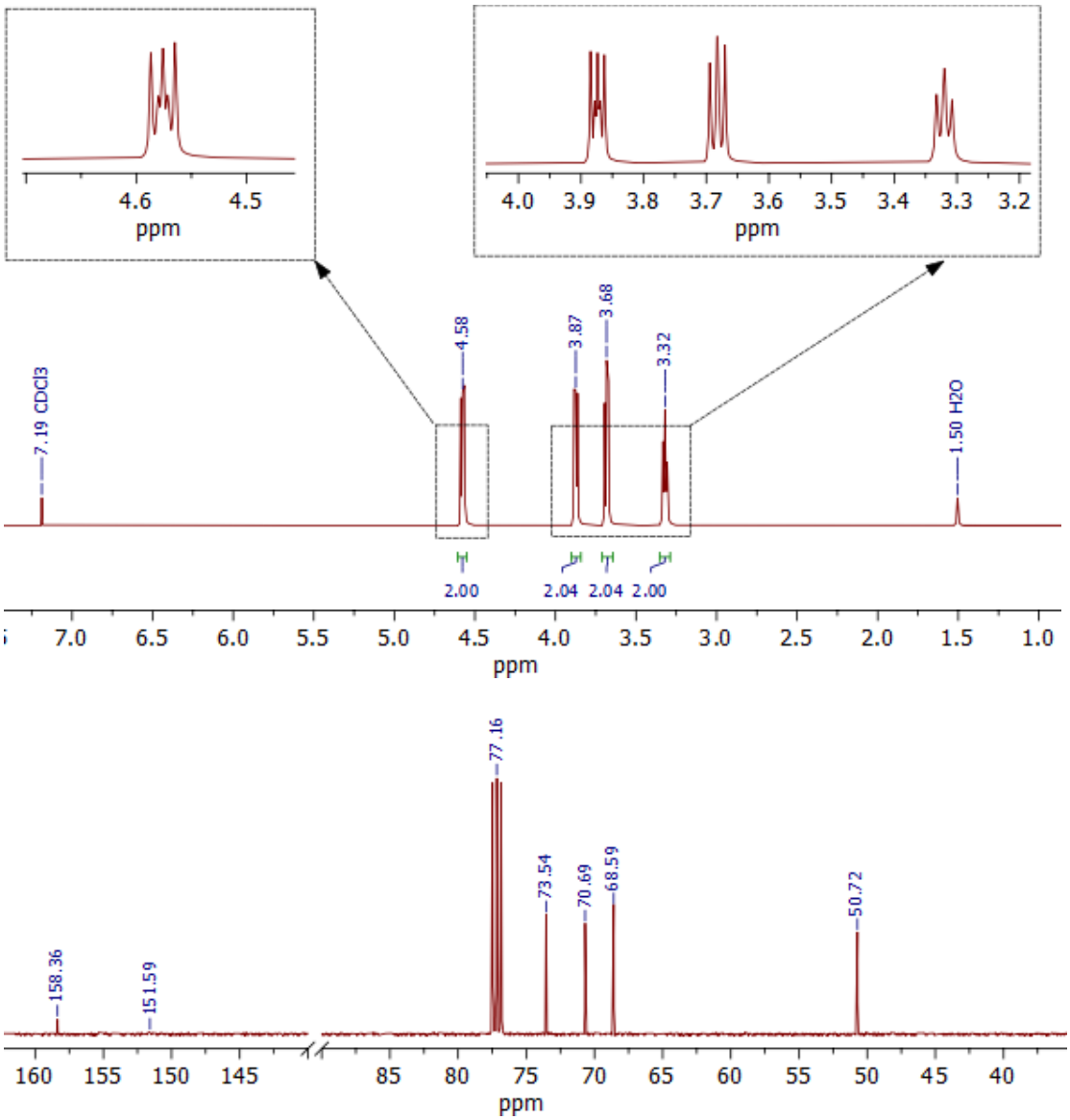

Figure 3 ^{1}H (above) and ^{13}C NMR spectra (below) of NFPEG2N3 in $CDCl_3$.

6.4.2 Impact sensitivity

Impact sensitivity (IS) was measured according to Council Regulation (EC) No 440/2008 [26] and DIN 13631-4 [27]. These specifications differ in terms of the distance between the steel cylinders. Depending on the regulation, 1 mm or 2 mm is specified. When measuring liquids, small changes can have a big impact. Studies have shown that the gap distance has a significant impact on the measured IS for liquids. For example, an IS of 5 J at a distance of 1 mm and an IS of 1 J at a distance of 2 mm have been reported for nitromethane, depending on the gap distance. If the nitromethane is placed in the center of the lower steel cylinder and not, as specified, at the edge between the lower cylinder and the hollow cylinder, a value >50 J has been reported [28]. However, our tests using

both distances with NFPEG2N3 placed at the edge between the lower cylinder and the hollow cylinder did not reveal any difference (Table 1). There was a reaction accompanied by smoke and a quiet bang even with a 1 J impact load, which is the lowest load at the BAM drop hammer. After each conversion, we found liquid residues in the hollow cylinder and on the drop hammer, indicating that the conversion was only partial.

Table 1 Impact sensitivity of NFPEG2N3.

	Council Regulation (EC) No 440/2008	DIN EN 13631
Gap between steel cylinders [mm]	1.0	2.0
IS [J]	<1	<1
Test series: Impact load [J] (reaction [a])	6(x), 3(x), 1(x), 1(x)	10(x), 3(x), 1(o), 2(x), 1(x), 1(x)

[a] Observation of a bang and/or a flame (x), no response (o).

NFPEG2N3 exhibits a very high impact sensitivity, which is undesirable from a handling and processing standpoint. However, this value is comparable to that of established nitrate ester plasticizers, such as trimethylolethane trinitrate (TMETN, typical reported IS of <1 J), which has been used in service-qualified double-base propellants [29]. This demonstrates that such sensitivities can be managed with the appropriate industrial controls. In practical composite formulations, the energetic plasticizer constitutes only a small percentage of 5-10%. The overall sensitivity of a GAP-based system is dominated by the binder matrix. Consequently, although NFPEG2N3 is a sensitive neat liquid, its use at modest loadings is not expected to significantly increase the sensitivity of the bulk formulation.

6.4.3 Infrared spectroscopy

Infrared spectroscopy (IR) is an analytical technique with the capacity to identify and characterize molecular structures based on their vibrational transitions. NFPEG2N3 was analyzed using IR spectroscopy. The spectrum obtained was then compared with a theoretical spectrum calculated using density functional theory (DFT) (Figure 4). The B3LYP functional was utilized in conjunction with the 6-31G* basis set to facilitate the requisite calculations. This combination is widely recognized for its accuracy in predicting molecular properties and vibrational frequencies. The experimental infrared

(IR) spectrum of NFPEG2N3 exhibited distinct absorption peaks corresponding to different vibrational modes. A comparison of these peaks with the DFT-calculated spectrum enabled the assignment of individual peaks to molecular vibrational modes (Table 2).

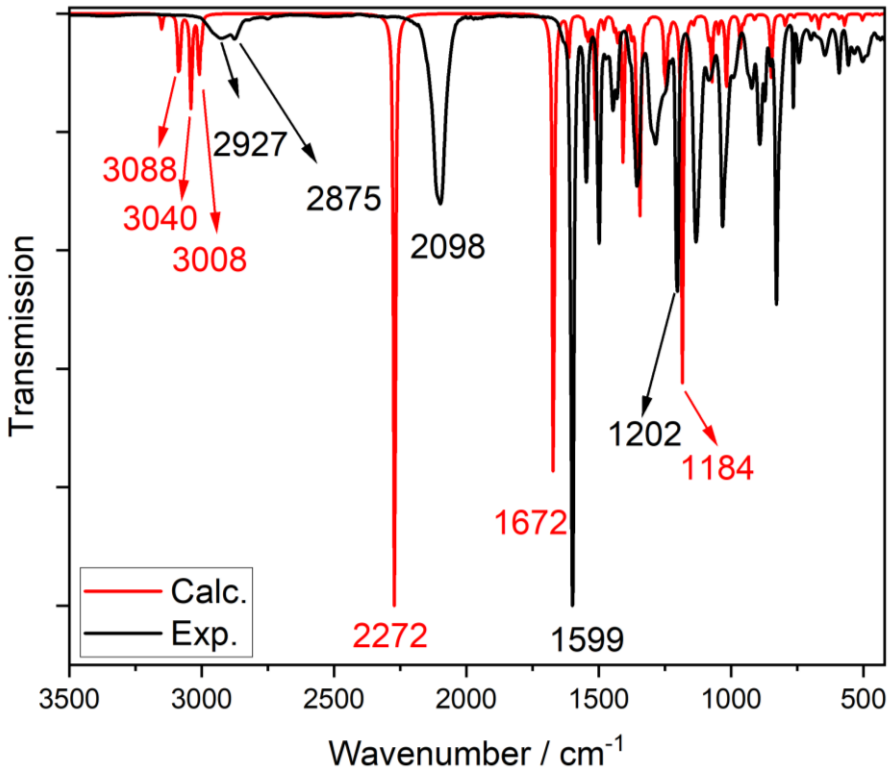

Figure 4 Calculated (red) and experimental (black) infrared spectra of NFPEG2N3. The calculated spectrum was obtained by DFT calculation with the functional/basis set combination B3LYP/6-31G*.

Table 2 Overview of the relevant vibration modes of NFPEG2N3.

Vibrational mode	Experiment		Calculation	
	Energy [cm^{-1}]	Shape	Energy [cm^{-1}]	Shape
C-H stretching	2927	broad weak	3088	sharp weak
C-H stretching	2875	broad weak	3040	sharp weak
C-H stretching	-	-	3008	sharp weak
Azide stretching	2098	broad medium	2272	sharp strong
Nitro asymmetric N=O stretching	1599	sharp strong	1672	sharp strong
C-O stretching	1202	sharp medium	1184	sharp medium

Figures 5-7 illustrate the molecular structure of NFPEG2N3 and the displacements of the individual atoms during the characteristic molecular vibrations listed in Table 1.

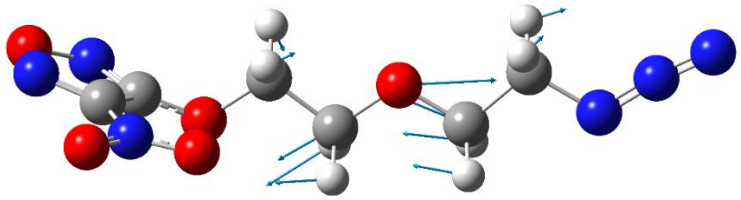

Figure 5 Molecular structure of NFPEG2N3; the blue arrows correspond to the displacement of the individual atoms in the vibrational mode (C-O stretching) at 1184 cm^{-1}.

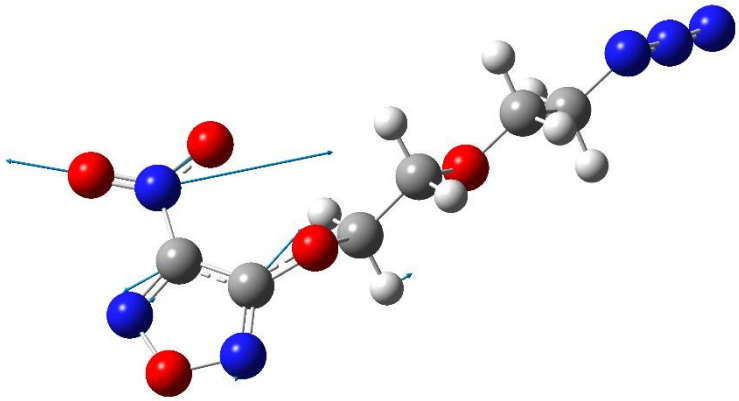

Figure 6 Molecular structure of NFPEG2N3; the blue arrows correspond to the displacement of the individual atoms in the vibrational mode (N=O stretching) at 1672 cm^{-1}.

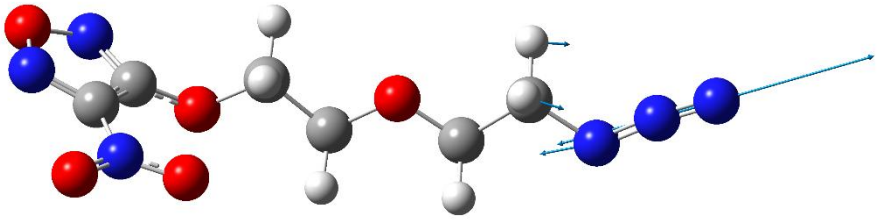

Figure 7 Molecular structure of NFPEG2N3; the blue arrows correspond to the displacement of the individual atoms in the vibrational mode (azide stretching) at 2272 cm^{-1}.

6.4.4 Thermochemical properties

Properties of NFPEG2N3 are presented in Table 3. Data from the plasticizers in use N-butyl-N-nitratoethyl nitramine (Bu-NENA) and bis-(2,2-dinitropropyl)acetal/ formal (BDNPA/F) as well as NFPEG3N3 are provided for comparison. NFPEG3N3 differs from NFPEG2N3 in that it has an ethyl ether chain that is one unit longer. Compared to the other compounds, NFPEG2N3 exhibits the highest enthalpy of formation of 164 kJ/mol

and the highest heat of explosion of 4024 J/g. This makes the new molecule the most energy-rich within the compounds compared. Additionally, it shows a lower T_g of -75 °C, compared to -72 °C for NFPEG3N3. The DSC and TGA curves of NFPEG2N3 are shown in Figure 8.

Table 3 Properties of NFPEG2N3 compared to selected energetic plasticizers.

Plasticizer	Bu-NENA [30]	BDNPA/F [30]	NFPEG3N3 [6]	NFPEG2N3
Sum formula	$C_6H_{13}N_3O_5$	$C_{7.5}H_{13}N_4O_{10}$	$C_8H_{12}N_6O_6$	$C_6H_8N_6O_5$
Mol weight [g/mol]	207.19	319.20	288.22	244.17
OB_{CO2}[a] [%]	-104.2	-57.6	-88.8	-72.1
T_g[b] (inflection p.) [°C]	-82	-67	-72	-75
T_{TGA}[c] (inflection p.) [°C]	152	182	167	156
T_{dec}[d] (onset) [°C]	173	207	179	186
Density [g/cm³]	1.22	1.39	1.34	1.375
$\Delta_f H^0(l)$[e] [kJ/mol]	-192	-620	-42	164
Heat of explosion [J/g]	3573	3469	3421	4024

[a] Oxygen balance assigned to CO_2. [b] Glass transition temperature. [c] Thermogravimetric analysis. [d] Differential scanning calorimetry (decomposition in closed crucible). [e] Enthalpy of formation.

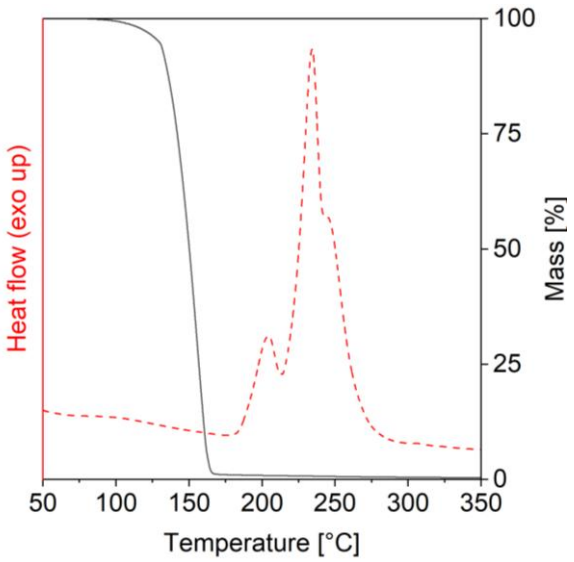

Figure 8 DSC (closed crucible) heat flow curve and TGA mass loss curve of NFPEG2N3.

6.4.5 Calculation of the enthalpy of formation

The standard enthalpy of formation is a critical thermodynamic quantity. Accurate determination of this parameter is essential for comprehending the stability and reactivity of chemical substances. In the case of substance NFPEG2N3, the standard enthalpy of formation was calculated using various methods of density functional theory (DFT). These calculation methods enable the prediction of thermodynamic properties

based on quantum mechanical principles. The methodology for these calculations is described in detail in the Experimental section. It delineates the specific DFT functionals and basis sets employed, in addition to the calculation parameters. The results obtained for the calculated enthalpies are summarized in Table 4.

Table 4 Summary of the enthalpies for NFPEG2N3.

NFPEG2N3	[kJ/mol]
$\Delta_f H^0(g)$	243.85
ΔH^0_{vap}	80.29
$\Delta_f H^0(l)$	163.55

6.4.6 Impact on the thermal and rheological properties of GAP diol

The azide functionality of NFPEG2N3 makes it incompatible with common HTPB-based binders, as azides can undergo ene-azide cycloaddition reactions with the unsaturated double bonds present in HTPB. These reactions lead to the formation of unstable triazolines that gradually decompose, releasing nitrogen gas and compromising the long-term stability of the propellant. [31] Consequently, NFPEG2N3 is better suited for use in formulations based on azide-compatible binders such as GAP. The plasticizing effect of NFPEG2N3 on GAP was investigated by measuring T_g and viscosity of mixtures. A significant reduction in both factors indicates effective plasticization. The viscosity of pure GAP diol at 20°C is 4560 mPa·s. This consistency is similar to that of thick honey or corn syrup. With NFPEG2N3 proportions of 10wt%, 20wt%, and 30wt%, the viscosity could be reduced to 2464 mPa·s (-46%), 1369 mPa·s (-70%), and 764 mPa·s (-83%), respectively. Figure 9 illustrates the reduction of viscosity between 10 °C and 50 °C for mixtures with NFPEG2N3 and NFPEG3N3. NFPEG2N3 causes a slightly stronger reduction in viscosity.

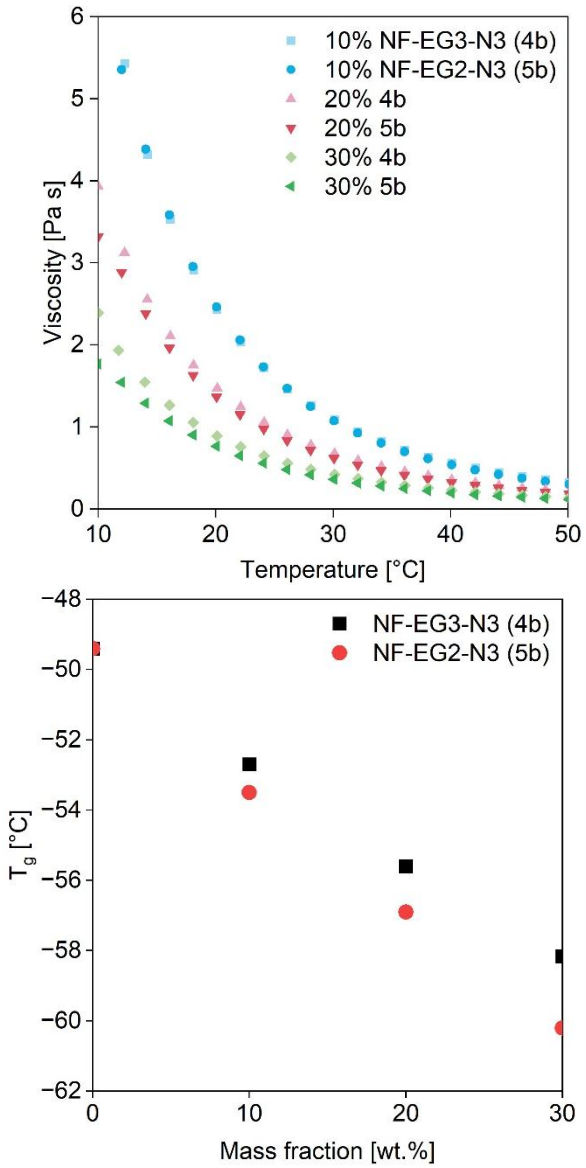

Figure 9 a) Viscosity of mixtures of GAP diol with 10, 20 and 30wt% of NFPEG3N3 and NFPEG2N3 at temperatures ranging from 10 °C to 50 °C. b) Tg of mixtures of GAP diol with 10, 20 and 30wt% of NFPEG2N3 and NFPEG3N3.

Figure 10 shows the viscosity of mixtures of GAP diol with 10wt% of plasticizer. Compared to Bu-NENA, DNDA-57, and BDNPA/F, the mixture with NFPEG2N3 has the lowest viscosity.

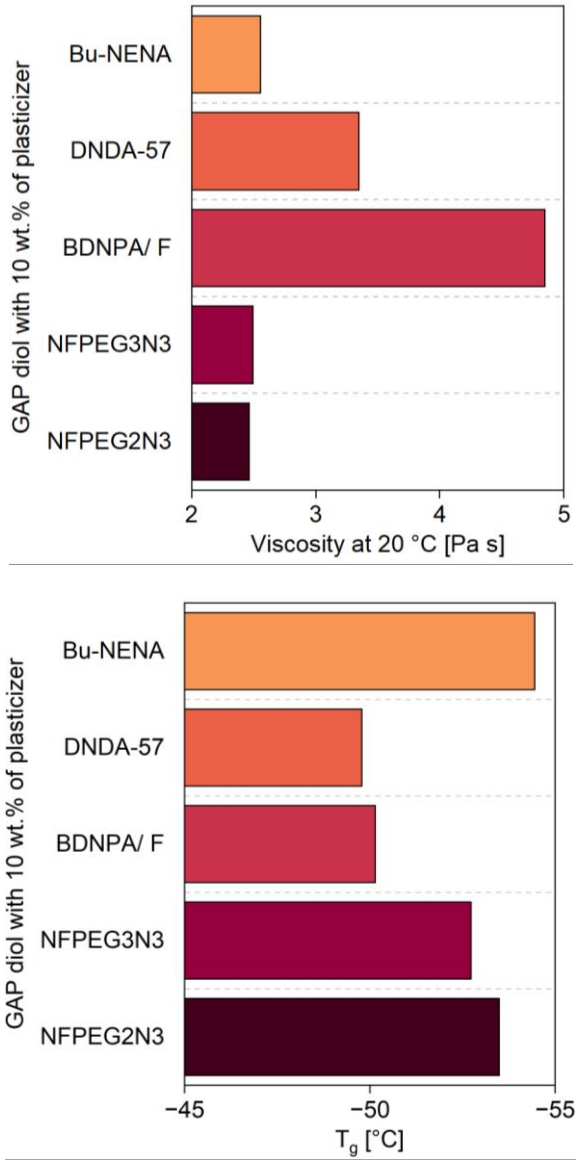

Figure 10 a) T_g of mixtures of GAP diol with 10wt% of plasticizers. b) Viscosity at 20 °C of mixtures of GAP diol containing 10wt% of plasticizers.

6.4.7 Performance evaluation for use in propellant applications

Thermodynamic calculations were conducted to evaluate the effect of NFPEG2N3 as an energetic plasticizer on a nitrocellulose (NC)-based gun propellant and a GAP-based solid rocket propellant. Assuming NC with a nitrogen content of 12.6%, the study examined how varying proportions of NFPEG2N3 influence specific energy and temperature of explosion (Tex). Ideally, a higher specific energy at a lower Tex is desirable, as it enhances performance while minimizing barrel wear. The results indicate that increasing NFPEG2N3 content achieves this balance, with a peak in specific energy observed at 20wt% (Figure 11). Beyond this concentration, the benefit plateaus or diminishes. Compared with conventional energetic plasticizers, NFPEG2N3 performs

between Bu-NENA and DNDA-57 in terms of temperature reduction at a given specific energy gain. Interestingly, NFPEG2N3 significantly outperforms its structural analog NFPEG3N3 and bisazidotriethylene glycol (BATEG) in terms of specific energy. The shorter ethyl ether chain in NFPEG2N3 contributes to this improved energetic performance.

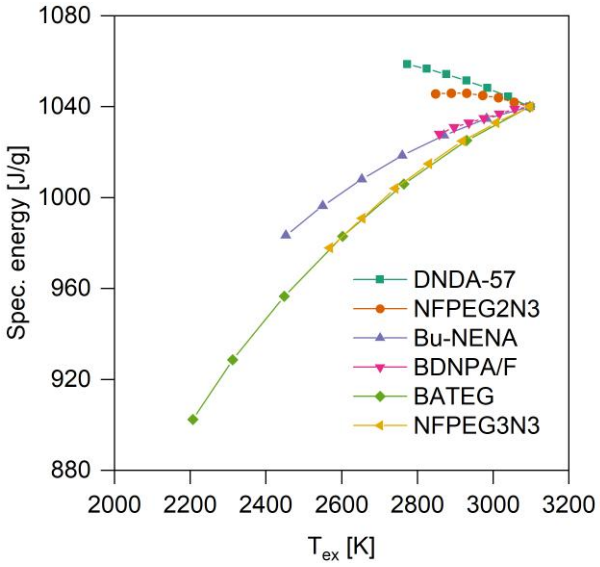

Figure 11 Specific energy and temperature of explosion of a mixture of NC (12.6% nitrogen content) with different amounts of NFPEG2N3 and selected energetic plasticizers. One point corresponds to an additional 5wt% of plasticizer. All curves start with pure NC.

To evaluate the impact of NFPEG2N3 in composite propellants, a formulation containing 30% binder, 60% ammonium perchlorate, and 10wt% HMX was selected for thermodynamic calculations. The binder contained GAP with a plasticizer content ranging from 0 to 15%. We investigated the influence of NFPEG2N3 on both the volume- and mass-specific impulses and benchmarked its performance against Bu-NENA and BDNPA/F (Figure 12). DNDA-57 was excluded from the comparison due to its low glass transition temperature of -52 °C, which is unsuitable for the intended application. BATEG was excluded due to its low energy content. Results indicate that both NFPEG2N3 and BDNPA/F contribute to an increase in volume-specific impulse, while Bu-NENA shows only marginal influence. Notably, in comparison with Bu-NENA and BDNPA/F, NFPEG2N3 delivers the highest mass-specific impulse at plasticizer loadings between 5 and 10wt%, suggesting a favorable balance of energetic contribution and formulation density. The results suggest that NFPEG2N3 is advantageous in both

surface-near and space applications as it offers a high volume-specific and mass-specific impulse.

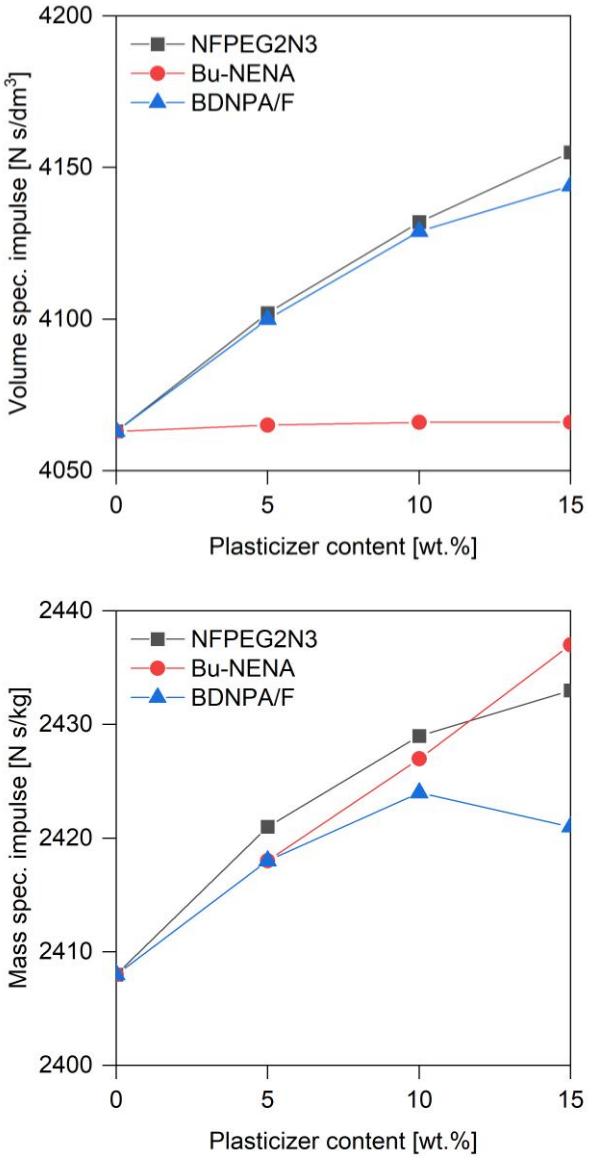

Figure 12 (a) Volume spec. impulse of a GAP-based composite propellant with NFPEG2N3 compared to other energetic plasticizers (b) Mass spec. impulse of a GAP-based composite propellant with NFPEG2N3 compared to other energetic plasticizers.

6.5 Conclusion

NFPEG2N3 couples a high-energy nitrofurazanyl core with a flexible azidodiethoxyethyl chain to deliver both energetic contribution and improved processability. Relative to established energetic plasticizers and the longer-chain analog NFPEG3N3, it provides a superior enthalpy of formation and heat of explosion, while

modestly lowering GAP T_g and more strongly reducing mixture viscosity, thereby widening the practical processing window. One limitation of NFPEG2N3 is that it exhibits very high impact sensitivity, comparable to that of common nitrate esters. Thermodynamic modeling indicates a favorable energy–temperature of explosion trade-off in NC systems with an optimum near 20wt% and, in GAP/AP/HMX composites, the highest mass-specific impulse at 5–10wt% alongside gains in volume-specific impulse compared to Bu-NENA and BDNPA/F.

6.6 Acknowledgment and Funding

The authors thank H. Schuppler for performing TGA and DSC measurements, T. Jahnke for performing density measurement, U. Förter-Barth for performing viscosity measurements, S. Lauinger for performing the elemental analysis and M. Jung for performing sensitivity measurements. Financial support from WTD91 of the German Ministry of Defense is also gratefully acknowledged.

6.7 Conflict of interest

The authors declare no conflicts of interest.

6.8 Supporting information

The elemental analysis data, Raman spectrum, TGA curve, and DSC curve of NFPEG2N3 have been included in the Supporting Information (S1-4).

6.9 References

[1] [1a] H. G. Ang, S. Pisharath, Energetic polymers: Binders and plasticizers for enhancing performance, 1st ed., Wiley-VCH-Verl., Weinheim 2012; [1b] T. M. Klapötke, Chemistry of high-energy materials, 6th ed., De Gruyter, Berlin, Boston 2022;

[2] M. K. Shukla, V. M. Boddu, J. A. Steevens, R. Damavarapu, J. Leszczynski, Energetic Materials: From the cradel to the grave, Springer International Publishing, Cham 2017.

[3] S. K. Shee, S. T. Reddy, J. Athar, A. K. Sikder, M. B. Talawar, S. Banerjee, M. A. Shafeeuulla Khan, Probing the compatibility of energetic binder poly-glycidyl nitrate with energetic plasticizers: thermal, rheological and DFT studies, RSC Adv. 2015, 5, 101297–101308, https://doi.org/10.1039/C5RA16476A.

[4] K. Selim, S. zkar, L. Yilmaz, Thermal characterization of glycidyl azide polymer (GAP) and GAP-based binders for composite propellants, J. Appl. Polym. Sci. 2000, 77, 538–546, https://doi.org/10.1002/%28SICI%291097-4628%2820000718%2977%3A3%3C538%3A%3AAID-APP9%3E3.0.CO%3B2-X.

[5] S. Ek, J. Johansson, M. Brantlind, H. Ellis, M. Skarstind, Synthesis and characterisation of tri- and tetraethyleneglycoldiazide for their use as energetic plasticisers, New Trends in Research of Energetic Materials (NTREM) 2019, 81–87.
[6] P. Lieber, U. Schaller, T. M. Klapötke, Synthesis and characterization of novel nitrofurazanyl ethers as potential energetic plasticizers, RSC Adv. 2025, 15, 12577–12584, https://doi.org/10.1039/D5RA01282A.
[7] K. Y. Suponitsky, A. F. Smol'yakov, I. V. Ananyev, A. V. Khakhalev, A. A. Gidaspov, A. B. Sheremetev, 3,4-Dinitrofurazan: Structural Nonequivalence of ortho -Nitro Groups as a Key Feature of the Crystal Structure and Density, ChemistrySelect 2020, 5, 14543–14548, https://doi.org/10.1002/slct.202004020.
[8] H. Wei, C. He, J. Zhang, J. M. Shreeve, Combination of 1,2,4-Oxadiazole and 1,2,5-Oxadiazole Moieties for the Generation of High-Performance Energetic Materials, Angew. Chem., Int. Ed. Engl. 2015, 54, 9367–9371, https://doi.org/10.1002/anie.201503532.
[9] Y. Wu, Y. Liu, K. Liang, X. He, Y. Liu, C. Xiao, Y. Wang, Design and Synthesis of 3-Amino-4-azidoethoxyfurazan: A Supramolecular Energetic Material with Insensitivity Properties, JACS Au, in press, https://doi.org/10.1021/jacsau.5c00511.
[10] P. Lieber, U. Schaller, T. M. Klapötke, Energetic plasticizers for GAP-based formulations with ADN: compatibility and performance evaluation of a nitrofurazanyl ether, RSC Adv. 2025, 15, 37006–37011, https://doi.org/10.1039/D5RA05154A.
[11] P. Lieber, U. Schaller, T. M. Klapötke, Amine oxidation under challenging conditions: implementation of a flow-chemistry procedure for 3,4-dinitrofurazan synthesis, in: Proceedings of the 26th Seminar on New Trends in Research of Energetic Materials (NTREM), Pardubice, Czech Republic 2024.
[12] M. J. Frisch, G. W. Trucks, H. B. Schlegel, G. E. Scuseria, M. A. Robb, J. R. Cheeseman, G. Scalmani, V. Barone, G. A. Petersson, H. Nakatsuji, X. Li, M. Caricato, A. V. Marenich, Bloino, J., Janesko, B.G., Gomperts, R., Mennucci, B., Hratchian, H.P., Ortiz, J.V., Izmaylov, A.F., Sonnenberg, J.L., Williams-Young, D., Ding, F., Lipparini, F., Egidi, F., Goings, J., Peng, B., Petrone, A., Henderson, T., Ranasinghe, D., Zakrzewski, V.G., Gao, J., Rega, N., Zheng, G., Liang, W., Hada, M., Ehara, M., Toyota, K., Fukuda, R., Hasegawa, J., Ishida, M., Nakajima, T., Honda, Y., Kitao, O., Nakai, H., Vreven, T., Throssell, K., Montgomery Jr., J.A., Peralta, J.E., Ogliaro, F., Bearpark, M.J., Heyd, J.J., Brothers, E.N., Kudin, K.N., Staroverov, V.N., Keith, T.A., Kobayashi, R., Normand, J., Raghavachari, K., Rendell, A.P., Burant, J.C., Iyengar, S.S., Tomasi, J., Cossi, M., Millam, J.M., Klene, M., Adamo, C., Cammi, R., Ochterski, J.W., Martin, R.L., Morokuma, K., Farkas, O., Foresman, J.B., Fox, D.J., Gaussian 16 Revision C.01, Gaussian, Inc., Wallingford, USA 2016.
[13] [13a] W. Kohn, A. D. Becke, R. G. Parr, Density Functional Theory of Electronic Structure, J. Phys. Chem. 1996, 100, 12974–12980, https://doi.org/10.1021/jp960669l; [13b] R. G. Parr, in: Horizons of Quantum Chemistry: Proceedings of the Third International Congress of Quantum Chemistry (Eds.: B. Pullman, K. Fukui), Springer Netherlands, Dordrecht 1980, pp. 5–15; [13c] D. Sholl, J. A. Steckel, Density functional theory: A practical introduction, Wiley, Hoboken, NJ 2009;
[14] [14a] A. D. Becke, A new inhomogeneity parameter in density-functional theory, J. Chem. Phys. 1998, 109, 2092–2098, https://doi.org/10.1063/1.476722; [14b] B. Miehlich, A. Savin, H. Stoll, H. Preuss, Results obtained with the correlation energy density functionals of becke and Lee, Yang and Parr, Chem. Phys. Lett. 1989, 157, 200–206, https://doi.org/10.1016/0009-2614(89)87234-3;
[15] A. D. Becke, Density-functional exchange-energy approximation with correct asymptotic behavior, Phys. Rev. A 1988, 38, 3098–3100, https://doi.org/10.1103/PhysRevA.38.3098.

[16] W. J. Hehre, R. Ditchfield, J. A. Pople, Self—Consistent Molecular Orbital Methods. XII. Further Extensions of Gaussian—Type Basis Sets for Use in Molecular Orbital Studies of Organic Molecules, J. Chem. Phys. 1972, 56, 2257–2261, https://doi.org/10.1063/1.1677527.
[17] D. E. Woon, T. H. Dunning, Theory of hypervalency: recoupled pair bonding in SF(n) (n = 1-6), J. Phys. Chem. A 2009, 113, 7915–7926, https://doi.org/10.1021/jp901949b.
[18] P. Politzer, Y. Ma, P. Lane, M. C. Concha, Computational prediction of standard gas, liquid, and solid-phase heats of formation and heats of vaporization and sublimation, Int. J. Quantum Chem. 2005, 105, 341–347, https://doi.org/10.1002/qua.20709.
[19] [19a] B. Rice, Predicting heats of formation of energetic materials using quantum mechanical calculations, Combust. Flame 1999, 118, 445–458, https://doi.org/10.1016/s0010-2180(99)00008-5; [19b] E. F. C. Byrd, B. M. Rice, Improved prediction of heats of formation of energetic materials using quantum mechanical calculations, J. Phys. Chem. A 2006, 110, 1005–1013, https://doi.org/10.1021/jp0536192;
[20] W. M. F. Fabian, Accurate thermochemistry from quantum chemical calculations?, Monatsh Chem 2008, 139, 309–318, https://doi.org/10.1007/s00706-007-0798-8.
[21] [21a] G. A. Petersson, M. A. Al-Laham, A complete basis set model chemistry. II. Open-shell systems and the total energies of the first-row atoms, J. Chem. Phys. 1991, 94, 6081–6090, https://doi.org/10.1063/1.460447; [21b] K. P. Somers, J. M. Simmie, Benchmarking Compound Methods (CBS-QB3, CBS-APNO, G3, G4, W1BD) against the Active Thermochemical Tables: Formation Enthalpies of Radicals, J. Phys. Chem. A 2015, 119, 8922–8933, https://doi.org/10.1021/acs.jpca.5b05448;
[22] L. A. Curtiss, P. C. Redfern, K. Raghavachari, Gaussian-4 theory using reduced order perturbation theory, J. Chem. Phys. 2007, 127, 124105, https://doi.org/10.1063/1.2770701.
[23] [23a] L. A. Curtiss, P. C. Redfern, K. Raghavachari, Gaussian-4 theory, J. Chem. Phys. 2007, 126, 84108, https://doi.org/10.1063/1.2436888; [23b] S. Rayne, K. Forest, A G4MP2 and G4 Theoretical Study into the Thermochemical Properties of Explosophore Substituted Tetrahedranes and Cubanes, Propellants, Explos., Pyrotech. 2011, 36, 410–415, https://doi.org/10.1002/prep.201000165;
[24] J. W. Ochterski, Thermochemistry in Gaussian 2000.
[25] S. Kelzenberg, P. B. Kempa, M. Herrmann, T. Fischer, F. Volk, H. Bathelt, ICT Thermodynamic Code V2017.1.1, Fraunhofer ICT, Pfinztal, Germany 2017.
[26] Council of the European Union, Council Regulation (EC) No 440/2008 of 30 May 2008 laying down test methods pursuant to Regulation (EC) No 1907/2006 of the European Parliament and of the Council on the Registration, Evaluation, Authorisation and Restriction of Chemicals (REACH) 2008.
[27] DIN German Institute for Standardization, DIN EN 13631-4, Explosives for civil uses - High explosives - Part 4: Determination of sensitiveness to impact of explosives, DIN Media GmbH, Berlin, Germany 2002.
[28] R. K. Wharton, J. A. Harding, A study of some factors that affect the impact sensitiveness of liquids determined using the BAM Fallhammer apparatus, J. Hazard. Mater. 1994, 37, 265–276, https://doi.org/10.1016/0304-3894(94)00004-2.
[29] R. Meyer, J. Köhler, A. Homburg, Explosives, 6th ed., Wiley-VCH, Weinheim 2007.
[30] U. Schaller, J. Lang, V. Gettwert, J. Hürttlen, V. Weiser, T. Keicher, 4-Amino-1-Butyl-1,2,4-Triazolium Dinitramide – Synthesis, Characterization and Combustion of a Low-Temperature Dinitramide-Based Energetic Ionic Liquid (EIL), Propellants, Explos., Pyrotech., in press, https://doi.org/10.1002/prep.202200054.
[31] M. F. Lemos, L. C. Mendes, M. Bohn, T. Keicher, Application of azide-containing molecules as modifiers of HTPB, J. Therm. Anal. Calorim. 2019, 137, 411–419, https://doi.org/10.1007/s10973-018-7968-2.

6.10 Supplementary information

Supporting information (SI)

All spectra and curves shown are unprocessed raw data.

S1 Elemental analysis (EA) of NFPEG2N3.

Sample	Composition [wt%]				
	Nitrogen	Carbon	Hydrogen	Oxygen	Mass balance
1	16.59	40.03	5.03	37.14	
2	16.51	40.41	5.09	36.86	
3	16.72	40.34	5.07	37.17	
MW	16.61	40.26	5.06	37.05	98.98
STABW	0.09	0.16	0.02	0.14	
Theory	*16.21*	*41.70*	*5.05*	*37.03*	

S2 Raman spectrum of NFPEG2N3.

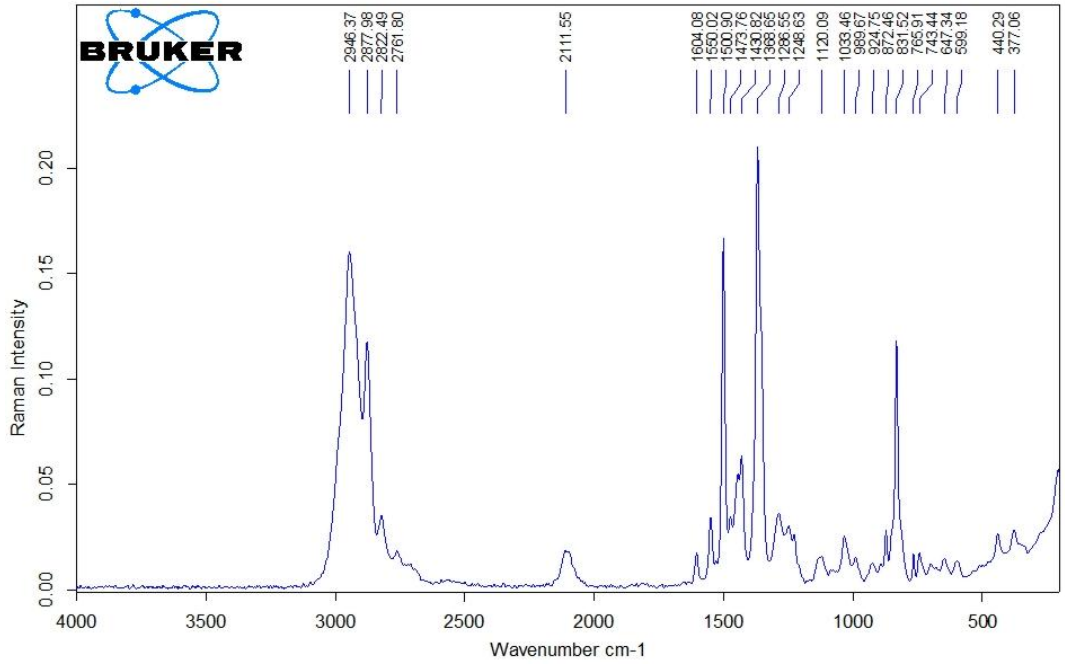

S3 TGA curve (blue) and first derivative (green, dTGA) of NFPEG2N3.

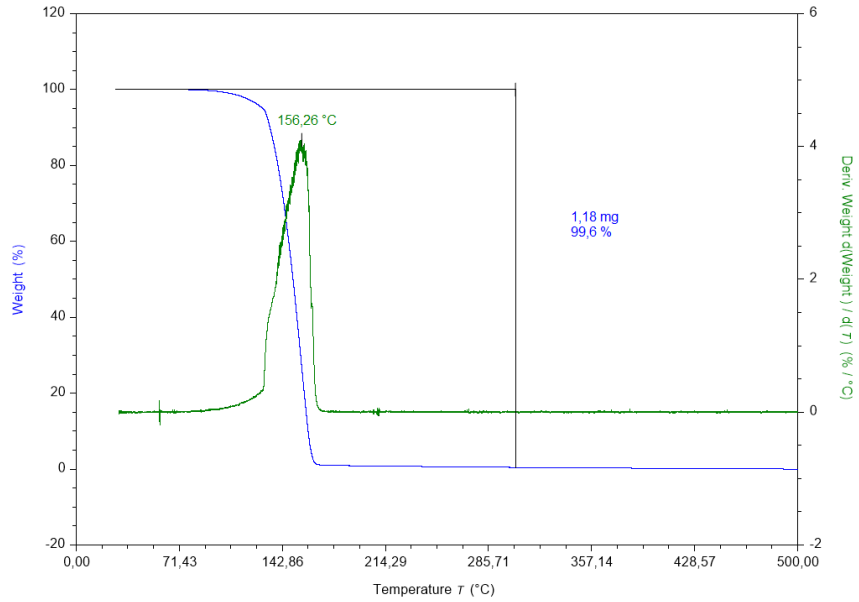

S4 DSC curve (closed steel crucible) of NFPEG2N3.

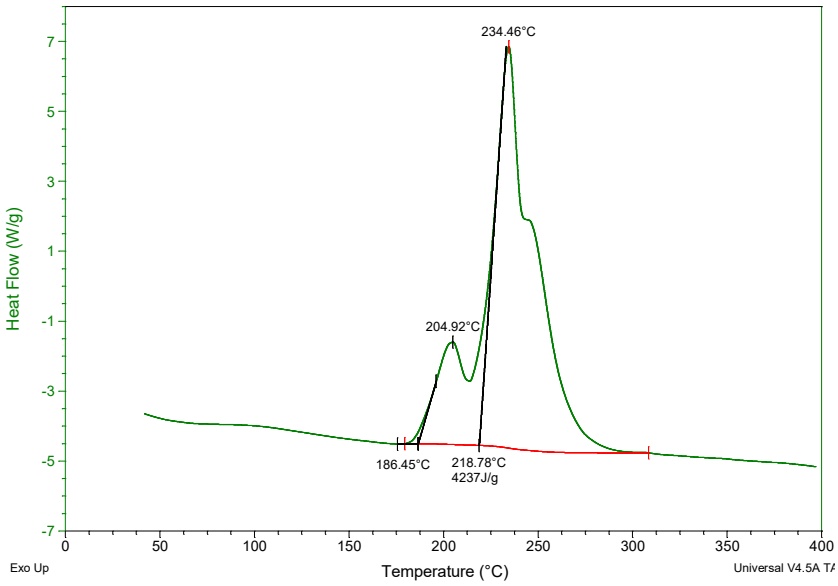

7 Summary and conclusion

This dissertation presents new energetic compounds that were designed, synthesized, characterized, and evaluated according to the workflow depicted in Figure 1. The order of the chapters reflects the iterative process of developing new molecules for a given application.

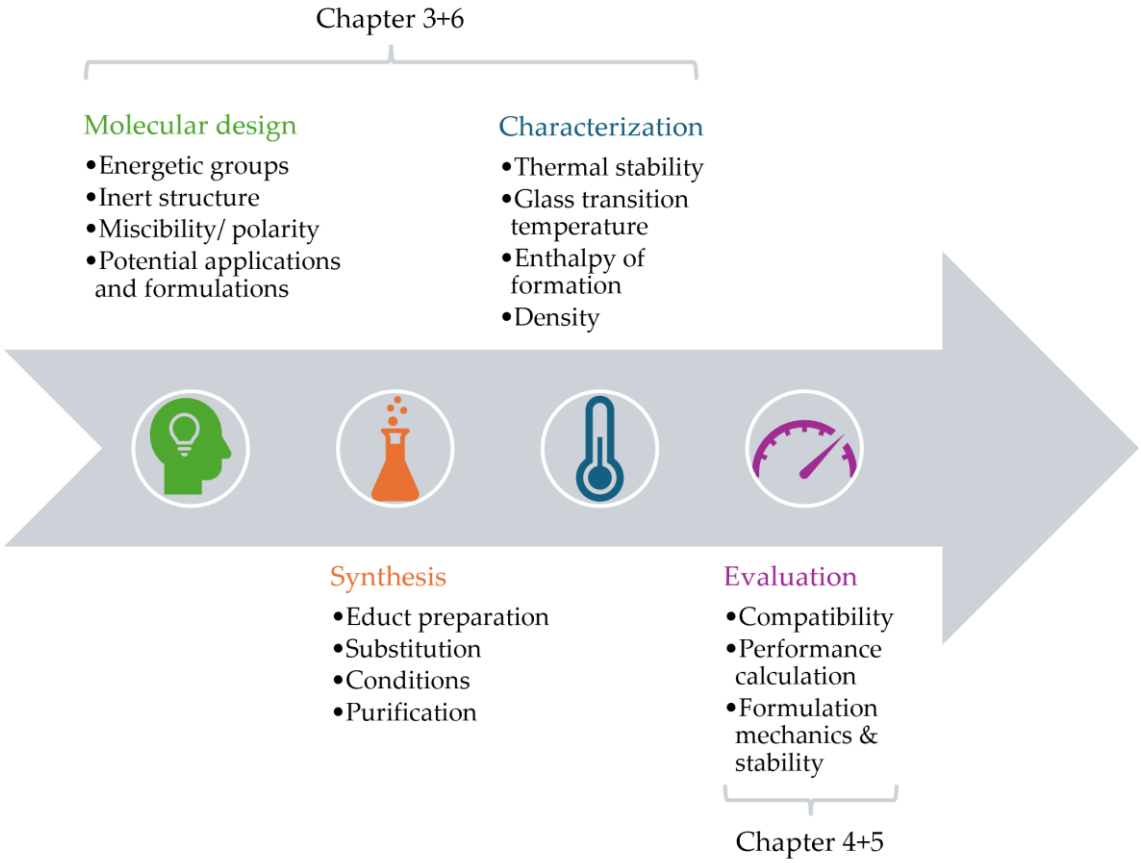

Figure 1 General workflow of this dissertation.

Chapter 3 introduces the concept of energetic plasticizers based on nitrofurazanyl ethers. A variety of compounds with distinct side chains were screened to study the fundamental properties of these novel molecules. Chapter 4 built on this work with experimental compatibility and theoretical performance studies of the most promising molecule NFPEG3N3. Chapter 5 contains a comprehensive investigation of a new formulation and comparisons with formulations produced using common energetic plasticizers. Chapter 6 describes the synthesis and characterization of NFPEG2N3, a more energy-rich nitrofurazanyl ether that was designed based on the previous results with NFPEG3N3.

Chapter 3 presents nitrofurazanyl ethers as a novel class of energetic plasticizers. Four ethers were synthesized via nucleophilic substitution of DNF with linear alkoxides. The presence of ethylene glycol side chains was the decisive factor in achieving good plasticizing properties. NFPEG2Me and especially NFPEG3N3 achieved very low glass transition temperatures (T_g −69 to −72 °C). NFPEG3N3 combines low viscosity (32 mPa·s, 20 °C), high density (1.34 g/cm³), competitive energy (calculated heat of explosion 3421 J/g), and superior thermal behavior (closed crucible DSC onset 179 °C). In GAP diol mixtures, 10wt% NFPEG3N3 reduced viscosity by ~45% and lowered the T_g by 3.3 °C. There was no adverse shift in GAP decomposition, and separate TGA peaks indicated no destabilizing interaction. Nitrofurazanyl ethers are feasible and tunable energetic plasticizers. Within the study NFPEG3N3 delivers the optimal balance of low T_g, thermal stability, density, insensitivity, and processability, decisively outperforming Bu-NENA in decomposition temperature and oxygen balance. It is a strong candidate for GAP-based formulations and merits compatibility and cured-formulation studies.

Chapter 4 deals with the compatibility and performance of NFPEG3N3 with key components. GAP diol, HMX, Desmodur N100 (HDI-biuret), and ADN were assessed per STANAG 4147 using dynamic thermogravimetry (TG) and heat-flow microcalorimetry (HFMC). The compatibility of NFPEG3N3 with GAP diol, HMX, and the isocyanate N100 was confirmed using both methods. ADN met the 1% heat-of-explosion criterion, but TG showed 5.2% excess mass loss (above the 4% threshold). This indicates long-term thermal incompatibility with untreated ADN. Thermodynamic modeling of a representative ADN/HMX/GAP propellant clearly showed that replacing 15wt% GAP with NFPEG3N3 increased the volume-specific impulse by 77 N·s/dm³ and improved oxygen balance versus Bu-NENA, with performance close to BDNPA/F. NFPEG3N3 is compatible with GAP, HMX, and N100 and improves volume-efficiency in ADN-containing propellants. Its pairing with uncoated ADN is questionable and corresponding mitigation measures (e.g., use of polymer-coated ADN) should be explored. NFPEG3N3's high density, low T_g, and stability make it a clear choice for advancement to cured formulation and aging studies, with a priority on energetic formulations that avoid direct contact with untreated ADN.

Chapter 5 benchmarks NFPEG3N3 against BDNPA/F, Bu-NENA, DNDA-57, and a plasticizer-free reference in a fixed GAP/HMX composite (77wt% HMX; binder: 18.4wt% GAP + 4.6wt% plasticizer). NFPEG3N3 delivered the lowest formulation T_g (−50.9 °C) and strongest plasticization, with a peak tensile strength comparable to Bu-NENA/DNDA-57 (0.36–0.38 MPa), the highest ductility (3.8% strain at max stress), and the lowest Youngs modulus (16.7 MPa). All formulations met stability criteria (VST, HFMC, mass loss), with NFPEG3N3 showing distinctly lower heat release and mass loss than nitrate-ester references. Combustion tests found no significant change in burn rate at 7 MPa, but NFPEG3N3 reduced the pressure exponent by 16.5% (to 0.792), improving robustness. NFPEG3N3 outperformed the plasticizer-free reference in detonation pressure and temperature in a PBX formulation. As a propellant, it matched Bu-NENA in mass-specific impulse and exceeded it in volume-specific impulse. NFPEG3N3 offers clear advantages: superior low-temperature mechanics, stability, and improved combustion pressure sensitivity. This positions it as a promising alternative to nitrate-ester plasticizers for GAP/HMX systems.

Chapter 6 presents NFPEG2N3, a shorter-chain azido nitrofurazanyl ether engineered to enhance energy while maintaining optimal plasticization. NFPEG2N3 is a dense liquid (ρ = 1.375 g/cm³) with very low T_g (−74.9 °C), TGA mass-loss midpoint 156 °C, and closed crucible DSC onset 186 °C. It was synthesized via substitution of DNF with lithium 2-(2-azidoethoxy)ethanolate. It has the highest enthalpy of formation (164 kJ/mol) and heat of explosion (4024 J/g) among comparators (BDNPA/F, Bu-NENA, NFPEG3N3). Blending with GAP reduces viscosity by 70% at 20wt%. The neat liquid is highly impact sensitive (<1 J), but at typical loadings the overall formulation sensitivity is dominated by the binder. Furthermore, the mechanical sensitivity of many nitrate ester plasticizers in use is comparable. Modeling clearly indicates favorable energy–temperature trade-offs in NC systems (optimum ~20wt%) and in GAP/AP/HMX propellants, with top mass-specific impulse at 5–10wt% and higher volume-specific impulse than Bu-NENA. NFPEG2N3 combines exceptional energy with effective rheological control. Despite high neat-liquid sensitivity, it is well-suited to GAP.

In summary, this dissertation makes an overall contribution to the field of energetic heterocycles by adding new furazan-based materials. For the first time, it introduces

nitrofurazanyl ethers as plasticizers and highlights their potential as essential components in GAP-based formulations. This achievement stems not only from synthesizing and characterizing new compounds, but also from conducting comprehensive evaluation studies that align with NATO standards, including compatibility and long-term stability tests. Additionally, energetic formulations were manufactured and compared. Due to the superior properties of the two most promising molecules, NFPEG3N3 and NFPEG2N3, documented in this work, they could potentially substitute for Bu-NENA as an energetic plasticizer.

8 Limitations and perspective

Looking ahead, the immediate priority is to consolidate compatibility and aging margins while preparing the chemistry for scaling up. First, borderline behavior of NFPEG3N3 with untreated ADN should be revisited using polymer-coated ADN prills. Then, a structured aging program should be conducted (isothermal HFMC/TG per STANAG, Arrhenius matrices at 60–90 °C, and humid/thermal cycling) to quantify long-term stability and establish clear usage parameters. The compatibility of NFPEG2N3 with ADN should also be investigated. The shorter side chain has the potential to lead to compatibility due to a presumably lower solubility of ADN. In parallel, plasticizer retention must be evaluated through migration and volatility studies and correlated with T_g drift and modulus changes in order to develop predictive retention models. Additionally, mechanical characterization should extend beyond quasi-static tensile tests to include dynamic mechanical analysis (DMA) over temperature and low-temperature tensile testing. Curing studies like FTIR/NIR conversion and swelling/DMA for network density will clarify whether the observed property changes arise from true plasticization or from an altered polyurethane network formation process. Formulation safety should be extended to include ESD, migration and small flame tests.

From a broader perspective, azide functionalities are incompatible with hydroxyl-terminated polybutadiene (HTPB), the most widely used binder in modern composite propellants and plastic-bonded explosives. This limits the use of straightforward methods to energize HTPB with new azide-containing nitrofurazanyl ether plasticizers, which maintains reliance on specialized energetic binders such as GAP. A promising approach is to introduce groups that are energetically compatible with HTPB, such as nitro groups or carefully designed nitrate ester moieties. However, this approach must be balanced against stability concerns, such as the acid-induced, autocatalytic decomposition of nitrate esters and their incompatibility with isocyanate crosslinkers. To ensure miscibility and prevent migration, the polarity of the new molecules may need to be adjusted by modifying the inert structures. In the future, using truly HTPB-compatible energetic plasticizers could accelerate the development of nitrofurazanyl ether-based energetic plasticizers faster than pathways dependent on energetic specialty binders.

All of the new compounds presented here are derived from DNF. It is a mechanically sensitive liquid that is difficult to obtain and handle. However, it has been successfully stored at Fraunhofer ICT for several years at low temperatures and in darkness without any loss of quality. Its common precursor, DAF, is expensive but commercially available. The flow chemistry synthesis developed during this dissertation enabled the production of sufficient DNF for the synthesis of nitrofurazanyl ethers on a laboratory scale. A conference paper with a detailed description of the DNF flow synthesis can be found in Appendix B. However, significant improvements in the efficiency, throughput, and operability of DNF synthesis are still needed for larger-scale formulation studies with the new plasticizers. Flow chemistry offers a practical and safe pathway through numbering up (parallelization) of reactor compartments rather than traditional scaling up. Future work on the application of nitrofurazanyl ethers should therefore include research on preparing and safely handling DNF. This will facilitate the translation of advances in nitrofurazanyl ether plasticizers from the laboratory to the production of energetic materials that are economically viable and readily available.

Furthermore, a large number of new energetic molecules can still be obtained through the substitution of DNF, as demonstrated in this dissertation. This opens ample opportunities for preparative organic chemists in the future, assuming sufficient quantities of the starting material are available.

Appendix A: Lists of publications and presentations

A.1 List of first author publications

P. Lieber, U. Schaller, T. M. Klapötke, Synthesis and characterization of novel nitrofurazanyl ethers as potential energetic plasticizers, *RSC Adv.* **2025**, *15*, 12577–12584, https://doi.org/10.1039/D5RA01282A.
Published on April 22, 2025.

P. Lieber, U. Schaller, T. M. Klapötke, Energetic plasticizers for GAP-based formulations with ADN: compatibility and performance evaluation of a nitrofurazanyl ether, *RSC Adv.* **2025**, *15*, 37006–37011, https://doi.org/10.1039/D5RA05154A.
Published on October 6, 2025.

P. Lieber, U. Schaller, T. M. Klapötke, Comparative assessment of energetic plasticizers including NFPEG3N3 in a GAP/HMX formulation: mechanics, stability, combustion, and performance, *Propellants, Explos., Pyrotech.*, in press, **2025**, https://doi.org/10.1002/prep.70095.
Accepted for publication on November 17, 2025.

P. Lieber, A. Omlor, U. Schaller, T. M. Klapötke, Synthesis and characterization of an azido nitrofurazanyl ether as energy-rich heterocyclic plasticizer with a low glass transition temperature for GAP and NC formulations.
Submitted to *Propellants, Explos., Pyrotech.* on November 03, 2025.

A.2 List of conference publications, posters and presentations

P. Lieber, Continuous flow synthesis of dichloroglyoxime, in: *Proceedings of the 24th Seminar on New Trends in Research of Energetic Materials (NTREM*), Pardubice, Czech Republic **2022**.
Oral presentation and conference paper: April 6-8, 2022.

P. Lieber, U. Schaller, T. M. Klapötke, Investigation of 3, 5-diamino-1, 2, 4-oxadiazole as a precursor for energetic salts, in: *Proceedings of the 25th Seminar on New Trends in Research of Energetic Materials (NTREM*), Pardubice, Czech Republic **2023**.
Poster and conference paper: April 19-21, 2023.

P. Lieber, P. Schultz, U. Schaller, T. M. Klapötke, Synthesis and Characterization of a 3,5-Diamino-1,2,4-Oxadiazole-based Perchlorate and Dinitramide Salt, in: *52nd Annual International Conference of Fraunhofer ICT (poster session)*, Karlsruhe, Germany **2023**.
Poster: Juni 27-30, 2023.

P. Lieber, U. Schaller, T. M. Klapötke, Amine oxidation under challenging conditions: implementation of a flow-chemistry procedure for 3,4-dinitrofurazan synthesis, in: *Proceedings of the 26th Seminar on New Trends in Research of Energetic Materials (NTREM)*, Pardubice, Czech Republic **2024**.
Oral presentation and conference paper: April 17-19, 2024.

P. Lieber, U. Schaller, T. M. Klapötke, Energetic plasticizers for GAP-based formulations with ADN: Compatibility and performance evaluation of a nitrofurazanyl ether, in: *Proceedings of the 48th International Pyrotechnics Society Seminar*, Munich, Germany **2025**.
Oral presentation and conference paper: September: 8-12, 2025.

Appendix B: Conference publications

The appendix contains a collection of conference publications from this dissertation, spanning from April 2021 to December 2025.

B.1 Continuous flow synthesis of dichloroglyoxime

Patrick Lieber*

As published in: *Proceedings of the 24th Seminar on New Trends in Research of Energetic Materials (NTREM)*, **2022**.

Abstract

Dichloroglyoxime is an intermediate in the synthesis of the promising energetic material dihydroxylammonium-5,5'-bistetrazole-1,1'-diolate (TKX-50). The classical synthesis by chlorination of glyoxime with elemental chlorine in a batch procedure has numerous disadvantages concerning safety and scalability due to the exothermic and heterogeneous nature of the reaction. Because of the high reactivity of chloronitroso intermediates and to prevent an over-chlorination to nitrosyl chlorides, cooling of the dispersion to at least -20°C is necessary. This requires strong cooling capacity, slow dosing and intense mixing, but still poses the risk of thermal runaway and a large toxic inventory. In order to overcome these drawbacks and still utilize the high atomic economy and the low cost of chlorine as a chlorination reagent, a continuous flow synthesis was developed. The resulting process has decisive advantages for scale-up the synthesis, such as significantly higher reaction temperature and increased safety. The low volume of the flow reactor provides a lower toxic inventory during the reaction compared to a conventional batch reactor. With a lab bench-scale setup a dichloroglyoxime throughput of 31 g/h was achieved with a yield of 70%, comparable to the batch reaction. Moreover, the reaction temperature in the flow reactor could be increased to 20 °C and the chlorine gas is fed into a closed reaction system and fully conversed.

Keywords: flow chemistry; heterogeneous reactions; dichloroglyoxime; chlorination.

Introduction

Dihydroxylammonium-5,5'-bistetrazole-1,1'-diolate (TKX-50) is currently one of the most interesting molecules to meet the need for high-performing, insensitive and

environmentally friendly explosives [1-3]. It's synthesis can be performed in a few steps by inexpensive and available chemicals [4]. Nevertheless, the search for efficient and safe processes is subject of current research [5, 6].

An important step in the synthesis of TKX-50 is the formation of dichloroglyoxime (DCG). It is obtained by the chlorination of glyoxime, which can be easily synthetized from abundantly available aqueous solution of glyoxal [7, 8]. Elemental chlorine has the lowest cost and highest atomic efficiency as a chlorinating agent, but it is also extremely reactive and toxic and therefore difficult to handle. Due to strong heat generation, reactive intermediates and the risk of over-chlorination to toxic nitrosyl chlorides, the traditional batch synthesis of dichloroglyoxime by chlorination with elemental chlorine in ethanol must be conducted at least at -20 °C.

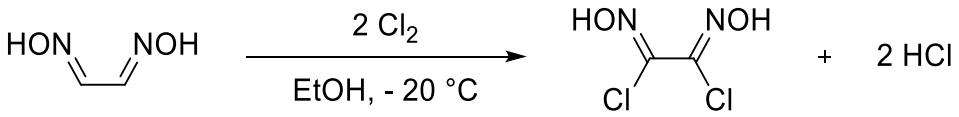

Figure 1 Reaction equation for the synthesis of dichloroglyoxime under traditional batch conditions.

The reaction proceeds in two steps, first monochlorglyoxime is formed and then chlorinated again to dichloroglyoxime. In each step chlorine is added to the aldoxime double bond and hydrogen chloride is eliminated followed by a rearrangement of the chloronitroso compound to chloroxime [9].

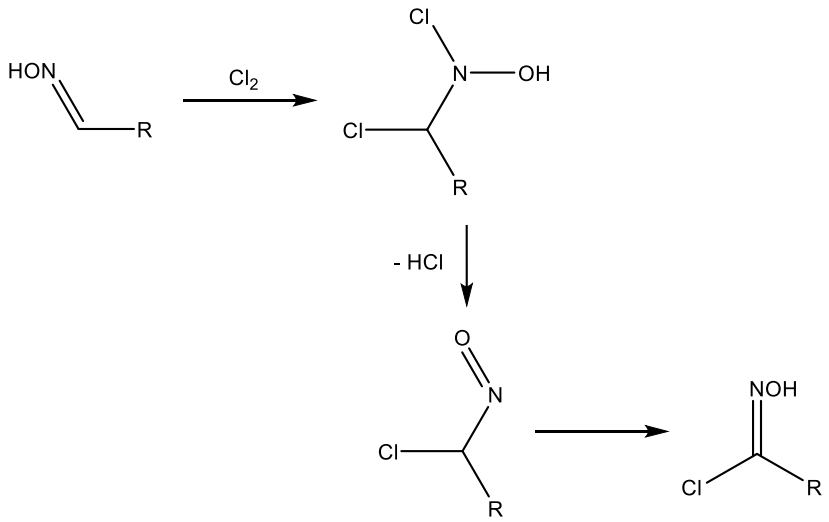

Figure 2 Oxime chlorination mechanism.

Recently, flow chemistry by using micro- an mesofluidic reaction devices has been successfully used to harness highly exothermic and dangerous reactions. The high atomic economy and outstanding reactivity of reagents that were previously considered as forbidden or uncontrollable can be exploited this way in laboratory as well as in technical scale [10]. This is enabled through the advantages of flow processing including rapid mass and heat transfer, accurate residence time control, easier reaction scale-up and full process automation [11].

In particular mass transport in gas-liquid heterogeneous systems benefits from the segmented flow regime where bubbles of gas are separated by slugs of a liquid. The secondary flow patterns formed in both the liquid and gas segments enhance the mixing and increase mass transfer [12]. Strongly exothermic reactions benefit by the high surface-to-volume ratio that allows for a fast cooling, heating and precise temperature control. This way, hot spots that could lead to a thermal runaway can be prevented [10]. The ability to precisely control the residence time of the molecules in the reactor can make it possible to prevent the decomposition of products by overreaction and to improve handling of reactive intermediates [13].

Since the characteristics of flow chemistry offer clear potential to perform the chlorination of glyoxime more safely and effectively, the aim of this study was to establish and evaluate such a process for small-scale synthesis.

Experimental

Continuous flow setup

A flow setup consisting of a PEEK T-piece as mixing element and PTFE tubes of 1.6 mm internal diameter as coiled tubular reactor was used to perform the reaction (Figure 2, 3). The liquid phase was dosed by a syringe pump and the gas phase by using a pressure regulator and a calibrated digital mass flow controller. Temperature control was achieved by placing the mixer and the reactor in a bath thermostat. The separation of the product solution from gaseous components was carried out continuously during the synthesis in the collection bottle. A nitrogen purge was finally used to remove remaining chlorine and gaseous by-products from the collected product solution. Resulting exhaust gas was guided into a saturated sodium hydroxide solution for cleaning.

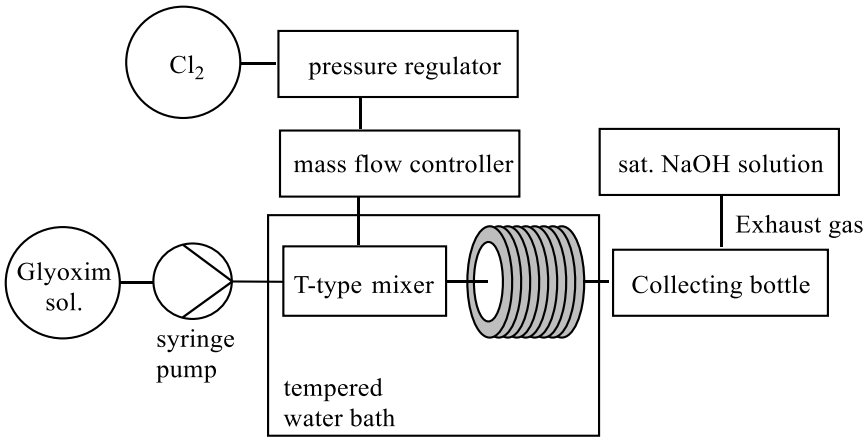

Figure 3 Schematic representation of the continuous flow setup.

Figure 4 Experimental setup in the fume hood.

Parameters

For all experiments, glyoxime was solved in ethanol as 0.7 M solution and chlorine was taken without further purification from the bottle. Reaction temperatures between -20 °C and 20 °C and residence times from 10 min to 6.7 min were investigated. For the optimization with regard to the necessary amount of chlorine, the gas was dosed with 2.9 mmol/min (73 ml/min) to 8.4 mmol/min (208 ml/min) while glyoxime was dosed with 1.4 mmol/min (2 ml/min). For experiments at maximum product capacity, the glyoxime solution was dosed with 4.2 mmol/min (6 ml/min) and the chlorine with 500 ml/min (4.8 equivalents). The reaction temperature was 20 °C and the residence time 6.7 minutes. Dichloroglyoxime was obtained with a yield of 75%.

Purification and analysis

The solvent was evaporated and the resulting solid was washed with chloroform. Dichlorogyloxime was recived as white solid. It was analyzed by DSC, IR and Raman spectroscopy. DSC (5 °C min^{-1}): 199 °C (dec.); IR (ATR, cm^{-1}): ũ = 3241 (s), 3074 (m), 2864 (m), 1620 (w), 1409 (m), 1335 (m), 999 (vs), 850 (vs), 683 (vs), 665 (vs), 490 (m); Raman (1064 nm, 350 mW, 25 °C, cm^{-1}): ũ = 3245 (0.03), 1596 (2.0), 1470 (0.7), 1249 (0.5), 1206 (0.02), 1052 (0.05), 689 (0.4), 605 (0.1), 446 (0.2), 342 (0.4), 276 (0.5).

Results and Discussion

Initially the influences of reaction temperature and reaction time were investigated. Temperature was varied by changing the temperature of the bath whereas the residence time was increased or decreased by adjusting the length of the reactor. The experiments were carried out with constant flow rate and 2.1 equivalents chlorine.

Within the temperature range of -20 to 10 °C, a strong temperature increase in the collection vessel as well as a large amount of chlorine in the exhaust gas was observed which indicated incomplete reaction. Increasing the residence time from 6 min to 10 min did not have influence on that. Complete reaction without heat generation from the product solution in the collection vessel was reached at a reaction temperature of 15 °C and a residence time of 10 min. In this case, dichloroglyoxime was obtained with 47% isolated yield as a pale pink powder.

Concerning the flow regime an unsteady segmented flow of gas bubbles and liquid slugs was first observed. The volume of the gas bubbles decreased along the reactor tube until the gas phase almost disappeared while the reaction mixture was passing the reactor. This indicates an almost complete dissolution of chlorine, dichloroglyoxim, hydrogen chloride and other by-products in the liquid phase. However, the by-products quickly outgassed after collection in the bottle. This became apparent by a decolorization of the initially brownish product solution.

After suitable conditions for a continuous synthesis were found as described, the amount of chlorine was optimized. Chlorine amounts between 2.1 and 6 equivalents were investigated (Table 1). Due to the high solubility of chlorine in the liquid phase, no significant change in residence time was observed at different chlorine levels. Within the studied range, a maximum yield of 72% was observed using an excess of 5 equivalents

of chlorine. Higher or lower quantities resulted in a reduced yield. Despite a slight pale pink coloration at small amounts of chlorine, no contamination with monochloroglyoxime or glyoxime could be detected by Raman spectroscopy. A persistent slightly bluish coloration of the product solution was observed with an excess of 6 equivalents. This can be attributed to the formation of nitrosyl chlorides by over-chlorination. However, the completely colorless product obtained from the 6 equivalents excess experiment did not show any impurities but a 10% reduced yield compared with the maximum yield.

Table 1 Optimization of the chlorine dosage.

Chlorine [ml/min]	equivalents	DCG is. yield %
73	2.1	47
104	3	58
139	4	59
174	5	72
208	6	62

In the next step, the same setup was further optimized in order to increase throughput. By further increasing the temperature to 20 °C, the residence time could be reduced to 6.7 min. An increase of the reactor volume to 40 ml resulted in a dichloroglyoxime throughput of 30 g/h with an isolated yield of 75% (Table 2). This enabled a threefold increase of the initial throughput.

Table 2 Selected parameters and isolated yields.

Glyoxime [mmol/min]	Chlorine equivalents	Residence time [min]	Bath temperature [°C]	DCG is. yield %	DCG [g/h]
1.4	5	10.0	15	72	9.3
4.2	4.8	6.7	20	75	30

Conclusion

A continuous flow approach for the chlorination of glyoxime using elementary chlorine was successfully implemented. Compared to the batch synthesis, advantageous reaction conditions and increased safety were achieved. The reactions temperature could be increased from -20 °C to 20 °C and a comparable yield of 72-75% was achieved. The flow-reactor allows a reduction of the toxic inventory by its small volume to a minimum and allows additionally the reaction of chlorine in a closed system. With a bench scale setup,

a dichloroglyoxime capacity of 30 g/h was achieved. The developed procedure satisfies and even exceeds the preparative demands at a laboratory level with simple means but could also be an interesting starting point for an industrial process.

References

[1] Klapötke, Thomas M., and Muhamed Suceska. "Theoretical evaluation of TKX-50 as an ingredient in rocket propellants." Zeitschrift für anorganische und allgemeine Chemie 647(5), p. 572-574, 2021.

[2] Gottfried, Jennifer L., Thomas M. Klapötke, and Tomasz G. Witkowski. "Estimated Detonation Velocities for TKX-50, MAD-X1, BDNAPM, BTNPM, TKX-55, and DAAF using the Laser–induced Air Shock from Energetic Materials Technique." Propellants, Explosives, Pyrotechnics 42(4), p. 353-359, 2017.

[3] Klapötke, Thomas M., et al. "Toxicity Assessment of Energetic Materials by Using the Luminescent Bacteria Inhibition Test." Propellants, Explosives, Pyrotechnics 46(1), p. 114-123, 2021.

[4] Fischer, Niko, et al. "Pushing the limits of energetic materials–the synthesis and characterization of dihydroxylammonium 5, 5′-bistetrazole-1, 1′-diolate." Journal of Materials Chemistry 22(38), p. 20418-20422, 2012.

[5] Ha, Heun-Jong, et al. "Synthesis of TKX-50 via 2-Methoxyisopropyl-Protected Diazidoglyoxime as an Insensitive Intermediate." Propellants, Explosives, Pyrotechnics 46(5), p. 732-736, 2021.

[6] Golenko, Yulia D., et al. "Optimization Studies on Synthesis of TKX-50." Chinese Journal of Chemistry 35(1), p. 98-102, 2017.

[7] Wingard, Leah A., Pablo E. Guzmán, and Jesse J. Sabatini. "A chlorine gas-free synthesis of dichloroglyoxime." Organic Process Research & Development 20(9), p. 1686-1688, 2016.

[8] Willer, R. L. U.S. Patent Number 4539405 A, 1985.

[9] Kukushkin, Yuri N., et al. "Different chlorination modes of oximes: chlorination of salicylaldoxime coordinated to platinum." Inorganica chimica acta 285(1), p. 116-121, 1999.

[10] Movsisyan, Marine, et al. "Taming hazardous chemistry by continuous flow technology." Chemical Society Reviews 45(18), p. 4892-4928, 2016.

[11] Plouffe, Patrick, et al. "On the scale-up of micro-reactors for liquid–liquid reactions." Chemical Engineering Science 143, p. 216-225, 2016.

[12] Tan, J., et al. "Mass transfer performance of gas–liquid segmented flow in microchannels." Chemical Engineering Journal 181, p. 229-235, 2012.

B.2 Investigation of 3,5-diamino-1,2,4-oxadiazole as a precursor for energetic salts

Patrick Lieber*, Uwe Schaller, Thomas M. Klapötke

As published in: *Proceedings of the 25th Seminar on New Trends in Research of Energetic Materials (NTREM)*, **2023**.

Abstract

1,2,4-Oxadiazole is an attractive backbone for energetic materials as it shows a positive impact on the oxygen balance compared to other heterocycles like imidazole or triazole. The suitability of 1,2,4-oxadiazole as a cation in energetic salts should be evaluated, as ionic compounds are known for high densities and low vapor pressure. 3,5-Diamino-1,2,4-oxadiazole (AOA) as a starting material can be easily synthesized from sodium dicyanamide and hydroxylammonium chloride. Despite indications in the literature to be acid sensitive, AOA hydrochloride was successfully synthesized. To the best of our knowledge, this is the first report of an AOA-based salt. The synthesized compound was characterized by NMR, IR spectroscopy, Raman spectroscopy, ion chromatography and thermal analysis.

Keywords: precursor; 3,5-diamino-1,2,4-oxadiazole; hydrochloride.

Introduction

Oxadiazole rings are promising building blocks for the synthesis of energetic materials due to their high enthalpy of formation and good oxygen content. Among the four oxadiazole isomers, historically furazans have received significant attention in Russia since they show the highest enthalpy of formation (Figure 1) [1, 2]. Despite their high energy content, furazan-based materials are often more sensitive towards impact and heat compared to 1,2,4- and 1,2,4-oxadiazoles [3]. 1,2,3-Oxadiazole has not been considered suitable for energetic materials as it tends to tautomerize to diazoketones [4]. 1,2,4- and 1,3,4-oxadiazole-based compounds have received limited attention so far for use in energetic materials. The 1,2,4-oxadiazole shows a lower enthalpy of formation compared to furazan and triazole. However, its stronger N-O bond, which leads to thermal stability, and higher oxygen content (compared to triazole) make it a potentially promising candidate for balancing performance, oxygen balance and stability [5].

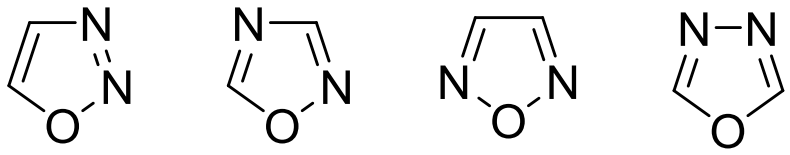

Figure 1 Oxadiazole-Isomers.

An easily accessible starting material for 1,2,4-oxadiazole-based energetic materials is 3,5-diamino-1,2,4-oxadiazole (AOA) [6]. Although high performing AOA-based energetic materials as the 1,2-bis (3-nitro-1,2,4-oxadiazole-5-yl) diazene and guanidinium bis (3-nitro-1,2,4-oxadiazole-5-yl) amide have been published recently, very low yields and an uncertain chemical durability remain as a challenge (Figure 2) [7, 8]. In contrast to these neutral or anionic molecules, little energetic materials with an AOA-based cation are known. However, Qiong et al. report a hydrolytic ring opening at the 1,2,4-oxadiazole in acidic solutions that makes the stability of a protonated AOA cation look uncertain. (Figure 3) [9].

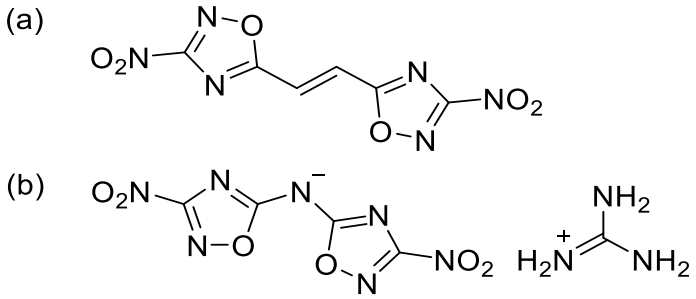

Figure 2 (a) 1,2-Bis (3-nitro-1,2,4-oxadiazole-5-yl) diazene, (b) guanidinium bis (3-nitro-1,2,4-oxadiazole-5-yl) amide.

Numerous energetic salts of diaminofurazan are already known in the Russian literature [10]. The preparation of analogous compounds based on the diaminofurazan-isomer AOA could lead to new energetic materials with the same oxygen balance and higher stability. The aim of this work is to verify the acid sensitivity of AOA, prepare the AOA hydrochloride (AOA·HCl) and characterize its substance properties.

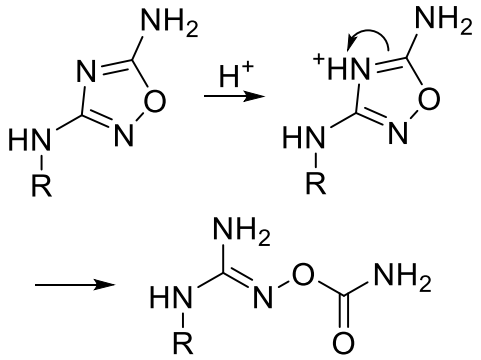

Figure 3 Proposed mechanism for a hydrolytic ring opening of 1,2,4-oxadiazole [9].

Results and discussion

Synthesis

3,5-Diamino-1,2,4-oxadiazole (AOA) was synthesized from sodium dicyanamide and hydroxylammonium chloride according to literature (Figure 4) [6]. By extending the reaction time to 72 h, the yield could be increased from 45% to 75%. The product was recrystallized twice from water to remove reactant residues. Without recrystallization, a brownish discoloration occurs on the surface of the raw product during storage.

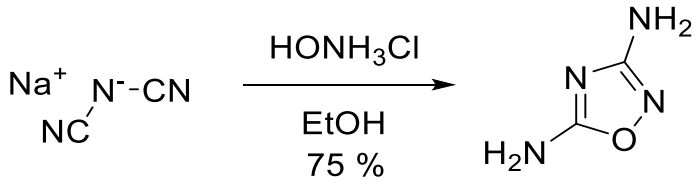

Figure 4 Reaction equation for the preparation of AOA.

AOA hydrochloride (AOA·HCl) can be obtained by precipitation from acetonitrile using concentrated hydrochloric acid (Figure 5). A disadvantage is the low solubility of AOA in acetonitrile. By adding two percent by volume of water the solubility can be increased to 12.3 g/L without disturbing the precipitation. The product is dried overnight in the fume hood and AOA·HCl is obtained as a white solid in 89% yield. No hygroscopic tendency was observed after a rigorous wash with acetonitrile.

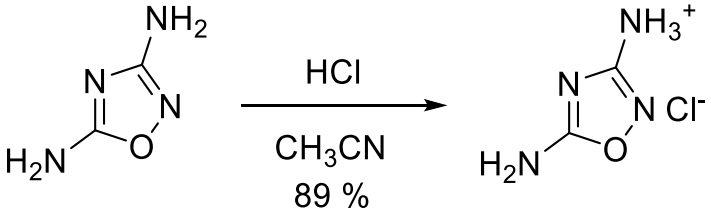

Figure 5 Synthesis of AOA·HCl in acetonitrile by precipitation.

Ion chromatography

AOA hydrochloride was analyzed by ion chromatography using an ICS-3000 from Dionex. An IonPac AS11-HC 2x250 mm with pre-column AG11-HC 2x50 mm was used as column and water (100 mM NaOH 70:30) as eluent. The flow rate was 0.38 ml/min at 30 °C. A conductivity detector with chemical suppression was used as the detector. A mass fraction of 26.85% chloride was determined. This corresponds to a 1:1 stoichiometry of the oxadiazole cation and the chloride, revealing AOA hydrochloride as a monochloride.

NMR spectroscopy

The identity and purity of the synthesized AOA was confirmed by NMR spectroscopy: ^{1}H-NMR δ_H (400 MHz, DMSO-d6) 7.26 (2H, s, NH2), 5.59 (2H, s, NH2); ^{13}C-NMR δ_C (100 MHz, DMSO-d6) 170.2, 168.6.

The received AOA·HCl does not show any ^{1}H-NMR signals in deuterated protic solvents, due to the proton exchange. Only one signal at 8.30 ppm is found in DMSO-d6 at our 60 MHz benchtop NMR. ^{13}C-NMR spectroscopy exhibits two signals corresponding to the two carbon atoms in the ring: ^{13}C-NMR δC (100 MHz, D_2O) 167.9, 164.2.

IR and Raman spectroscopy

Solid spectra of AOA and AOA·HCl were recorded by FTIR and Raman spectroscopy: AOA IR (ATR, cm^{-1}) = 3394 (s), 3307 (br), 3176 (br), 3088 (br), 1688 (s), 1641(s), 1600 (m), 1576 (m) C=N, 1452 (s), 1432 (s) ring mode, 1361 (m) ring mode, 1133 (m) ring-breathing, 1064 (m), 999 (m), 887 (m) N-O, 798 (w), 758 (m), 684 (m), 656 (m), 573 (m), 529 (m), 433 (m); Raman (1064 nm, 600 mW, 25 °C, cm^{-1}): ũ = 3399, 3337, 3179, 3081, 1670, 1645, 1566 C=N, 1473, 1370 ring mode, 1168, 1060, 1005, 890, 792, 666, 507; AOA·HCl IR (ATR, cm^{-1}) ũ = 3160 (br), 3054 (br), 2903 (br), 2807 (br), 2640 (br), 1709 (m), 1654 (s), 1630 (w), 1590 (w), 1536 (s), 1341 (w), 1109 (w), 1070 (w), 1047 (s), 1016 (m), 860 (m), 777 (w), 757 (w), 733 (m), 679 (w), 658 (w), 599 (m), 520 (w), 510 (w); Raman (1064 nm, 600 mW, 25 °C, cm^{-1}): ũ = 3159, 2653, 1719, 1657, 1613, 1544, 1393, 1352, 1113, 1070, 1051, 1018, 864, 778, 746, 650, 512.

Based on the literature-documented ring opening of a similar 1,2,4-oxadiazole derivate in acidic solution, the question of the acid sensitivity of AOA and AOA·HCl arises [9].

For this purpose, 1 M aqueous solutions of AOA were prepared with different equivalents of conc. hydrochloric acid. The solutions were analyzed by Raman spectroscopy to study the proton concentration dependent behavior of AOA. Increasing acidity from zero to four equivalents of HCl leads to a stepwise change of the Raman spectrum from pristine AOA over mixed spectra to pure AOA·HCl. No evidence of a decomposition or ring opening is found. At a concentration of four equivalents of HCl no AOA bands are measurable anymore. As a result, AOA is entirely protonated.

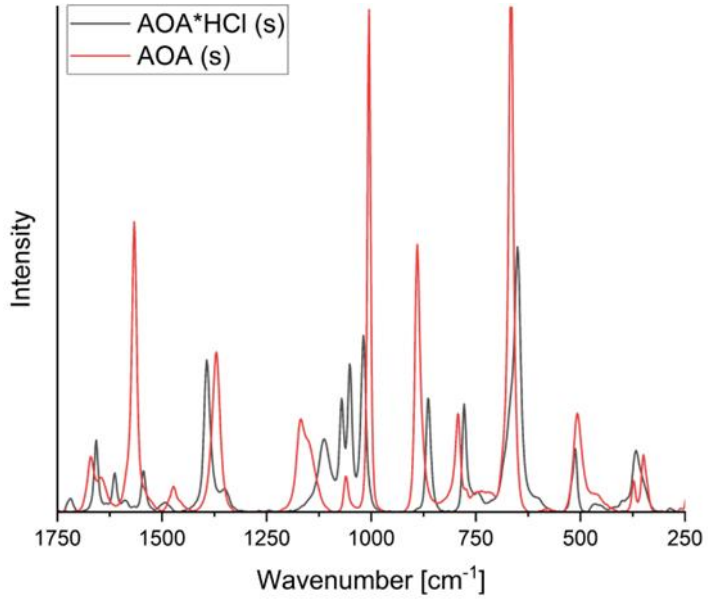

Figure 6 Raman spectra of AOA and AOA·HCl.

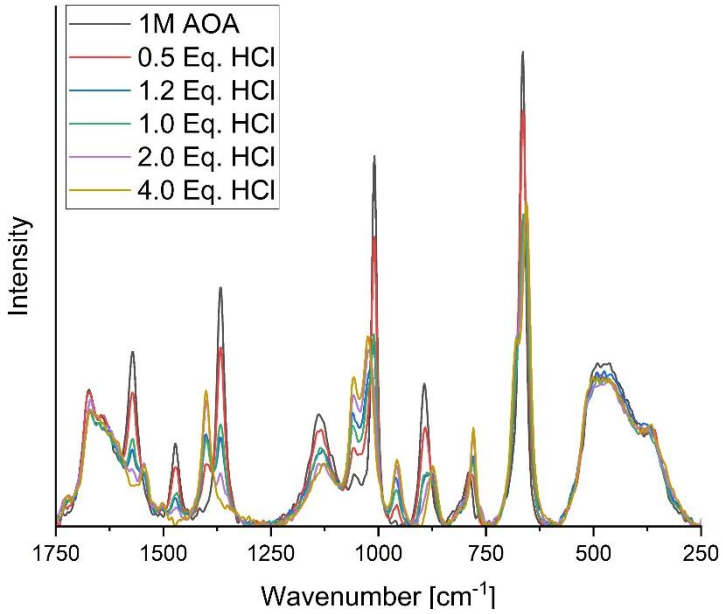

Figure 7 Raman spectra of 1 M solutions of AOA containing various Eq. of conc. HCl.

Thermal properties

Thermal properties of AOA and AOA·HCl were investigated by differential scanning calorimetry (DSC) in a closed crucible and thermogravimetric analysis (TGA) under inert gas flow. Heat rates of 5 °C min^{-1} and 10 °C min^{-1} were used. The DSC analysis of AOA shows a melt at 168 °C followed by decomposition. AOA hydrochloride decomposes at 135 °C for 5 °C min^{-1} and at 143 °C for 10 °C min^{-1} (Figure 8). The TGA exhibits for AOA·HCl a first mass loss at 118 °C for 5 °C min^{-1} and at 122 °C for 10 °C min^{-1} which could be caused by release of hydrochloric acid (Figure 8).

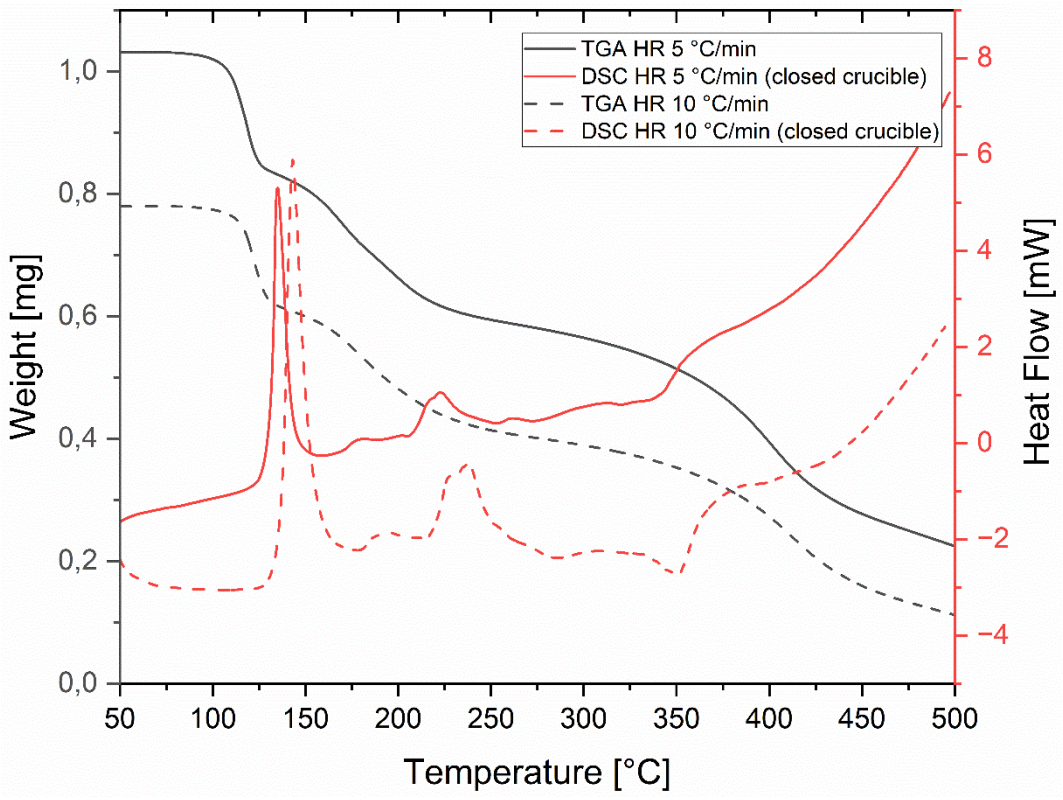

Figure 8 Thermal analysis of AOA·HCl.

Conclusion

The reactivity of AOA towards hydrochloric acid in aqueous solutions was investigated. No evidence of decomposition or reaction other than protonation could be found by Raman spectroscopy. AOA·HCl precipitates in high yield during its synthesis in acetonitrile. It can be stored at room temperature and shows no tendency to hygroscopic behavior. The thermal analysis of AOA·HCl suggests that HCl is released at temperatures above 100 °C. AOA·HCl could be an easily accessible starting material for energetic salts with good oxygen balance. Due to its low decomposition temperature, it

must be investigated if a sufficient thermal stability is obtained with stronger acids like perchloric acid (p K_a -10) and dinitramidic acid (p K_a -6) [11, 12].

Acknowledgment

Thanks to the WTD 91 of the German ministry of defense for the financial support of this work within the framework of the DBES project. I also thank G. Wolf for performing the ion chromatography and H. Schuppler for conducting the thermal analysis. Thanks to W. Schweikert and S. Müller for their assistance in the spectroscopy lab.

References

[1] Fershtat, Leonid L., et al. "Assembly of nitrofurazan and nitrofuroxan frameworks for high-performance energetic materials." ChemPlusChem 82(11), p. 1315-1319, 2017.

[2] Sheremetev, Aleksei B., Nina N. Makhova, and Willy Friedrichsen. "Monocyclic furazans and furoxans." Advances in Heterocyclic Chemistry 78, p. 65-188, 2001.

[3] R. A. Olofson, and J. S. Michelman. "Furazan*, 1, 2." The Journal of Organic Chemistry 30(6), p. 1854-1859, 1965.

[4] J. A. Joule, K. Mills, G. F. Smith, Heterocyclic Chemistry, 3rd ed., Taylor & Francis, New York, 1995.

[5] Wei, Hao, et al. "Combination of 1, 2, 4-oxadiazole and 1, 2, 5-oxadiazole moieties for the generation of high-performance energetic materials." Angewandte Chemie International Edition 54(32), p. 9367-9371, 2015.

[6] Huttunen, Kristiina M., et al. "Towards metformin prodrugs." Synthesis 2008(22), p. 3619-3624, 2008.

[7] Li, Xin, et al. "C4N8O6: A promising ternary CNO-compound with good detonation performance and low sensitivity." Propellants, Explosives, Pyrotechnics 46(8), p. 1286-1291, 2021.

[8] Pang, Fuqing, et al. "Preparation and characteristics of 1, 2, 4-oxadiazole-derived energetic ionic salts with nitrogen linkages." New Journal of Chemistry 42(6), p. 4036-4044, 2018.

[9] Yu, Qiong, et al. "An interesting ring cleavage of a 1, 2, 4-oxadiazole ring." New Journal of Chemistry 41(12), p. 4797-4801, 2017.

[10] I.V. Vigalok, V.I. Kovalenko and Petrova G.G. “Salts of aminofurazanes.” Khimiya Geterotsiklicheskikh Soedinenii 7, p. 998-999, 1991.

[11] Yoshida, Eri. "Control of micellization induced by disproportionation of 2, 2, 6, 6-tetramethylpiperidine-1-oxyl supported on side chains of a block copolymer." Colloid and Polymer Science 287(11). p. 1365, 2009.

[12] Ermolin, N. E., and V. M. Fomin. "On the mechanism of thermal decomposition of ammonium dinitramide." Combustion, Explosion, and Shock Waves 52, p. 566-586, 2016.

B.3 Synthesis and characterization of a 3,5-diamino-1,2,4-oxadiazole-based perchlorate and dinitramide salt

Patrick Lieber*, Peter Schultz, Uwe Schaller, Thomas M. Klapötke

As presented at the poster session of the *52nd Annual International Conference of Fraunhofer ICT*, **2023**.

Introduction

1,2,4-Oxadiazole is an attractive backbone for energetic materials as it has a better impact on the oxygen balance compared to other heterocycles like imidazole or triazole [1]. The suitability of 1,2,4-oxadiazole as a cation in energetic salts should be evaluated, as ionic compounds are known for low vapor pressure. 3,5-Diamino-1,2,4- oxadiazole (AOA) as a starting material can be easily synthesized from sodium dicyanamide and hydroxylammonium chloride [2]. Despite indications in the literature that it is acid- or moisture-sensitive, stable AOA perchlorate and dinitramide salts were successfully synthesized under ambient conditions. To the best of our knowledge, this is the first report of the single crystal structure of an AOA dinitramide salt.

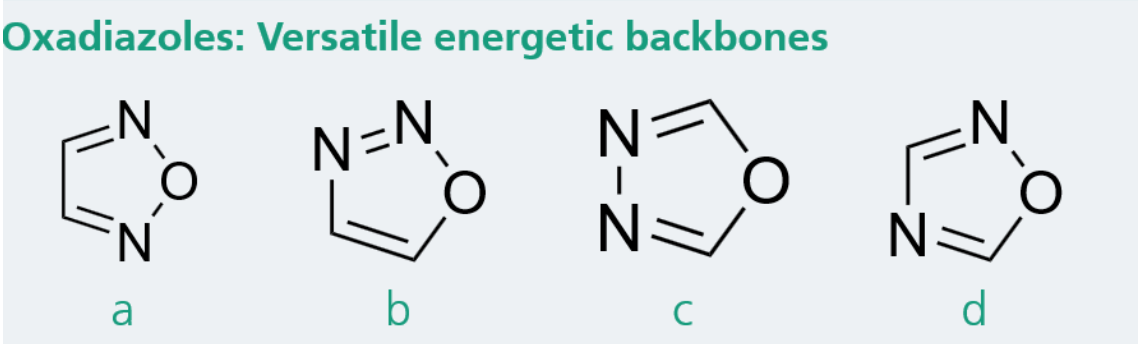

Figure 1 Oxadiazole isomers.

Furazan-based materials (Figure 1a) have received significant attention in Russia since they show the highest enthalpy of formation [4,5]. 1,2,3-Oxadiazole (Figure 1b) has not been considered suitable for energetic materials as it tends to tautomerize to diazoketones. 1,3,4- (Figure 1c) and 1,2,4-oxadiazole-based compounds (Figure 1d) have received limited attention so far for use in energetic materials. The 1,2,4-oxadiazole (Figure 1d) shows a lower enthalpy of formation compared to furazan and triazole. However, its stronger N-O bond, which leads to thermal stability, and higher oxygen content (compared to triazole) make it a potentially promising candidate for balancing

performance, oxygen balance and stability [1]. Moisture sensitive salts of diaminofurazan are already known in the literature [6]. In a previous study we could show that AOA forms a hydrochloride (AOA·HCl), that is stable at ambient conditions [7].

Synthesis

Perchlorate $[AOAH]^+[ClO_4]^-$ was synthesized via direct protonation from perchloric acid in trifluoroacetic acid with a yield of 87% as white solid. Attempts to receive the product from salt metathesis of AOA·HCl and anhydrous sodium perchlorate resulted in an impure product. Dinitramide salt $[AOAH]^+[N_3O_4]^- \cdot ½\ H_2O$ was synthesized from $[AOAH]^+[ClO_4]^-$ via salt metathesis with potassium dinitramide in methanol with a yield of 77% as slightly yellowish solid (Figure 2).

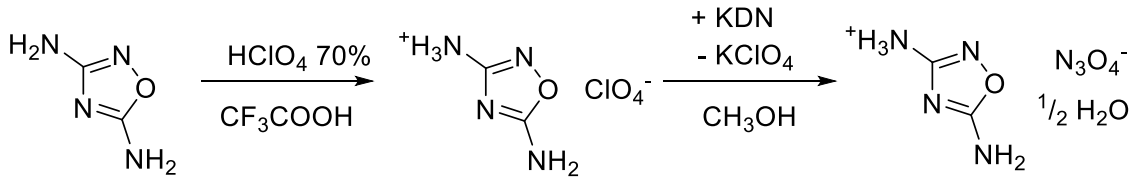

Figure 2 Synthesis of $[AOAH]^+[ClO_4]^-$ and $[AOAH]^+[N_3O_4]^- \cdot ½\ H2O$.

Single crystal X-ray diffractometry

The crystal structures of $[AOAH]^+[ClO_4]^-$ and $[AOAH]^+[N_3O_4]^- \cdot ½\ H_2O$ were determined by single crystal X-ray diffraction (Figure 3+4).

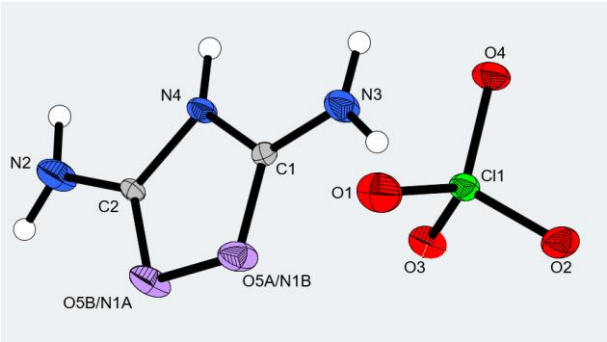

Figure 3 Molecular structure of $[AOAH]^+[ClO_4]^-$, space group $P2_1/c$, a = 10.124 Å, b = 7.117 Å c = 9.800 Å, β = 95.03°.

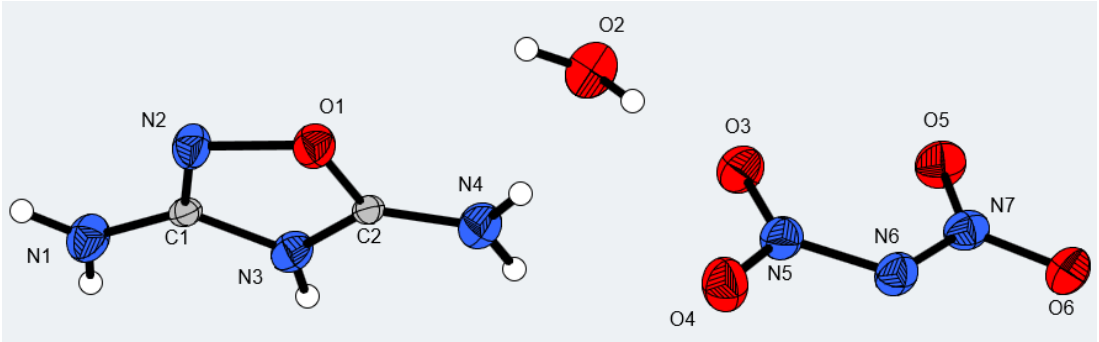

Figure 4 Molecular structure of $[AOAH]^+[N_3O_4]^- \cdot ½\ H_2O$, space group *C*2/*c*, a = 12.901 Å, b = 4.960 Å c = 25.15 Å, β = 102.35 °.

Table 1 Crystallographic data.

Sum formular	$[C_2H_5N_2O]^+[ClO_4]^-$	$[C_2H_5N_2O]^+[N_3O_4]^-$
Name	AOA perchlorate salt	AOA dinitramide salt
Crystal system	monoclinic	monoclinic
Space group	*P* 1 2_1/*c* 1	*C* 1 2/*c* 1
a (in Å)	10.1241(4)	12.9012(7)
b (in Å)	7.1168(3)	4.9495(2)
c (in Å)	9.7996(4)	25.1522(12)
B (in °)	95.026(2)	102.353(5)
Unit cell volume (in A^3)	703.36(5)	1568.9(1)
Z	4	4
Radiation	Mo- Kα	Mo- Kα
Temperature (K)	100	100
Calc. density at 100 K (g/cm^3)	1.894	1.830
d*min* (in Å)	0.90	0.79
Reflections	15290	2649
Independent reflections	1753	2482
GooF	1.069	1.082
R1 (all data / for F2 > 2σ(F2))	0.031/ 0.035	0.071/ 0.068
wR2 ((all data / for F2 > 2σ(F2))	0.077/ 0.079	0.186/ 0.183
Δρmax , Δρmin (in e/$Å^3$)	0.34/ -0.45	0.31/ -0.37

Thermal analysis

The 1,2,4-oxadiazol salts undergo thermal decomposition at temperatures below 172 °C. $[AOAH]^+[ClO_4]^-$: DSC (5 °C min-1, closed crucible) onset: 134 °C (endothermic), 150 °C (exothermic). $[AOAH]^+[N_3O_4]^- \cdot ½\ H_2O$: DSC (5 °C min-1) onset: 107 °C (exothermic), 172 °C (exothermic).

NMR spectroscopy

$[AOAH]^+[ClO_4]^-$ ^1H NMR (400 MHz, [D3]ACN): δ = 7.78 (s, 2H, NH2), 7.46 (s, 3H, NH3+) ppm. ^{13}C NMR (125 MHz, [D3]ACN): δ = 166.4, 161.3 ppm.

[AOAH]$^{+}$[N_3O_4]$^{-}$ · ½ H_2O ^{1}H NMR (400 MHz, [D3]DMSO): δ = 7.86 (s, 2H, NH2), 6.97 (s, 3H, NH3+) ppm. ^{13}C NMR (125 MHz, [D6]DMSO): δ = 169.1, 166.6 ppm.

IR and Raman spectroscopy

As shown in Figure 5, the anions exhibit strong infrared (IR) bands: 1170-1040 cm^{-1} (perchlorate) and 1180-1010 cm^{-1} (dinitramide).

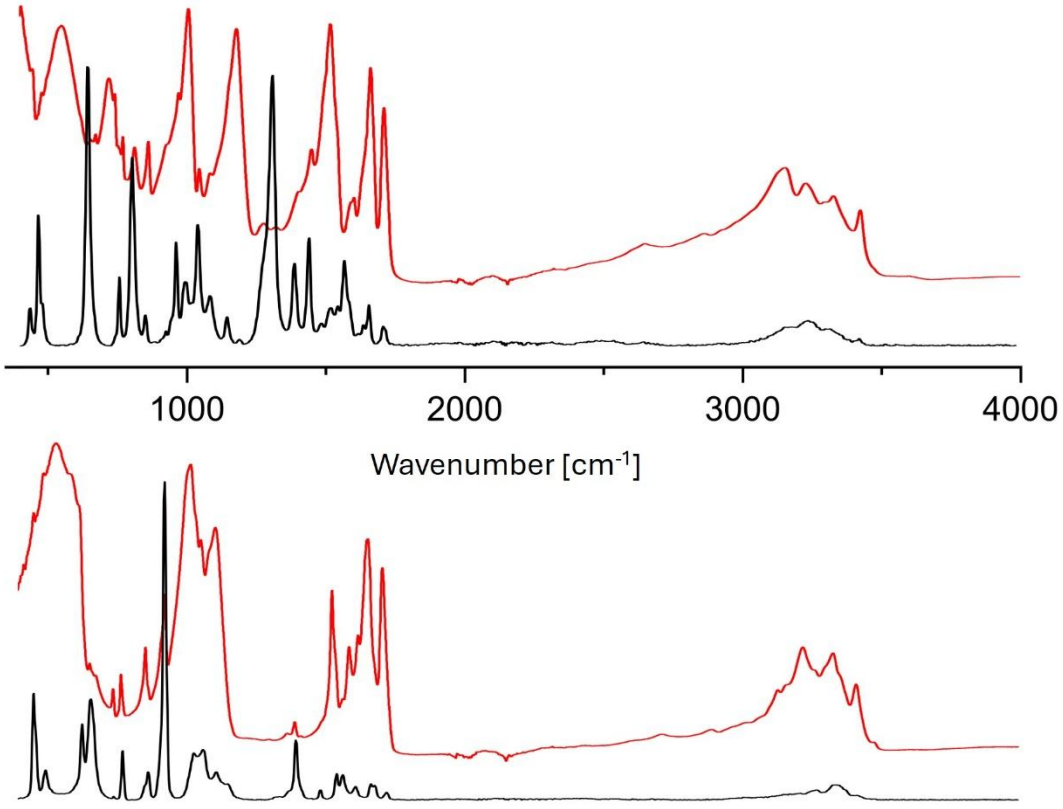

Figure 5 Raman- (black) and infrared (red) spectra of [AOAH]$^{+}$[N_3O_4]$^{-}$ · ½ H_2O (top) and [AOAH]$^{+}$[ClO_4]$^{-}$ (bottom).

Mechanical sensitivities

AOA·$HClO_4$ was investigated for friction and impact sensitivity. Sensitivities (BAM): impact > 10 J; friction > 120 N.

Conclusion

Despite an almost neutral oxygen balance of -8% and insensitivity to mechanical stimuli determined for AOA·$HClO_4$, both energetic salts show a disadvantageous low decomposition temperature. A remarkable feature is the protonation of the cyclic nitrogen in 4-position detected for the crystalline solids by X-ray structural analysis while in solution a protonation at the extra cyclic amine in 3-position was observed by

^{1}H NMR. A gain of crystal lattice energy caused by formation of intermolecular hydrogen bonds is assumed to be the reason for this constitution change.

Acknowledgement

We thank Bruker AXS Karlsruhe for performing the single crystal X-ray diffraction measurements.

References

[1] Wei, H. et al. "Combination of 1,2,4-oxadiazole and 1,2,5-oxadiazolemoieties for the generation of high-performance energetic materials." Angewandte Chemie International Edition 54(32), p. 9367-9371, 2015.

[2] Huttunen, K. M. et al. "Towards metformin prodrugs." Synthesis 2008(22), p. 3619-3624, 2008.

[3] Yu, Q. et al. "An interesting ring cleavage of a 1,2,4-oxadiazole ring." New Journal of Chemistry 41(12), p. 4797-4801, 2017.

[4] Fershtat, L. L. et al. "Assembly of nitrofurazan and nitrofuroxan frameworks for high performance energetic materials." ChemPlusChem 82(11), p. 1315-1319, 2017.

[5] Sheremetev, A. B., Makhova, Nina N. and Friedrichsen, Willy. "Monocyclic furazans and furoxans." Advances in Heterocyclic Chemistry 78, p. 65-188, 2001.

[6] Vigalok, I. V., Kovalenko, V. I. and Petrova G.G. "Salts of aminofurazanes." Khimiya Geterotsiklicheskikh Soedinenii 7, p. 998-999, 1991.

[7] Lieber, P., Schaller, U., Klapötke, T. M. “Investigation of 3,5-diamino-1,2,4-oxadiazole as a precursor for energetic salts.” Proceedings of the 25th Seminar on New Trends in Research of Energetic Materials, p. 382-387, 2023.

B.4 Amine oxidation under challenging conditions: implementation of a flow-chemistry procedure for 3,4-dinitrofurazan synthesis

Patrick Lieber*, Uwe Schaller, Thomas M. Klapötke

As published in: *Proceedings of the 26th Seminar on New Trends in Research of Energetic Materials (NTREM)*, **2024**.

Abstract

3,4-Dinitrofurazan (DNF) is both a liquid energetic material with unique properties and an excellent starting material for synthesis. Its batch synthesis is hazardous and time consuming. Therefore, we recently developed a novel microreactor based flow-chemistry procedure for the oxidation of DAF with commercially available hydrogen peroxide (70%) and concentrated sulfuric acid at elevated temperatures up to 60 °C. A yield of 32% DNF was received in preliminary experiments exploring suitable parameters for future studies. The herein presented process significantly increases safety in providing DNF on a laboratory scale and does not require the use of elemental fluorine or unusual reagents.

Keywords: 3,4-dinitrofurazan, flow-chemistry, N-oxidation.

Introduction

3,4-Dinitrofurazan (DNF) is a powerful energetic liquid that has good thermal stability and a positive oxygen balance of 10% [1-3]. Its reactivity gives access to new furazan compounds for various applications such as derivatives with show antiproliferative activity [4]. DNF shows potential uses as an additive for energetic plasticizers (Table 1).

Table 1 Comparison of selected physical properties of energetic plasticizers [5].

Energetic plasticizer	Decomposition temperature[a] [°C]	Heat of explosion[b] [J/g]	Oxygen balance [%]	Nitrogen content [%]
DNF	220	5992	+10.0	35.0
NG	143	6099	+3.5	18.5
BTTN	156	6022	-16.6	17.4
TMETN	155	5053	-34.5	16.5
DNDA57	159	3848	-72.3	30.9
BDNPA/F	182	3469	-57.6	17.6
Bu-NENA	152	3573	-104.3	20.3
C4 DN	188	3703	-93.8	39.7

[a] TGA, [b] calculated by ICT-thermodynamic code (water liquid). Nitroglycerin (NG), 1,2,4-butanetriol trinitrate (BTTN), trimethylolethane trinitrate (TMETN), dinitrodiazaalkanes (DNDA57), bis-2.2-dinitropropyl acetal/ formal (BDNPA/F), n-butylnitratoethylnitramine (Bu-NENA), 4-amino-1-butyl-1,2,4-triazolium dinitramide (C4 DN).

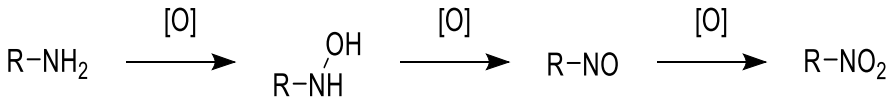

Figure 1 N-Oxidation of a primary amine in three steps to a nitro compound [7].

In batch syntheses, DNF can be received by oxidizing the commercially available solid 3,4-diaminofurazan (DAF) using concentrated mixtures of hydrogen peroxide, sulfuric acid and sodium tungstate (Figure 2) or a solution of hypofluorous acid in acetonitrile [8-9]. These procedures require the handling of extremely reactive or toxic substances. The use of concentratated hydrogen peroxide mixtures >90% is limited only to small batches because of the highly exothermic reaction and the potential risk of a thermal runaway. On the other hand, hypofluorous acid is only stable in diluted solutions and must be prepared freshly, requiring the handling of fluorine gas.

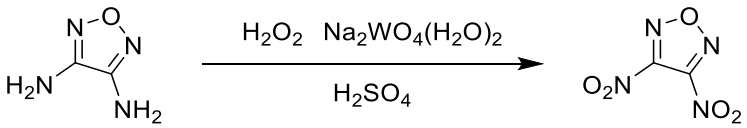

Figure 2 Synthesis of DNF through oxidation of DAF with a mixture of hydrogen peroxide 93%, conc. sulfuric acid and sodium tungstate as catalyst in the molar ration 2:1:0.05 published by Novikova et al. [8].

Recently, the use of micro- and mesofluidic reaction devices in flow chemistry has proven successful in handling highly exothermic and hazardous reactions. This

approach allows the utilization of reagents and conditions, which were previously considered too dangerous or uncontrollable. Flow chemistry enables the exploitation of these reagents in both laboratory and technical-scale applications [10]. This is enabled through the advantages of flow processing including rapid mass and heat transfer, accurate residence time control, easier reaction scale-up and full process automation [11]. Strongly exothermic reactions benefit by the high surface-to-volume ratio that enable a fast cooling, heating and precise temperature control. This way, hot spots that could lead to a thermal runway can be prevented [10].

The aim of this work was to establish a flow-chemistry setup for the synthesis of DNF which offers more safety than conventional methods and uses commercially available raw materials.

Experimental

Reagents and solutions

DAF 98% was purchased from Chemical Point UG, Deisenhofen. Hydrogen peroxide 70% was purchased from Evonik Industries AG, Essen. Sulfuric acid 98% was supplied by Merk KgaA, Darmstadt and sodium tungstate dihydrate ≥99% was supplied by Carl Roth GmbH & Co. KG, Karlsruhe. Solution A for the flow-chemistry synthesis was freshly manufactured by portionwise dissolution of 12.0 g sodium tungstate dihydrate in 40 ml of hydrogen peroxide at 0 °C. Solution B was prepared from DAF and sulfuric acid in a volumetric flask at a concentration of 0.05 g/ml DAF. The volume flow ratio of solution B to solution A during the here presented experiments was 0.33.

Analytical equipment

A high-pressure liquid chromatography system Agilent 1200 equipped with a ZorbaxBonus RP 4.6x2500mm column and a diode array detector was used to verify the yield and the purity of the synthesised DNF. ATR infrared spectra were recorded by a Thermo scientific iS 50 FTIR spectrometer.

Analytical methods

Assessment of the purity and estimation of the yield was performed by LC-DAD. Gradient determination of DNF was performed by injecting 5 µL of 1:50 by acetonitrile diluted samples of product solution. The mobile phase was acetonitrile/water with 0.1% trifluoroacetic acid (gradient from 20:80 to pure acetonitrile in 15 minutes) the flow rate

was 1.0 ml/min. The identification of DNF was based on retention time and UV spectra profile (190-400 nm). The retention times, resolution of peaks and spectra profiles of analytes were determined after injection of reference material from batch synthesis. Quantification was performed by peak integration and calibration curve.

Flow-chemistry setup

To perform the reaction, a flow setup was used, which consisted of an LTF-ST mixer and a coiled tubular reactor with a 0.8 mm internal diameter PTFE tube. The total volume of the mixer and reactor was 7.5 ml. Temperature control was achieved by using a water bath and a heating/ cooling circulator. Solution A was pumped from a reservoir, which was cooled by a ice bath, using a peristaltic pump. Solution B, on the other hand, was delivered at Ambient temperature using a syringe pump. The system pressure was measured by an integrated sensor in the peristaltic pump. Samples and waste were collected at Ambient temperature.

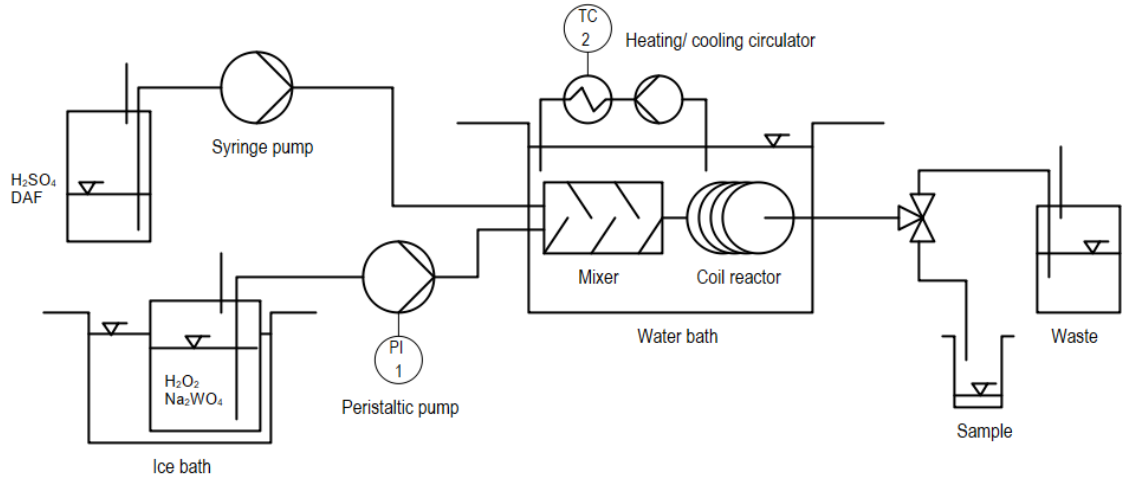

Figure 3 Schematic representation of the flow-chemistry setup.

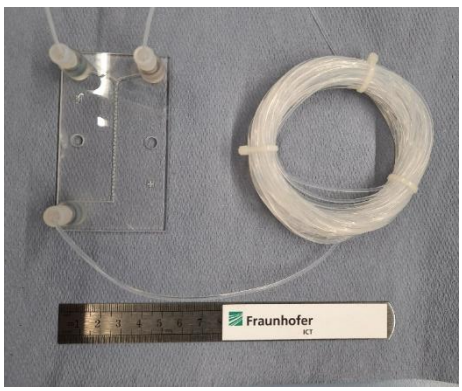

Figure 4 LTF-ST mixer and coil reactor from PTFE tube.

Batch synthesis of DNF

The synthesis of DNF in batch was carried out based on the method by Novikova et al. to provide a reference product [5]. However deviating from the original procedure commercial available aqeous hydrogen peroxide 70% was used instead of 93%

5.44 g of hydrogen peroxide 70% (111.9 mmol; 22.9 eq.) is placed in a 50 ml round-bottom flask equipped with a thermometer. The liquid is cooled down to -5 to 0 °C using an cooling bath of water, ice and sodium chloride. Then, carefully and dropwise under vigorous stirring, 7.84 g of sulfuric acid 98% (78.3 mmol, 16.0 eq.) are added keeping the temperature below 5 °C. The addition of the acid takes about one hour. Afterwards, 1.17 g of sodium tungstate dihydrate (3.51 mmol, 0.7 eq.) is added in three portions. The finished oxidation mixture is stirred for one hour at 0 °C. 500 mg DAF (4.89 mmol, 1.00 eq.) is added in small portions while keeping the temperature below 10 °C. A very intense dark green color appears and shows the reaction start. After the addition is complete, the ice bath is removed and the temperature was slowly allowed to increase to 20 °C using a water bath with little ice. The reaction mixture was stirred for 3 hours until complete decolorization occurred. It was then diluted with 20 ml of water and extracted with three portions of 10 ml DCM. The combined organic extracts were washed with two portions of 10 ml water and dried over sodium sulfate. The solvent was removed at 25 °C by argon stripping. The removal of the solvent was followed by IR spectroscopy. DNF was received with 21.7% isolated yield as a slightly yellow, clear liquid. It was subsequently characterized by HPLC (Figure 7), infrared spectroscopy and ^{13}C-NMR spectroscopy. ^{13}C-NMR (100 MHz, DMSO-D_6) δ = 152.74 (t, J=0.2) ppm. IR (ATR, 25 °C) = 1570, 1538, 1451, 1351, 1325, 1137, 1031, 902, 839, 803, 769, 734, 615, 475 cm^{-1}.

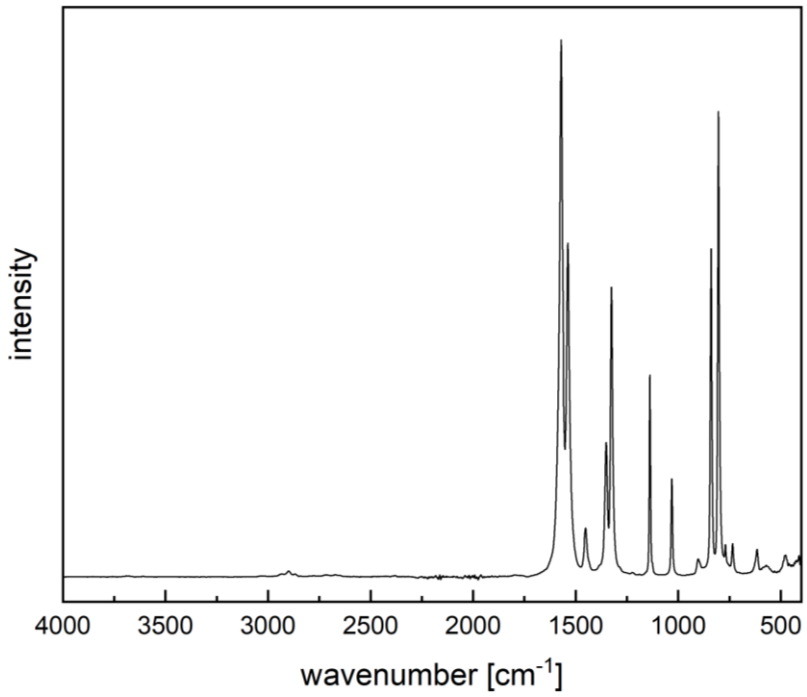

Figure 5 ATR FT-IR spectrum of DNF from batch synthesis.

Results and discussion

Solubility of reagents

The prerequisite for a well-functioning flow process is that all components remain in solution or in the gas phase during the process. In this case, the violent conditions of the reaction do not allow any auxiliary solvents other than dichloromethane and other perhalogenated substances. Therefore, the only question is which solids are pre-dissolved in which liquid reagent. Sodium tungstate turned out to be insoluble in sulfuric acid. So that only hydrogen peroxide remained with the disadvantage that the addition would immediately trigger a decomposition process with oxygen release (solution A). In order to minimize the degradation of hydrogen peroxide, the solution was prepared fresh and always cooled to 0 °C. The sulfuric acid proved to be a suitable solvent for DAF and no signs of a reaction such as discoloration or gas development could be observed (solution B).

Configuration of the flow process

To prevent the accumulation of oxygen from the decomposition of solution A in the syringes, a peristaltic pump was used. The solutions were mixed by a LTF-ST mixer in front of the 7.5 ml tubular reactor to ensure fast mixing. Solutions were pumped in a volume flow ratio of solution B/ solution A=0.33. Initially, the reaction was performed at

10°C with a residence time of 6.25 minutes. However, this resulted in incomplete conversion and a violent reaction in the waste collection flask. This fact also became clear when the still green reaction mixture left the reactor. The strong coloration of the reaction mixture is probably caused by nitroso intermediates. Increasing the water bath temperature to 40 °C improved the yield, but the most advantageous result of 32% was achieved at the highest tested temperature of 60 °C and a residence time of 12.5 minutes (Figure 6).

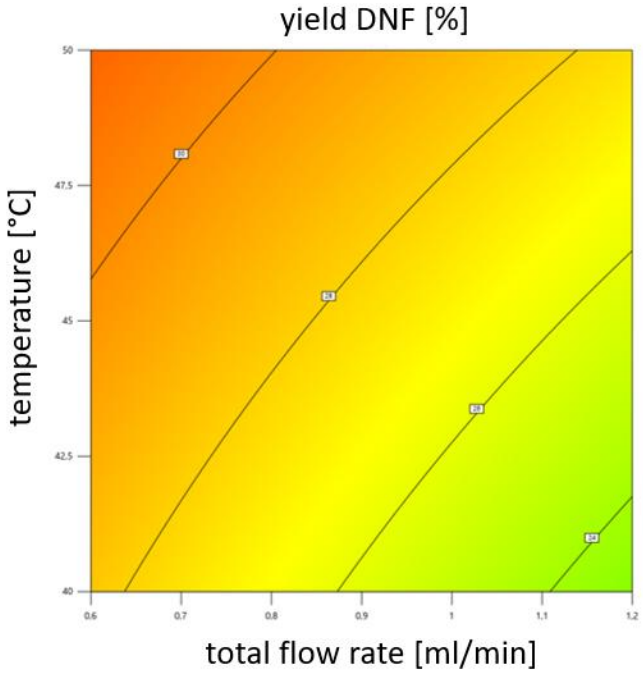

Figure 6 Response contour of DNF Yield (%) depending on temperature and total flow rate.

HPLC-DAD analysis of the yield

In order to verify the yield of the flow-chemistry reaction and the purity of the reference DNF a HPLC-DAD method was used. Due to a matching retention time and UV-spectrum, a compound of the flow-chemistry product solution could be assigned to the DNF reference from batch synthesis (Figure 7).

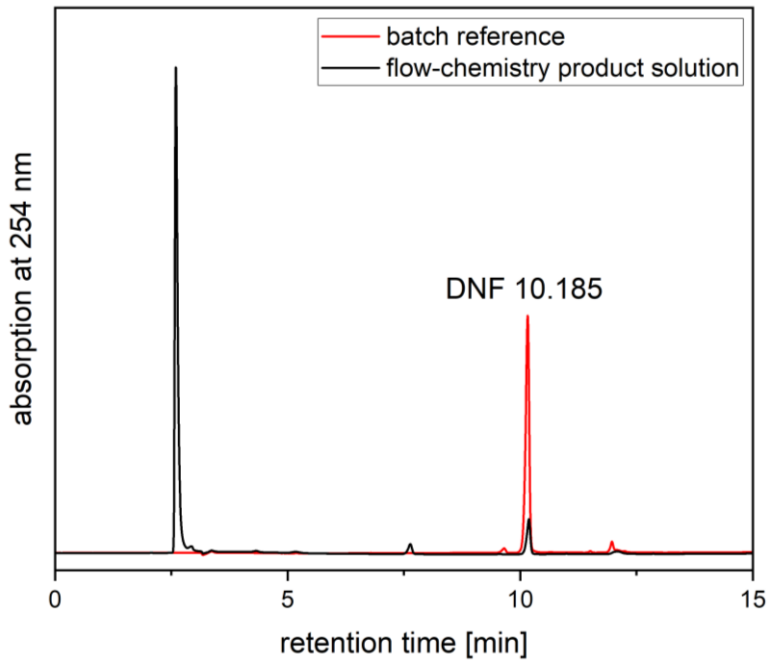

Figure 7 The chromatographs of reference DNF from batch synthesis (red) and a product solution of the flow-chemistry process (black).

Conclusion

Aim of this research is to develop a safe and effective method to synthesize DNF from commercialy available compounds. In this initial work a flow-chemistry setup for the synthesis of DNF was implemented. Preliminary experiments for exploration of suitable reaction conditions and the development of a HPLC-DAD-based analysis method were reported. The application of flow chemistry made it possible to successfully realize new reaction conditions such as a reaction temperature of 60 °C in practice. The goal of further studies will be to determine the influence of various reaction parameters to optimize the yield and gain a deeper understanding of N-oxidation reaction at elevated temperatures. In addition, efforts will continue to use safer and more available reagents.

Acknowledgment

Thanks to the WTD 91 of the German ministry of defense for the financial support of this work. We are particularly grateful to M. Schwarzer for performing the HPLC measurements. We also thank S. Panic for his support with the setup as well as S. Müller and W. Schweikert for help with the IR spectroscopy.

References

[1] A. V. Belyakov, V. A. Losev, A. N. Rykov, I. F. Shishkov, V. V. Kuznetsov, A. V. Khakhalev, A. B. Sheremetev. „Combined gas-phase electron diffraction and coupled cluster determination of the molecular structure of 3,4-dinitrofurazan - A propellant ingredient.“ Journal of Molecular Structure 1250, p. 131669, 2022.

[2] K. Y. Suponitsky, A. F. Smol'yakov, I. V. Ananyev, A. V. Khakhalev, A. A. Gidaspov, A. B. Sheremetev. „3,4-Dinitrofurazan: Structural Nonequivalence of ortho -Nitro Groups as a Key Feature of the Crystal Structure and Density.“ ChemistrySelect 5, p. 14543–14548, 2020.

[3] D. E. Dmitriev, Y. A. Strelenko, A. B. Sheremetev. „NMR spectroscopic study of 3-nitrofurazans.“ Russ Chem Bull 62, p. 504–515, 2013.

[4] A. B. Sheremetev, D. E. Dmitriev, N. K. Lagutina, M. M. Raihstat, A. S. Kiselyov, M. N. Semenova, N. N. Ikizalp, V. V. Semenov. „New functionalized aminofurazans as potential antimitotic agents in the sea urchin embryo assay.“ Mendeleev Communications 20, p. 132–134, 2010.

[5] B. Wu, X. Jiang, Y. Yang, H. Du, X. Shi, Z. Li, C. Pei. „Continuous-Flow Oxidation of Amines Based on Nitrogen-Rich Heterocycles: A Facile and Sustainable Approach for Promising Nitro Derivatives.“ Organic Process Research and Development 26, p. 2823–2829, 2022.

[6] R. W. Murray, M. Singh, N. Rath. „Stereochemistry in the oxidation of primary amines to nitro compounds by dimethyldioxirane.“ Tetrahedron: Asymmetry 7, p. 1611–1619, 1996.

[7] U. Schaller, J. Lang, V. Gettwert, J. Hürttlen, V. Weiser, T. Keicher. "4-Amino-1-Butyl-1, 2, 4-Triazolium Dinitramide–Synthesis, Characterization and Combustion of a Low-Temperature Dinitramide-Based Energetic Ionic Liquid (EIL)." Propellants, Explosives, Pyrotechnics 47(7), p. e202200054, 2022.

[8] T. S. Novikova, T. M. Mel’nikova, O. V. Kharitonova, V. O. Kulagina, N. S. Aleksandrova, A. B. Sheremetev, T. S. Pivina, L. I. Khmel’nitskii, S. S. Novikov. „An Effective Method for the Oxidation of Aminofurazans to Nitrofurazans.“ Mendeleev Communications 4, p. 138–140 1994.

[9] A. B. Sheremetev. „Efficient synthesis of nitrofurazans using HOF • MeCN.“ Russ Chem Bull 71, p. 1818–1820, 2022.

[10] M. Movsisyan, E. I. P. Delbeke, J. K. E. T. Berton, C. Battilocchio, S. V. Ley, C. V. Stevens „Taming hazardous chemistry by continuous flow technology.“ Chemical Society reviews 45, p. 4892–4928, 2016.

[11] P. Plouffe, M. Bittel, J. Sieber, D. M. Roberge, A. Macchi. „On the scale-up of micro-reactors for liquid–liquid reactions.“ Chemical Engineering Science 143, p. 216–225, 2016.

B.5 Energetic plasticizers for GAP-based formulations with ADN: Compatibility and performance evaluation of a nitrofurazanyl ether

Patrick Lieber*, Uwe Schaller, Thomas M. Klapötke

As published in: *Proceedings of the 48th International Pyrotechnics Society Seminar*, **2025**.

Extended abstract

Glycidyl azide polymer (GAP) diol is a hydroxyl-terminated polyether that contains azide groups in its side chains (Figure 1). Due to its high energy content and low sensitivity towards external stimuli, it is a promising energetic binder. When combined with the environmentally friendly oxidizer ammonium dinitramide (ADN), it offers good ballistic properties. [1] Although it has a positive enthalpy of formation and high density, its mechanical properties are poor compared to those of the widely used inert binder hydroxyl-terminated polybutadiene (HTPB). Therefore, sufficiently low glass transition temperature for GAP formulations can only be achieved by using a plasticizer. [2] This improves the formulation's mechanical properties at low temperatures by increasing flexibility and reducing brittleness. Compared to inert plasticizers, energetic plasticizers have the advantage of containing explosophores that increase the overall energy content of the formulation. The most common energetic plasticizers consist of a saturated, linear carbon backbone supplemented by explosophores containing side groups. Although the use of heterocyclic building blocks in other energetic materials has been extensively studied, literature on using heterocycles as energetic plasticizers is scarce. Among energy-rich heterocycles, oxadiazoles are of particular interest. They have a less negative impact on the oxygen balance than triazoles or tetrazoles. Among the four oxadiazole isomers, furazan (1,2,5-oxadiazole) has the highest enthalpy of formation. [3]

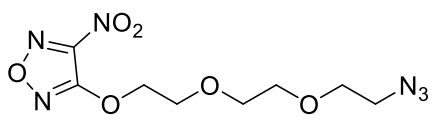

NFPEG3N3

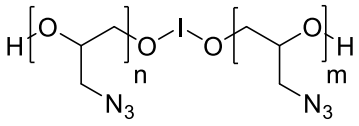

GAP diol
I=ethan-1,2-diol (diol initiator)

Figure 1 Molecular structures of NFPEG3N3 (3-(2-(2-(2-azidoethoxy) ethoxy) ethoxy)-4-nitro-1,2,5-oxadiazole) and GAP diol.

Recently, we succeeded in synthesizing new nitrofurazanyl compounds with interesting properties for use as energetic plasticizers (Figure 1). [4] The compound NFPEG3N3 has an impressive glass transition temperature of -72 °C. Initial tests of mixtures on the viscosity and glass transition temperature lowering of the prepolymer GAP diol were promising. This study investigates the compatibility of NFPEG3N3 with the formulation components GAP diol, HMX, Desmodur N100 and ADN. For this purpose, isothermal heat flow microcalorimetry (HFMC) and dynamic thermogravimetry (TG) were employed, according to STANAG 4147. [5] An overview of the results and criteria can be found in Table 1. Mixtures of NFPEG3N3 with HMX, GAP diol, and Desmodur N100 met the compatibility criteria. However, the NFPEG3N3-ADN mixture did not meet the compatibility criteria in the dynamic TG test. It passed the HFMC test when a heat generation reactivity limit of 1% of the mixture's heat of explosion was applied. [5] Nevertheless, its reactivity is clearly higher than that of the other mixtures. According to STANAG criteria, HMX, GAP diol, and Desmodur N100 are compatible with NFPEG3N3. Further investigation is needed to determine the exact compatibility between ADN and NFPEG3N3 because the measured reactivity could lead to long term stability issues.

Table 1 Summary of compatibility test results and criteria.

Compatibility test	Heat generation (HFMC), air, R_Q [J/g] after 10.6 days at 80 °C (*limit value*)	Weight loss (dynamic TG), nitrogen flow, R_W [%] at x °C	Total assmt.
Limit value	-1% of Q_{Ex}< R_Q<1% of Q_{Ex}	R_W<4%	
NFPEG3N3 + HMX	0.80 (*38.42*)	-10.6 at 175 °C	compatible
NFPEG3N3 + GAP diol	2.24 (*32.25*)	-17.5 at 172 °C	compatible
NFPEG3N3 + Desmodur N100	3.67 (*30.00**)	-19.1 at 183 °C	compatible
NFPEG3N3 + ADN	24.46 (*41.90*)	+5.2 at 158 °C	

* Thermodynamic data not available, general threshold value for NC-based formulations. [5]

The impact of NFPEG3N3 on the specific impulse of a GAP-based composite propellant containing 70wt% filler (58.7wt% ADN and 11.3wt% HMX) was evaluated using theoretical calculations with the ICT thermodynamic code. [6] By replacing 15wt% of GAP with NFPEG3N3 the mass-specific impulse of the formulation increased by 30 N s/kg.

Considering that the same proportion of an inert plasticizer reduces the mass-specific impulse by approximately 50 N s/kg, this is a considerable gain in performance. In comparison with the energetic plasticizers BDNPA/F and Bu-NENA, however, NFPEG3N3 shows a slightly smaller increase of the mass-specific impulse (Figure 2).

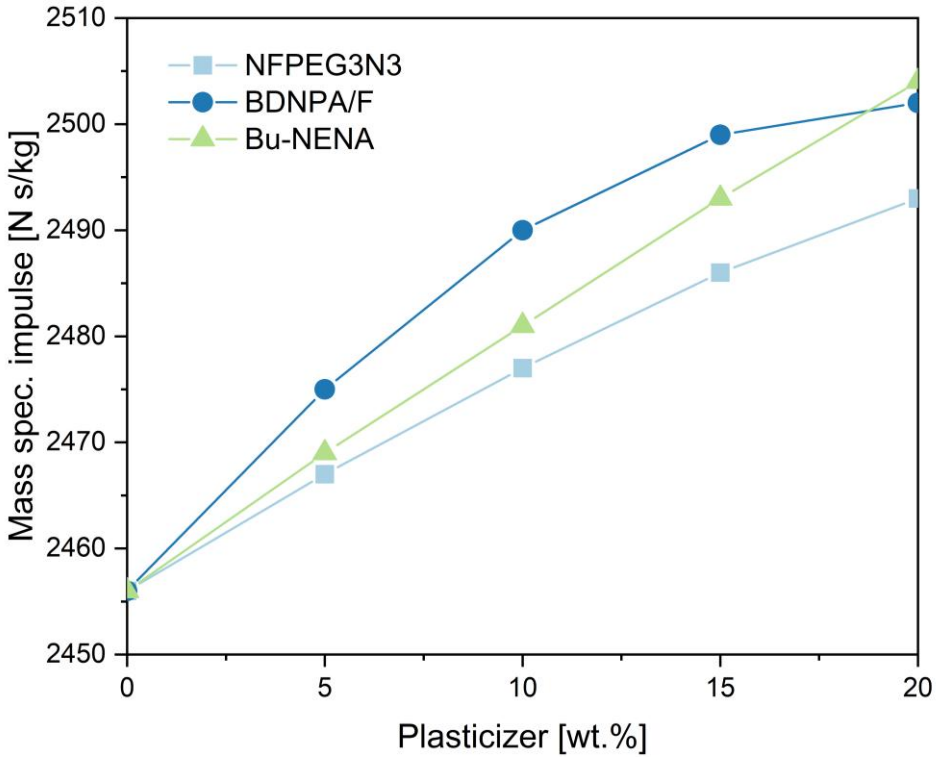

Figure 2 Impact of NFPEG3N3 and selected energetic plasticizers on the mass-specific impulse of a propellant formulation containing 10-30wt% GAP, 58.7wt% ADN and 11.3wt% HMX.

Nevertheless, NFPEG3N3 appears to be a promising new molecule due to its advantageous combination of properties, including a high TG decomposition temperature of 167 °C and a nitrogen content of 29.2%. 4 The NFPEG3N3 formulation also demonstrates a higher volume-specific impulse of 4043 N s/L and a more favorable oxygen balance of -20.4% than the Bu-NENA formulation, which exhibits a volume-specific impulse of 4001 N s/L and an oxygen balance of -22.0%. The results presented in this extended abstract will be submitted for publication in a peer-reviewed journal.

Acknowledgment

The authors gratefully acknowledge Dr. M. Heil for his valuable guidance and support throughout this study. We thank H. Schuppler for performing the TG measurements and

T. Grunwald for conducting the HFMC measurements. Funding from the WTD91 of the German Ministry of Defense is also gratefully acknowledged.

References

(1) Menke, K.; Heintz, T.; Schweikert, W.; Keicher, T.; Krause, H. Formulation and properties of ADN/GAP propellants. Propellants Explos. Pyrotech. 2009, 34(3), 218-230.
(2) Ek, S.; Johansson, J.; Brantlind, M.; Ellis, H.; Skarstind, M. Synthesis and characterisation of tri- and tetraethyleneglycoldiazide for their use as energetic plasticisers. New Trends in Research of Energetic Materials (NTREM) 2019, 81-87.
(3) Wei, H.; He, C.; Zhang, J.; Shreeve, J. N. M. Combination of 1, 2, 4-oxadiazole and 1, 2, 5-oxadiazole moieties for the generation of high-performance energetic materials. Angew. Chem. Int. Ed. 2015, 54(32), 9367-9371.
(4) Lieber, P.; Schaller, U.; Klapötke, T. M. Synthesis and characterization of novel nitrofurazanyl ethers as potential energetic plasticizers. RSC Adv. 2025, 15(16), 12577-12584.
(5) STANAG 4147 (edition 3), chemical compatibility of ammunition components with explosives (non-nuclear applications), NATO, 2023.
(6) Kelzenberg, S.; Kempa, P.-B.; Wurster, S.; Herrmann, M.; Fischer T. New version of the ICT-thermodynamic code. 45th International Annual Conference of ICT, 2014.